Radiating Graben-Fissure Systems in the Ulfrun Regio area, Venus

By

Duncan Studd

A thesis submitted to the Faculty of Graduate and Postdoctoral Affairs in partial fulfilment of the requirements for the degree of:

Master of Science

In

Earth Sciences

Carleton University

Ottawa, Ontario

Library and Archives Canada

Published Heritage Branch

395 Wellington Street
Ottawa ON K1A 0N4
Canada

Bibliothèque et Archives Canada

Direction du Patrimoine de l'édition

395, rue Wellington
Ottawa ON K1A 0N4
Canada

Your file Votre référence
ISBN:978-0-494-71726-4
Our file Notre référence
ISBN: 978-0-494-71726-4

Acknowledgements

I would like to thank my supervisors, Claire Samson (Carleton University) and Richard Ernst (Ernst Geosciences, Carleton University) for their aid, knowledge, and guidance throughout this project.

I would also like to thank Mikhail Ivanov (Vernadsky Institute) for providing a copy of his geological map of Venus, and for his comments and suggestions on various abstracts and posters during the last two years. Thanks, as well, to Jim Head (Brown University) and Eric Grosfils (Pomona College) for their comments and suggestions during this project; and to Don Desnoyers (Geological Survey of Canada) for helping solve data display and projection problems.

Thank you.

Abstract

Radiating graben-fissure systems are extensional tectono-magmatic structures which are found on Venus and believed to be underlain by dykes fed by magmatic centres which are located at the focus of the system. This study has mapped radiating graben-fissure systems in the Ulfrun Regio area (200°-240°E, 0°-25°N) on Venus. In the study area, 66 radiating centres comprised of 13,000 individual graben and having radii of up to 2000 km have been identified. Cross-cutting relations between these systems and with the Hecate Chasma rift zone and surface geology have been examined to provide a relative chronology of magmatic activity in the area. There is an apparent younging trend from the southwest to northeast of the study area. The widths of several long graben within these systems have been measured with respect to distance from their point of origin. A majority exhibit a general trend of decreasing width with distance for these graben.

Table of Contents

Table of Figures

1.0. Introduction

1.1. Venus: A Planetary Overview

While long thought of as Earth's sister planet due to its similarity in size and mass, Venus possesses several characteristics that differ greatly from those of Earth. In similarity, Venus has 81.5% the mass of Earth, 95.5% the density, and 95% the mean radius (Janle & Meissner, 1986). However, in great contrast to the Earth, the Venusian atmosphere is largely composed of carbon dioxide, which forms clouds that obscure any view of the surface from orbit and work very effectively to trap heat. The surface conditions are thus hostile to life as it exists on Earth, with a temperature of 450˚C and a pressure of 9030 kPa. Water is only present in miniscule amounts of between 1 ppm (part per million) to 100 ppm (Prinn & Fegley, 1987). Venus also lacks a significant magnetic field (Russell, 1980), and its surface temperature is sufficiently high that a magnetic record cannot be preserved within the rock (Head, 1999) – so we do not know if Venus ever did have a magnetic field.

The surface of Venus does not exhibit heavy cratering which has been interpreted as evidence that Venus underwent a global resurfacing event with a mean age of approximately 750 million years ago (McKinnon et al., 1997; Basilevsky and Head, 2002; Ernst and Desnoyers, 2004). According to recent studies, the duration of the resurfacing event could range from 300 to 500 million years (McKinnon et al., 1997) up to 900 million years or more (Ernst and Desnoyers, 2004). This is markedly different from previous estimates that had the resurfacing event lasting only 10 to 100 million years,

between 500 and 300 million years ago (Phillips et al., 1992; Schaber et al., 1992; Bullock et al., 1993; Herrick, 1994; Namiki & Solomon, 1994; Strom et al., 1994; Herrick et al., 1995; Strom et al., 1995; Head and Coffin, 1997). The Venusian lithosphere is about 80-200 km thick, the crust about 30 km, overlying a mantle with a potential temperature of approximately 1300°C, comparable to Earth's mantle (Nimmo & McKenzie, 1998).

Venus' crust does not appear to be subjected to plate tectonics; there are regions of extensional rifting, and others crowded with compressional "wrinkle ridges" but there are no separate plates or subduction of crust into the mantle (Phillips and Hansen, 1994). Wrinkle ridges are the surface expression of low-amplitude compressive anticlines and associated thrust faults and are found on 43% of Venus's volcanic plains (Bilotti & Suppe, 1999). Most of the topography of the planet lies within 1 km of the mean planetary radius (Pettengill et al. 1980). Three types of topography are recognized which make up almost the entirety of the surface: (1) low-lying plains with relatively little relief, called "planitia"; (2) rough, mountainous, volcanic highlands; and (3) rolling plains termed mesolands which are found in between planitia and highlands (Philips and Hansen, 1994). Data gathered by the Soviet Venera landers in the short time that they survived on the surface indicate that the surface composition is essentially basaltic (Surkov et al, 1986, 1986).

1.2. Magmatic Centres

Our research in this project focuses on the mapping and interpretation of radiating graben-fissure systems. Here, we summarize features on the surface of Venus which are related to radiating graben-fissure systems.

According to Crumpler and Aubele (2000), 1734 volcanic edifices, shield fields, calderas, and related features over 20 km in diameter have been identified on Venus. These volcanic centres exhibit two distinct styles: the larger and more earth-like volcanoes formed by large flows emanating from a vent; and regions of 100 to 200 km in diameter occupied by many small volcanic edifices, known as shield fields. Rather than being primarily dependent on magma type as on Earth, it seems likely that Venusian volcanic landforms are mainly basaltic in composition and the differences depend on magma flow rates: high rates result in large volcanoes, while low rates feed shield fields (Crumpler et al., 1997). Shield fields can alternatively be interpreted to represent shallow source melting over broad areas (Addington 2001; Ivanov and Head 2004).

1.2.1. Coronae

Coronae (Figure 1.1) are circular to elongate volcano-tectonic structures with an average diameter of 230 km and a maximum of 2600 km. They typically consist of an inner plateau surrounded by an annular ring of troughs and ridges and are sometimes associated with extensive volcanism (Stofan et al., 1992). They can be accompanied by large numbers of small volcanoes, extensive flow deposits, and radial fractures and ridges. There are approximately 513 coronae identified on Venus, with diameters

ranging from 37 km to 2600 km (Stofan et al., 2001, as modified in Glaze et al., 2002). It is believed that they are the result of mantle diapirs – pockets of buoyant material that rise through the mantle and may produce melts that ascend into the crust. Typically, this process blisters the lithosphere outwards. Then as the diapir thins and spreads laterally, the centre of the blister will collapse forming a depression (Stofan et al, 1997). While coronae-like structures are not as readily observed on Earth, it has been proposed that similar structures can be found, especially on the African plate and within the East African rift system (Lopez et al, 1999).

1.2.2. Arachnoids

Arachnoids (Figure 1.2) are volcano-tectonic features with a circular shape and a radiating system of ridges. It has been theorized that they are a subtype of coronae (Price and Suppe, 1995) or possibly an early stage of corona development (Hamilton and Stofan, 1996a). Arachnoids are associated with minor extrusive volcanism and generally exhibit a depressed topography. They are mostly found in clusters in the northern hemisphere (Aittola and Kostama, 2000).

1.2.3. Radiating Graben-Fissure Systems/Novae/Astra

Radiating graben-fissure systems (Figure 1.3) are volcano-tectonic features expressed as radiating fracture centres. Other terms to describe them, used in early work, include "radial corona-like feature" (Stofan et al, 1992), "failed corona" (Janes and

Turtle, 1996), "radially fractured dome" (Squyres et al, 1992), and "stellate fracture centre" (Crumpler et al, 1997). In all these cases, the patterns radiate from a point. They can be viewed as a type of radiating graben fissure system in which the focal point region (with graben-fissure convergence to a point) is preserved. The fractures are extensional in nature, likely the result of buoyant mantle diapirs deforming the crust (Stofan et al, 1992). The diameters of identified novae range from 50-300 km (Head et al, 1992). It is estimated that approximately half of all novae are found within coronae and approximately 60% are associated with rift zones. (Aittola and Kostama, 2000) Note that the term "nova" in the Venusian context is not recognized by the Planetary Nomenclature Group of the International Astronomic Union (IAU), as it is already used in astrophysics. The term "astrum" has been suggested by the IAU as a replacement, but since "nova" is commonly used and well-defined by those who study Venus, the use of the term has persisted. However, in some recent studies (e.g. Ernst et al. 2003) and also in the present study, the term radiating graben-fissure system is being used instead of novae and astra. It is realized that in some cases the radiating focal regions (i.e. nova) for radiating graben-fissure systems are obscured by younger lavas, and so the nova term cannot be used for these. Therefore the broader term, radiating graben-fissure system, is being used instead.

These radiating systems are believed to be the product of magmatic or tectonic processes. These are, respectively, a combination of the stresses of domical uplift above an ascending mantle diapir (Cyr and Melosh, 1993) and surface fracturing induced by

shallow dyke emplacement (Parfitt and Head, 1993). The more extensive systems are believed to be produced by the dyke swarm model (Grosfils and Head, 1994).

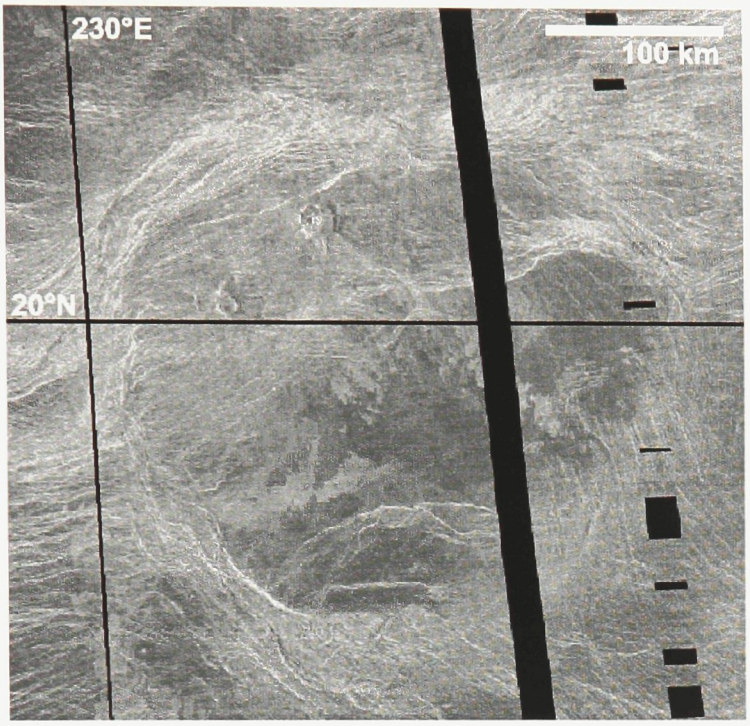

Figure 1.1. Pani Corona (19.9°N, 231.5°E) exhibits typical circular ridge forms.

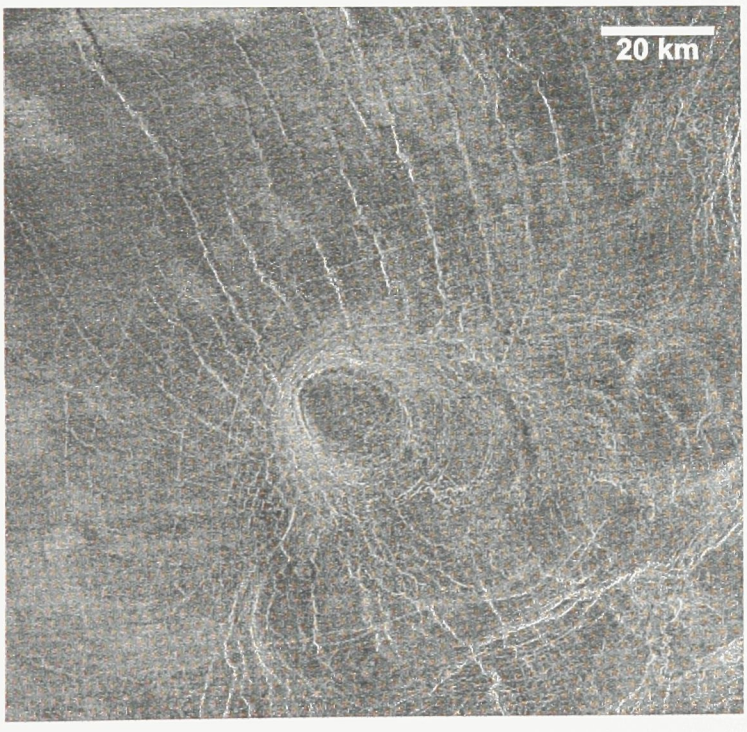

Figure 1.2. A typical arachnoid (22°N, 202°E), with a central circular structure and radiating ridges.

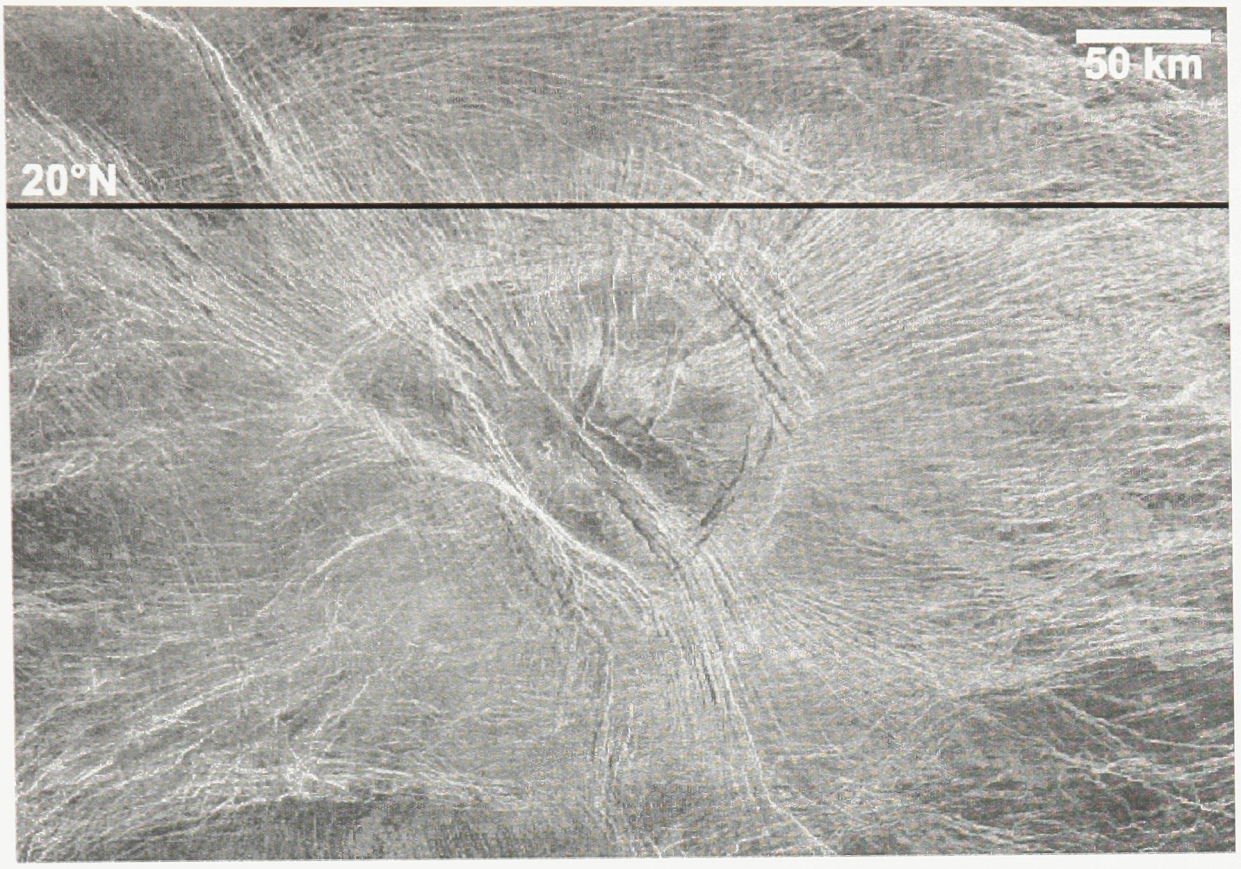

Figure 1.3. A nova/astrum/radiating graben-fissure system at (19°N, 227.5°E) centred within an irregularly shaped corona structure.

1.3. Research Objectives

In this project, a systematic mapping of all extensional lineaments (fractures, fissures, and graben) in the Ulfrun Regio area of Venus has been completed, using Synthetic Aperture Radar (SAR) data from the Magellan mission. The emphasis is on identifying radiating graben-fissure systems within and immediately adjacent to the study area. With the high density of linear extensional features that we have mapped, we are exploring the approach of using cross-cutting relationships between individual graben-fissure systems and geological units to ascertain relative ages. From the mapping, and using the geological map of Ivanov (2008), the relative ages of radiating systems with respect to their host geology and other major geological features are established. These data will provide a new context from which to examine the magmatic and tectonic evolution of the study area.

The radiating graben-fissure systems are of particular interest because (as mentioned above) they are largely acknowledged to be underlain by dyke swarms laterally emplaced from magmatic centres located at the foci of the systems (eg. Grosfils and Head, 1994; Ernst et al, 1995; Ernst et al, 2003). This study is concerned with these extensional lineaments – which we will collectively term graben when they are included in radiating graben-fissure systems. Note that graben are wider and have an observable floor, while fissures are trough- or V-shaped and typically narrower than graben (Grosfils and Head, 1994; Ernst et al., 2003).

For the sake of brevity, when referring to collections of lineaments (graben and fissures) within the radiating graben-fissure systems discussed in this thesis, the term graben will be used. Please be aware that future mentions of "graben" can be assumed to also refer to fissures. This study is part of the Venus Global Dyke Swarm Map Project (Ernst et al., 2009; Studd et al., 2010a, b, c), the goals of which are: to produce a global map of graben-fissure systems, to assess which of these systems are underlain by dyke swarms and to contribute to the understanding of the tectonic and magmatic history of the planet (Figure 1.4).

All mapping of graben in the study area has been completed by the author, the results of which have been presented to the scientific community through the following abstracts: Ernst et al., 2008; Ernst et al., 2009; Studd et al., 2009; Studd et al., 2010a; Studd et al., 2010b; and Studd et al., 2010c.

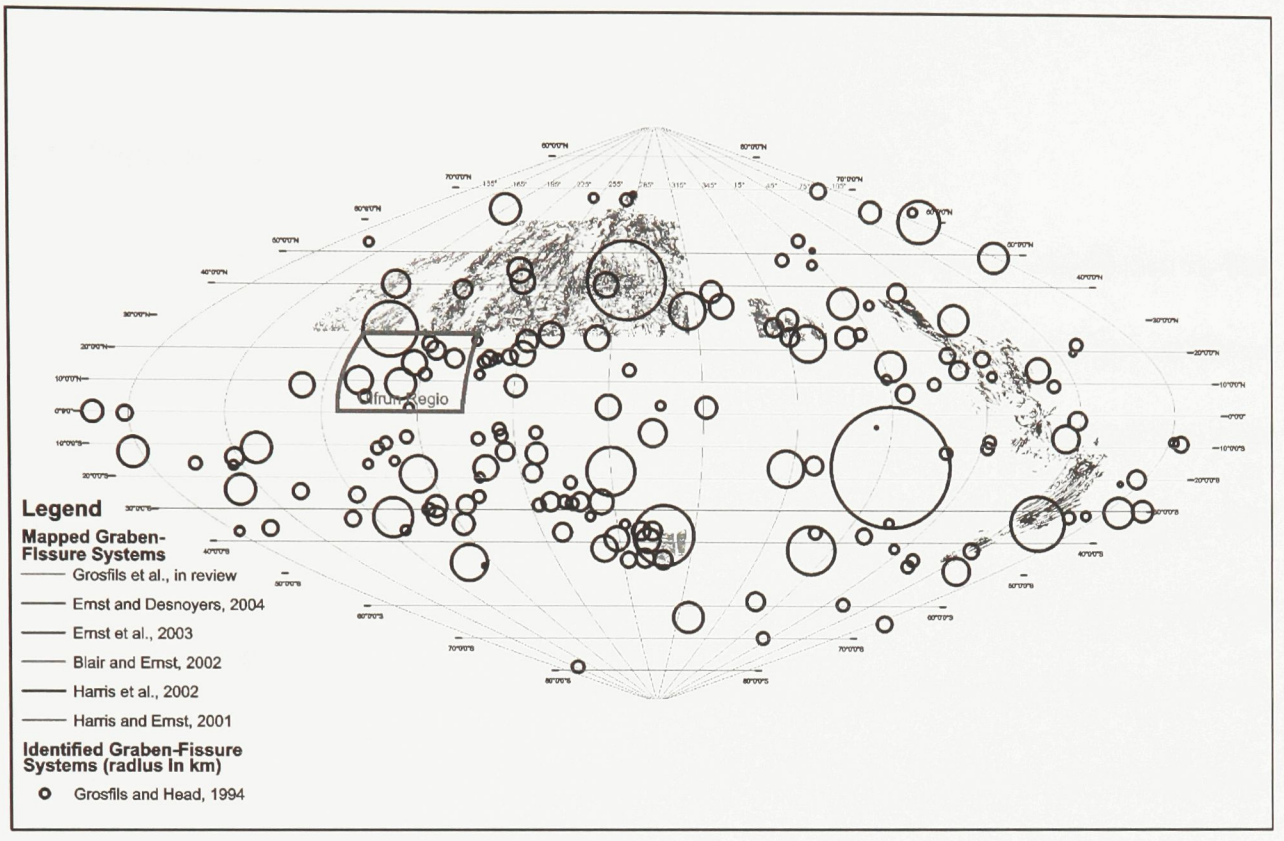

Figure 1.4. Present state of mapping in the Venus Global Dyke Swarm Map Project. The region studied in this thesis is outlined and labelled as Ulfrun Regio. From Studd et al., 2010c.

1.4. Tectono-Magmatic Setting of the Study Area

The Ulfrun Regio area (200-240°E, 0-25°N) was selected for this study due to the greater than average abundance of structural features, striking a fair balance between undeformed volcanic plains and highly deformed uplands terrains. Most of the area (specifically the Ulfrun Regio Quadrangle) is as yet unassigned for mapping by the NASA/USGS Planetary Mapping Program. The abundance of radial graben-fissure systems (greater than 100 in the study area) allows for ample study of their features, formation, and interaction with each other and with other tectonic and magmatic features in the region.

Ulfrun Regio, which lends its name to our study area, is an uplifted highland region. Ulfrun Regio is 4000 km from north to south, 800 km across, and rises up to 3000 m above surrounding plains. The highland is crossed by Hecate Chasma, a large-scale fracture belt and rift zone which runs west to east between Atla and Beta Regiones.

Atla Regio is a highland region at the western end of Hecate Chasma. Atla Regio has a 3200 km maximum diameter and is the site of abundant volcanism, including a newly discovered area of recent volcanic activity[1]. A portion of eastern Atla Regio, including the large volcano Ozza Mons (4.5°N, 201°E) is included in our study area.

---

[1] http://www.esa.int/SPECIALS/Venus_Express/SEMUKVZNK7G_0.html

The Beta-Atla-Themis region (BAT) is the area enclosed by and including Beta, Atla, and Themis Regiones (Figure 1.5). Three major rift zones are included in this area - Hecate, Devana, and Parga Chasmata. Beta Regio is a highland region at the eastern end of Hecate Chasma. Beta has a maximum diameter of 2,989 km. The highland Themis Regio marks the southernmost reach of the region. The BAT region is believed to be a zone of large-scale mantle upwelling (Squyres et al., 1992); it exhibits high amounts of volcanic flows and structures and is believed to be one of the geologically youngest areas on the planet.

Hecate Chasma is a discontinuous fracture belt and volcano-tectonic rift system over 8000 km long between Atla and Beta Regiones. Studies based on Magellan data have shown Hecate Chasma to be morphologically similar to the East African Rift (Hamilton and Stofan, 1996b; Foster and Nimmo, 1996). There is also an anomalous concentration of coronae in and proximal to Hecate Chasma, indicating likely sustained mantle activity (Hamilton and Stofan, 1996b). Linear sets of graben in the study area may be a product of the stresses involved in the rifting process (Hamilton and Stofan, 1996b).

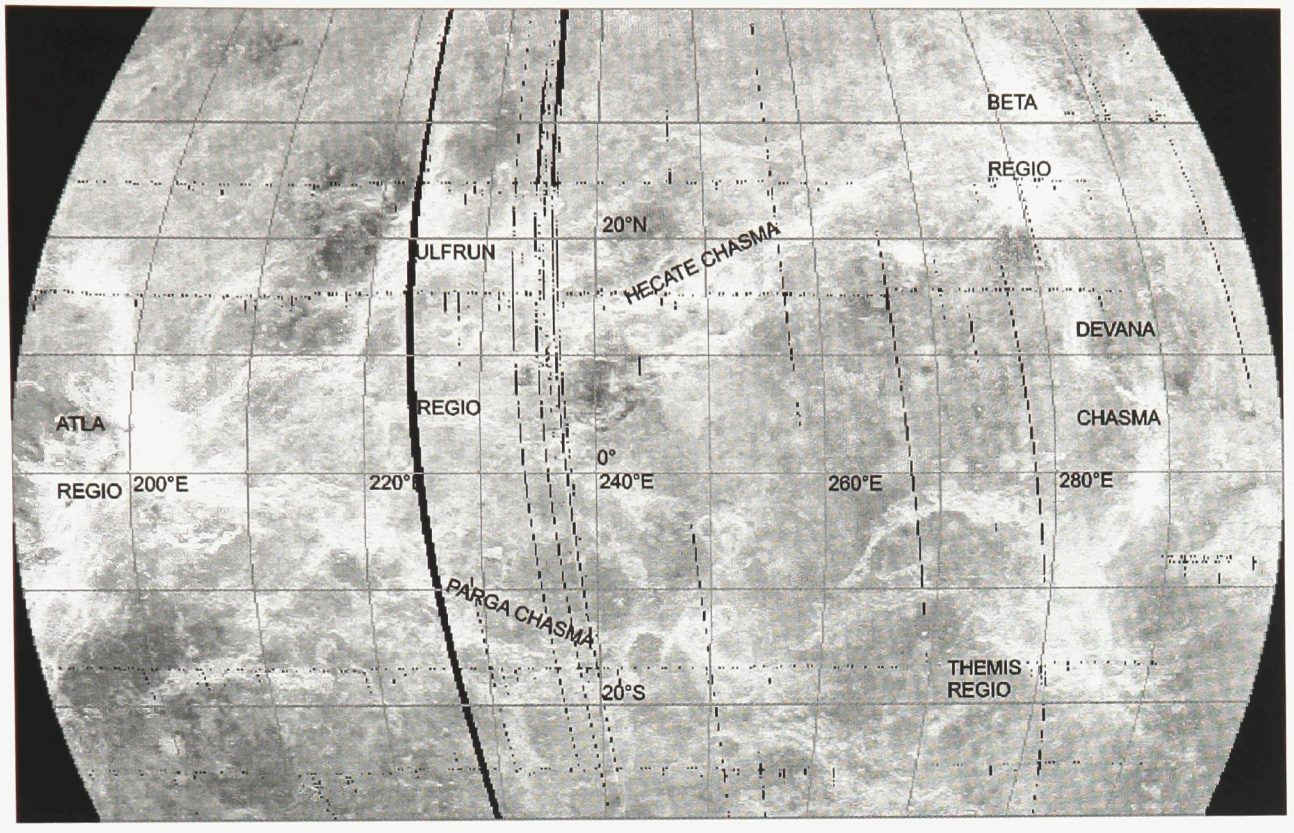

Figure 1.5. SAR radar image map of the Beta-Atla-Themis region.

1.5. Magellan Mission

The data used in this project were provided by the U.S. National Aeronautics and Space Administration (NASA) and collected by the Magellan spacecraft. Magellan was launched on May 4, 1989, arrived in the vicinity of Venus on August 10, 1990, and orbited Venus for four years, until it was commanded to enter the planet's atmosphere and crash on its surface on October 11, 1994, to obtain data on the atmosphere and the spacecraft's performance. At the end of its mission, Magellan had completed three 243-day mapping cycles, providing radar maps of 98% of the planet's surface[2].

Magellan was constructed on a tight budget, and many of its components were borrowed from other NASA projects: parts came from the Mariner, Voyager, Ulysses, Galileo, and Space Shuttle programs, as well as some other sources within NASA. Almost the only newly designed instrument was the Synthetic Aperture Radar (SAR) system, which had to be configured to work within the constraints imposed by the varied provenance of the components of the spacecraft. The radar used on Magellan transmitted microwaves with a wavelength of 12.6 cm, which are unaffected by the cloud cover, onto the planet's surface, using the delay and strength of the echoes to create an image of the surface. In SAR imaging, image resolution depends on the aperture of the instrument acquiring the image – that is the size of the receiving unit, such as a camera's lens or a radar system's antenna. As the antenna on Magellan was in motion while receiving the radar echoes from the surface, computers at NASA could

---

[2] http://www2.jpl.nasa.gov/magellan/

process the received information to simulate reception by an aperture much larger than the actual antenna. The size of this "synthetic" aperture was governed by the distance that Magellan travelled while a given point on the surface was within the antenna's field of view.

Magellan had three antennas: high- (HGA), medium- (MGA), and low-gain (LGA) units, as well as an altimeter antenna. The HGA was used for nearly all of Magellan's primary functions, including radar mapping and communication with Earth. The other two antennas were largely used to support the HGA and relay signals when the HGA could not be pointed directly at Earth. The altimeter provided one-dimensional readings of the height of the surface directly below the craft, which were used to calibrate the SAR data, as well as to adjust the orientation of the HGA during each mapping pass. Figure 1.6 shows the configuration of the Magellan components; Figure 1.7 shows a pre-launch image of Magellan.

During the mapping cycles, Magellan always followed the same data acquisition strategy (Figure 1.8). Starting at the North Pole of Venus, after leaving the window for communication with Earth, the HGA was pointed towards the surface to begin mapping. Due to constraints imposed by the orbit inclination, the HGA had to be slightly pointed to the left (with respect to the craft's motion) as it crossed the North Pole, so the first mapping cycle was completed with left-looking radar. For the second cycle, Magellan was rotated 180 degrees and the HGA pointed to the right. As the HGA was fixed to the Magellan and wasn't free to move itself, the whole craft had to be rotated in order to

point the antenna. For a multi-year mission, the amount of propellant required for all this movement would have far outweighed the amount available, so all rotation of the craft was carried out as to take maximum advantage of the basic laws of physics. Electric motors in Magellan spun small wheels (three of them, one for each axis) and in the absence of any external forces, the craft would turn in the opposite direction to the wheel. With the HGA pointed towards Venus, mapping would begin: the SAR system operated for 25-250 ms, then the altimeter sent signals through its antenna for 25 ms while the radar was switched off, then the HGA was turned back on to receive microwave energy naturally emitted from the surface for 50 ms, and the process would restart with the SAR mode once more (Figure 1.9). Once during every orbit, the HGA would be turned away from the planet to detect known stars in order to confirm that the Magellan was on the correct trajectory. At the end of each orbit, arriving at the North Pole, the HGA was pointed towards Earth to communicate data and receive orders. On Earth, the received data was recorded onto magnetic tapes, as electronic links were not advanced enough to handle the volume of data at the time. Three SAR mapping cycles were carried out, two looking left (at differing angles of incidence), and one looking right. Table 1.1 details some of the specifications of the Magellan SAR system.

The radar images produced by the Magellan were originally in the form of F-BIDRs (Full-resolution Basic Image Data Record), which include data from the 25 km by 16,000 km swathes produced by each orbit. After processing, the data were released in formats easier to exchange and analyze: F-MIDRs (Full-resolution Mosaicked Image Data

Records) and C-MIDRs (Compressed Mosaicked Image Data Records). The F-MIDRs were converted to FMAPs (Full-resolution radar Maps) as well. The radar images have a resolution of approximately 120 m, and the uncompressed images (F-MIDRS and F-MAPS) each pixel represents a 75 m by 75 m square of Venus' surface. The altimetry data for each cycle had a footprint of 10 km (i.e. there was one reading for every 10 km of surface travelled over on each mapping orbit) and a vertical resolution of 30 m.

For this work, we are using images at the full F-MIDR resolution (75 m/px). With modern internet technology, we have been freed from the constraints of the original data packaging system for the Magellan. Images can now be acquired which are customized to requested parameters (resolution, extent, projection) directly from the USGS Astrogeology Planetary Data System[3]. Specifically, we acquired our SAR data as 13 horizontal swaths in a sinusoidal projection centred on 220°E and stitched them together using image software before loading them into the ArcGIS 9.3 mapping software package[4].

---

[3] http://www.mapaplanet.org

[4] http://www.esri.com/software/arcgis/index.html

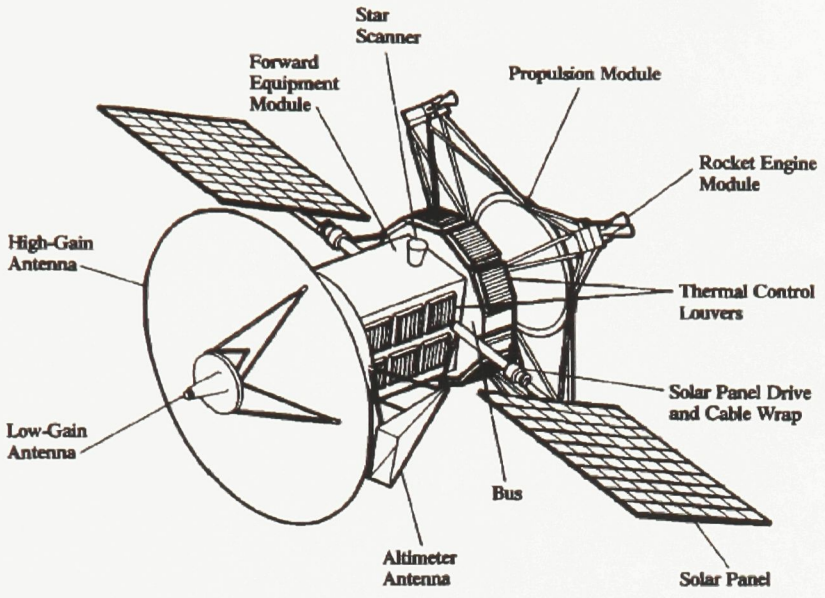

Figure 1.6. The Magellan spacecraft in mapping configuration. From Saunders et al, 1990.

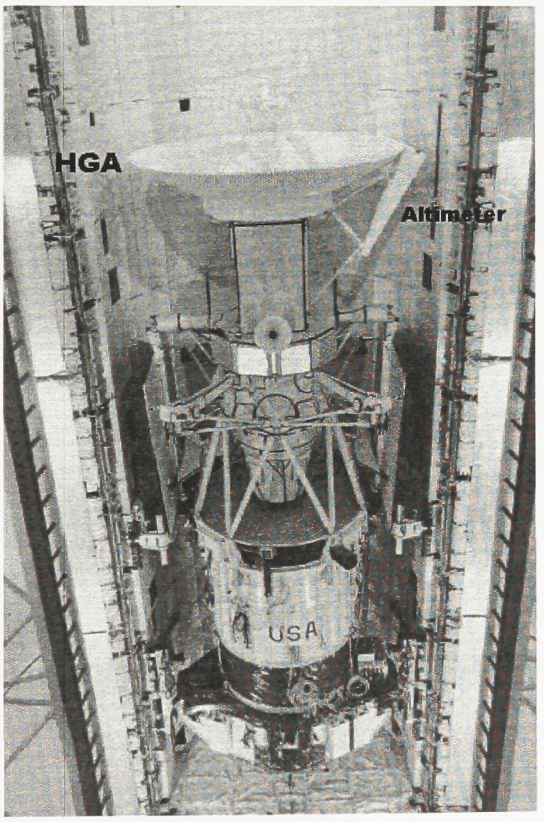

Figure 1.7. Magellan loaded into the cargo bay of the space shuttle Atlantis prior to launch. The HGA is mounted at the top, with the altimeter on its right. The lower half of the structure is the booster which was discarded after propelling Magellan towards Venus. From The Magellan Venus Explorer's Guide, 1990.

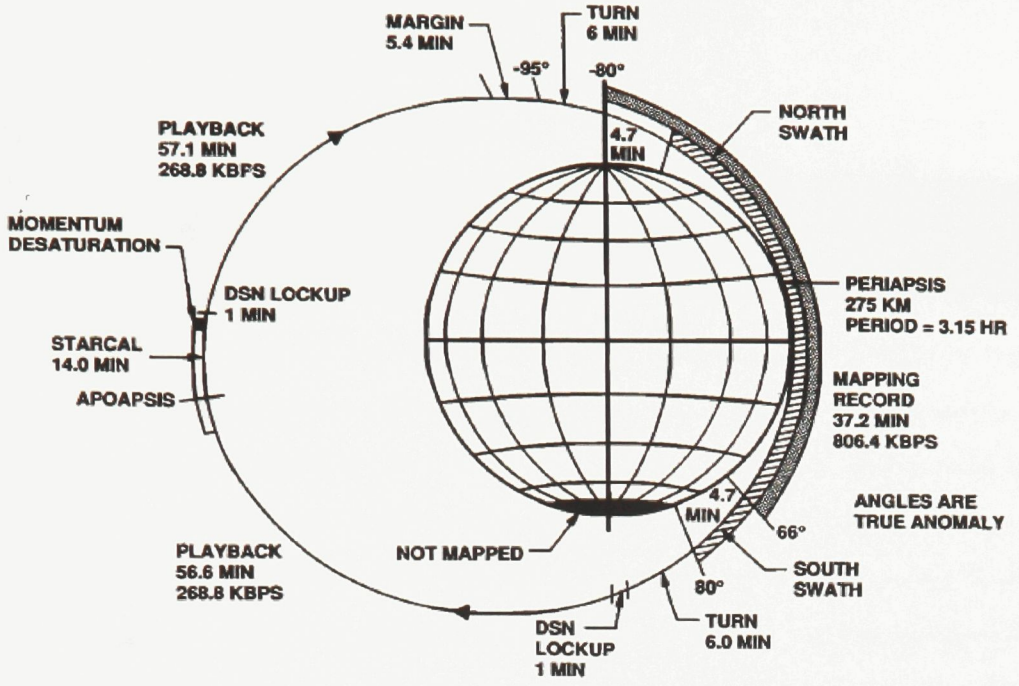

Figure 1.8. Mapping orbit of the Magellan spacecraft, including procedures for data playback and transmission to NASA's ground base. From Saunders et al., 1990.

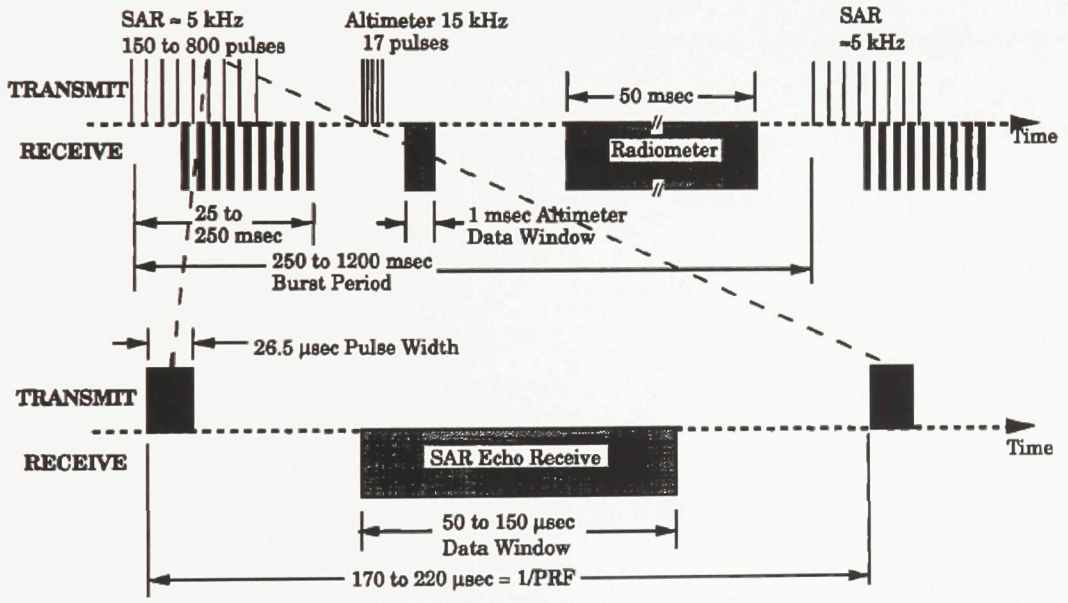

Figure 1.9. The instrument operation pattern for the Magellan probe during mapping passes. From Saunders et al., 1990.

Table 1.1. Specifications of the Magellan SAR system.

Parameter	Value
Nominal operating altitudes	*275-2100 km*
Incidence Angle	*18°-50°*
Radar Frequency	*2.385 GHz*
Radar Wavelength	*12.6 cm*
Transmitter Peak Power	*350 W*
Range Resolution	*120-360 m*
Azimuth Resolution	*120-150 m*
Swath Width	*25 km*
Orbit Period	*3.25 hours*
Orbit Inclination	*86°*
Planetary Radar Mapping Coverage	*98%*

1.6. Synthetic Aperture Radar (SAR)

While the images produced by SAR appear quite similar to aerial photographs, they operate on entirely different principles. In a SAR image, each pixel is representative of the amount of wave energy reflected back to the antenna from the sampled area. Radar images are therefore more of a measure of the roughness of the scattering surface than of its physical appearance. Typically, smooth surfaces appear dark and rough surfaces appear bright in SAR images, although this is dependent on the surface's geometry relative to SAR incidence angle (Oliver and Quegan, 2004).

In a SAR image, each pixel represents the calculated sum of all echoes returned from the geographical position that it represents. Pixels are generally compiled from several "looks" – data returned from several separate pulses while the ground is within the radar's footprint (Oliver and Quegan, 2004). In each Magellan SAR burst, there were 150 – 800 separate pulses; each point saw at least 4 looks (Saunders et al., 1990).

The side-looking nature of synthetic aperture radar leads to geometric distortions which can affect interpretation. This is compounded (beyond the case of optical perspective) by the nature of radar, in that it is dependent on echo time to map sources (Oliver and Quegan, 2004). For example, foreshortening is an apparent reduction in the width of topographic slopes which face towards the instrument. This produces features such as mountain peaks and ridges appearing displaced from their actual position. This is a result of the side-looking geometry of an SAR instrument: due to the difference in incidence angle and the difference in altitude of two features (the

peak of a mountain and the base of that same mountain), the difference in echo time for the radar waves is not the same as it would be if the two features were at the same altitude. The shorter-than-expected echo time from the peak of the mountain results in it being displaced towards the radar instrument when the data are processed and the final image is produced (Woodhouse, 2006). This type of distortion is increased by low incidence angles – which are typical of airborne SAR instruments. Satellite SAR tends to have higher incidence angles and hence less foreshortening (Woodhouse, 2006). Magellan SAR had an incidence angle which varied from 18° at the poles to 50° at the equator, with 70% of the surface mapped at above 30° to minimize the effects of foreshortening (Saunders et al, 1990).

Radar shadows are areas of an image from which no echo response was received by the instrument. These typically are found on the far side (relative to the radar) of steep topographical slopes. Where the local topographic slope relative to the radar's direction is greater than the angle of incidence, no radar signal will actually reach the surface, being reflected by the topographic high "in front" of it. The result in the image is an area of black (Woodhouse, 2006).

1.7. Previous Work

The geologic mapping of Venus is overseen by the United States Geological Survey (USGS). The planet has been divided into 62 "quadrangles" for high-resolution mapping, of which 22 maps have been published, 8 are yet unassigned, and the

remaining 32 are in progress. These maps are produced at 1:5M scale. Ivanov (2008) has recently completed a new [as yet unpublished] global geologic map, which we have been given a copy of and are using as our geologic base for this project. Our study area coincides with two quadrangles (V-26 and V-27), neither of which are assigned for mapping at this time.[5]

Other studies have been carried out in our study area and its vicinity. Hamilton and Stofan (1996b) looked at the morphology and evolution of Hecate Chasma. Aittola and Raitala (2005) studied the relationship between certain novae and coronae in the Hecate Chasma region. Ernst and Desnoyers (2004), Ernst et al (2003), and Grosfils et al (in review) have completed similar studies to our own in adjacent areas on Venus, while Blair and Ernst (2002), Harris et al (2002), and Harris and Ernst (2001) have worked in other areas on Venus on graben-fissure systems.

Grosfils and Head (1994) made a global study of radiating graben-fissure systems. Novae and arachnoids have also been catalogued by Crumpler and Aubele (2000). Krassilnikov and Head (2003) made a study of all identified novae on Venus, classifying them and theorizing on styles of evolution. Aittola and Kostama (2000, 2002) and Basilevsky et al (2009) each studied selected novae in differing areas of Venus.

---

[5] http://astrogeology.usgs.gov/Projects/PlanetaryMapping/MapStatus/VenusStatus/Status_Venus.html

2.0. Mapping Overview

Magellan F-MIDR (75 m/pixel) images and altimetry data from Ulfrun Regio, along with the global geological map from M. Ivanov (2008) were loaded into ArcGIS 9.3. Dividing the study area into five degree by five degree blocks (1 degree latitude is 105.625 km at the equator), visible graben and fissures were systematically mapped throughout the study area. Negative topographical features in SAR images have a characteristic signature – radar-dark on the downward sloping side closest to the radar instrument, and radar-bright on the far side. Graben and fissures were identified as being linear features with this radar signature. Wrinkle ridges, as a positive topographical feature, can be differentiated as their radar-dark and radar-bright sides are reversed. Centres of radiating graben-fissure systems were identified and were associated with graben related to them. This was largely accomplished by looking at the orientation of individual graben and fissures – those that "pointed" in towards a centre were likely to be related to that centre. The longer and better-defined graben were used to help in the assessment of smaller and shorter features, as well as those that were far from centres. It was assumed that graben with similar morphologies and parallel trends to prominent neighbours were related to the same radiating system. Where the graben and fissures were particularly dense, it was difficult to distinguish singular features and, as a consequence, the number of features mapped in those areas

is underestimated. The mapped centres and their defining features are detailed in Appendix 1.

The Magellan altimetry and nomenclature (officially named features[6]) of the study area are shown in Figure 2.1. The altimetry is extruded to three dimensions and overlain with Magellan SAR images to produce Figure 2.2. Figure 2.3 shows the Magellan SAR data for the study area, along with the locations of each of the 66 identified centres. Figure 2.4 displays all mapped graben and fissures in the study area, and Figure 2.5 shows only the graben and fissures attributed to radiating centres.

Within the study area over 47,000 individual graben and fissures and 66 radiating graben-fissure systems have been identified, ranging in radius from 10 km up to nearly 2000 km. Figure 2.6 displays the size distribution of these radiating systems. It should be noted that the great increase in identified systems over previous work includes higher amounts of systems of all sizes. Grosfils and Head (1994) identified 10 radiating systems with radii of 150-400 km. Figure 2.7 details the number of graben identified in each radiating system, comparing it to the overall extent of the system. A total of over 13,000 graben were attributed to the 66 radiating systems. The unassigned graben may belong to additional unidentified radiating systems, linear systems, or circumferential systems (Ernst et al., 2003). A positive correlation is observed between the number of graben and the size of the system.

---

[6] http://planetarynames.wr.usgs.gov/jsp/SystemSearch2.jsp?System=Venus

Figures 2.8 and 2.9 look at radiating systems where a central topographical uplift – termed dome following Grosfils and Head (1994) – is observed. These features are believed to be associated to uplift caused by rising mantle diapirs (Parfitt and Head, 1993), which are one of the driving forces behind the formation of radiating graben-fissure systems. While Grosfils and Head (1994) inferred that systems that extend beyond the edge of the central dome were not caused by the same process, a positive correlation between dome size (radius and height) and the size of the radiating graben-fissure systems suggests that mantle diapirs may still have an effect on how large the radiating system becomes.

The map produced in this effort can be found in Appendix 2.

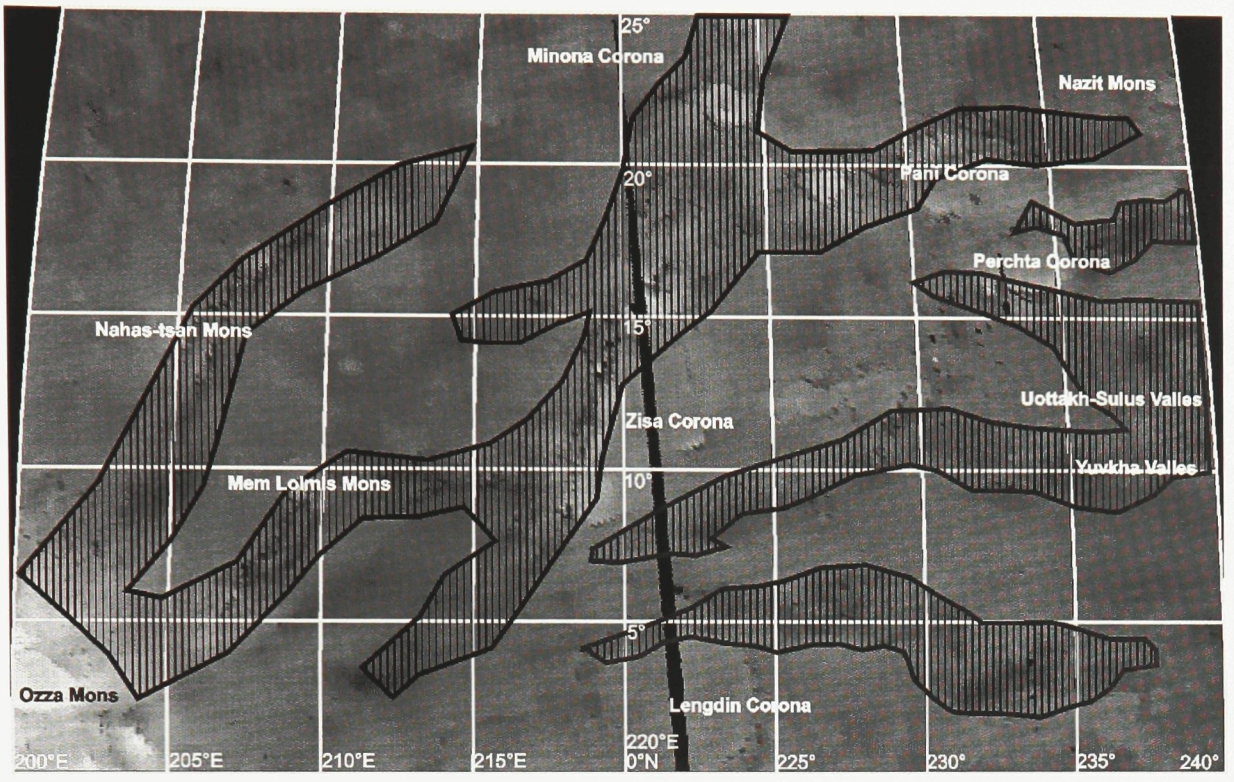

Figure 2.1. Magellan radar topography of the study area. Topography is a 256-colour greyscale image, ranging from 2.9 km below the planetary mean radius to 10.8 km above. Named magmatic features are labelled. The striped overlays indicate areas considered part of the Hecate Chasma rift system (Hamilton and Stofan, 1996).

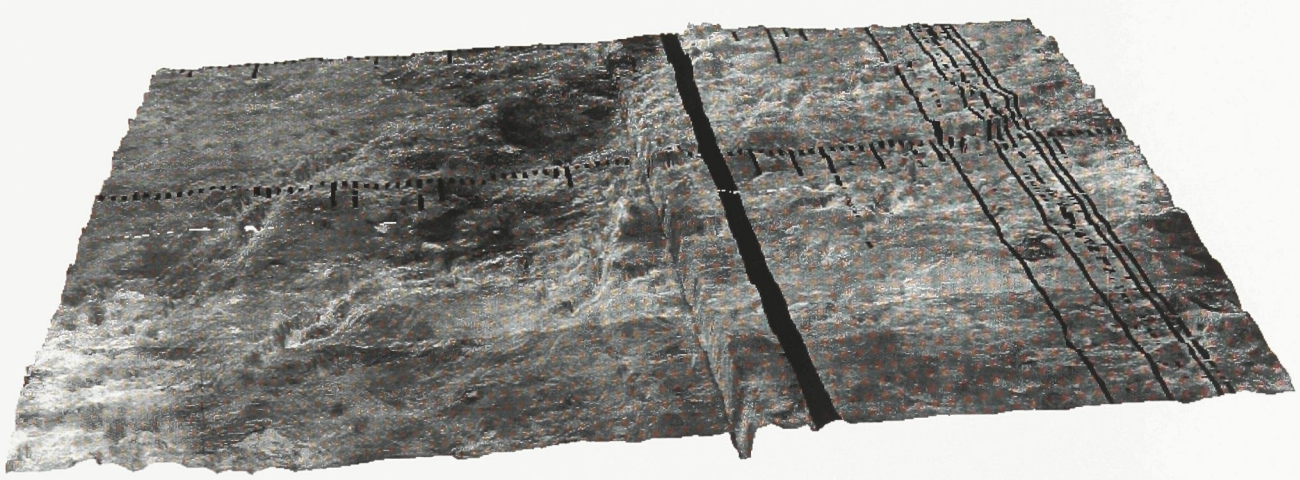

Figure 2.2. The study area extruded to three dimensions. The Magellan topography has been converted to a digital elevation model and the SAR data have been overlain. The wide swath of missing SAR data (the thick black stripe running from north to south) is echoed and offset (as the altimeter antenna pointed in a slightly different direction than the main antenna on Magellan) in the topographic data. The missing data are represented by a black bar in the topographic image, which is automatically assigned the lowest possible elevation in the three dimensional model. This produces the large trench seen in the model.

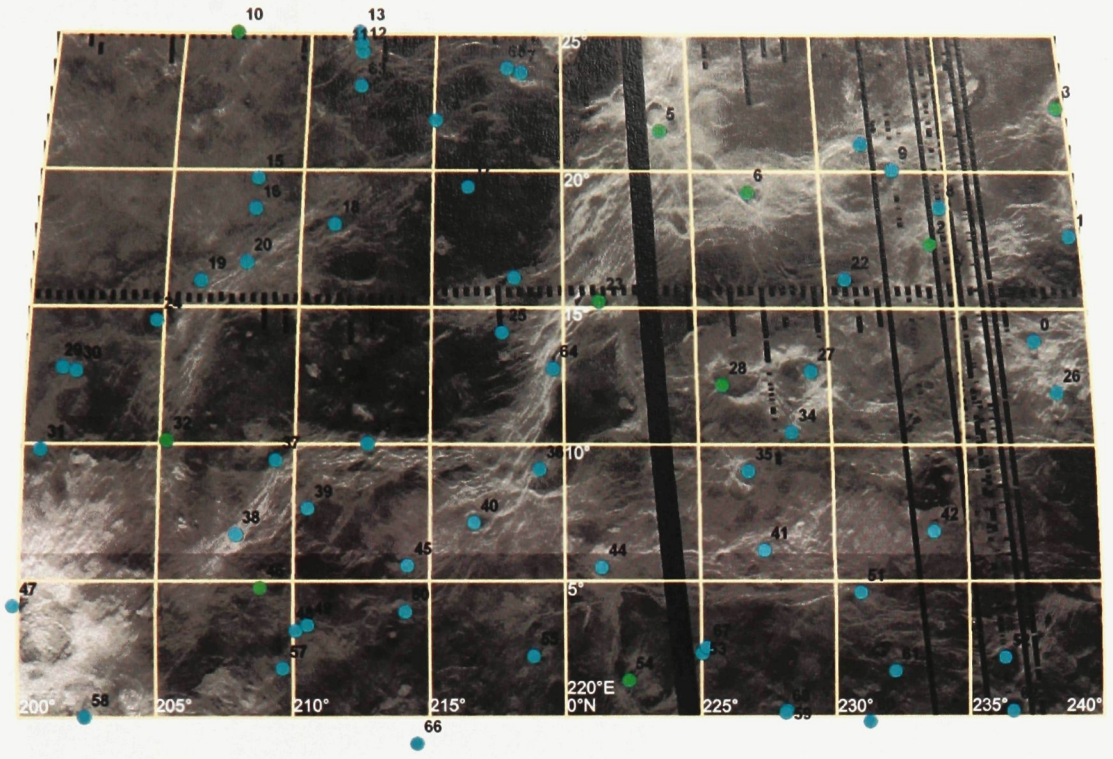

Figure 2.3. Magellan SAR image of the study area. Centres of radiating graben fissure systems are identified by blue dots, centres previously identified by Grosfils (1996) are green dots.

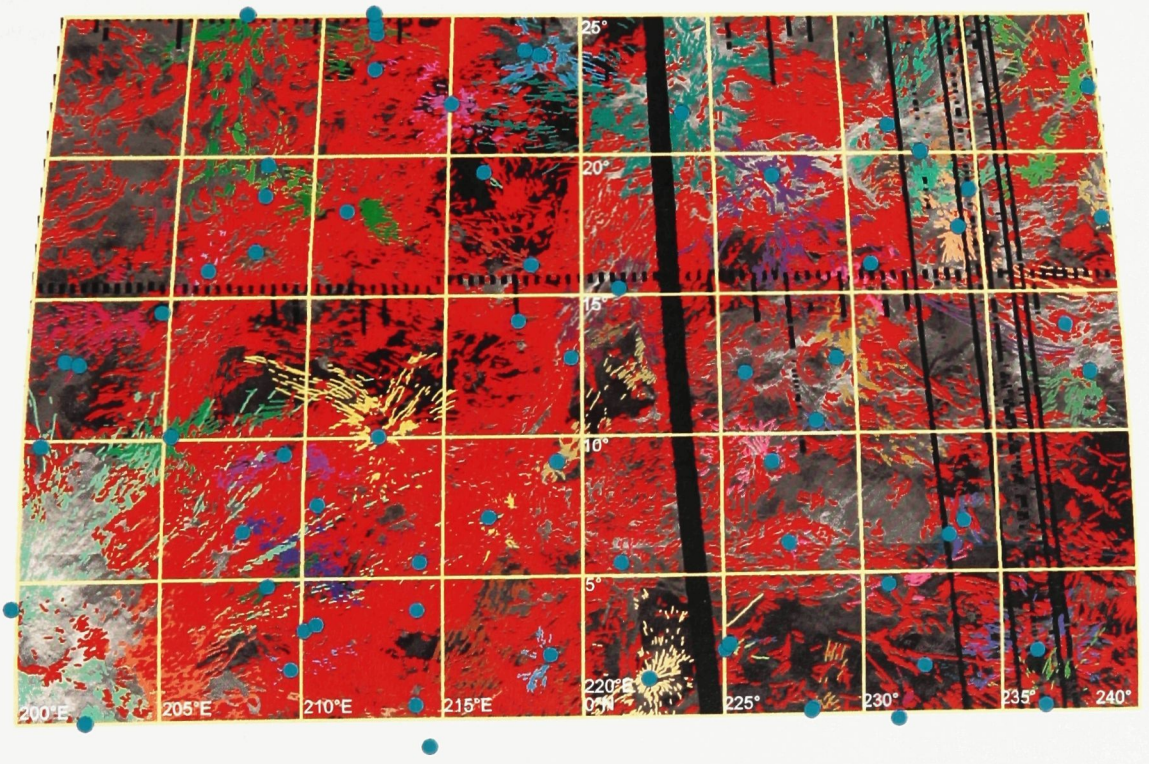

Figure 2.4. Mapped graben and fissures within the Ulfrun Regio study area. Red lines are features unassigned to radiating systems. Graben and fissures assigned to radiating systems are shown by lines of other colours. Unassigned graben may belong to linear, circumferential, or unidentified radiating systems.

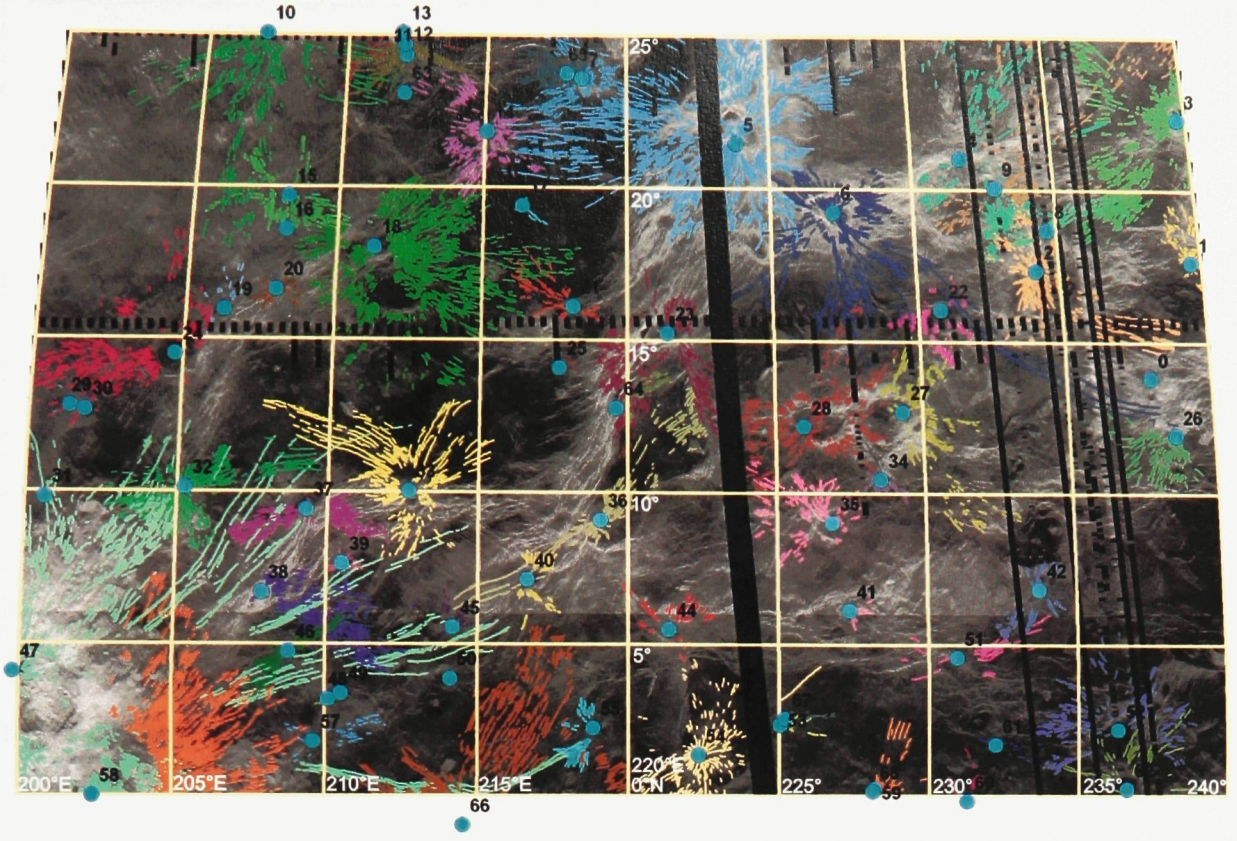

Figure 2.5. Radiating graben-fissure systems, distinguished from each other by colour, are overlain on Magellan SAR image. Centres are denoted by labelled blue dots.

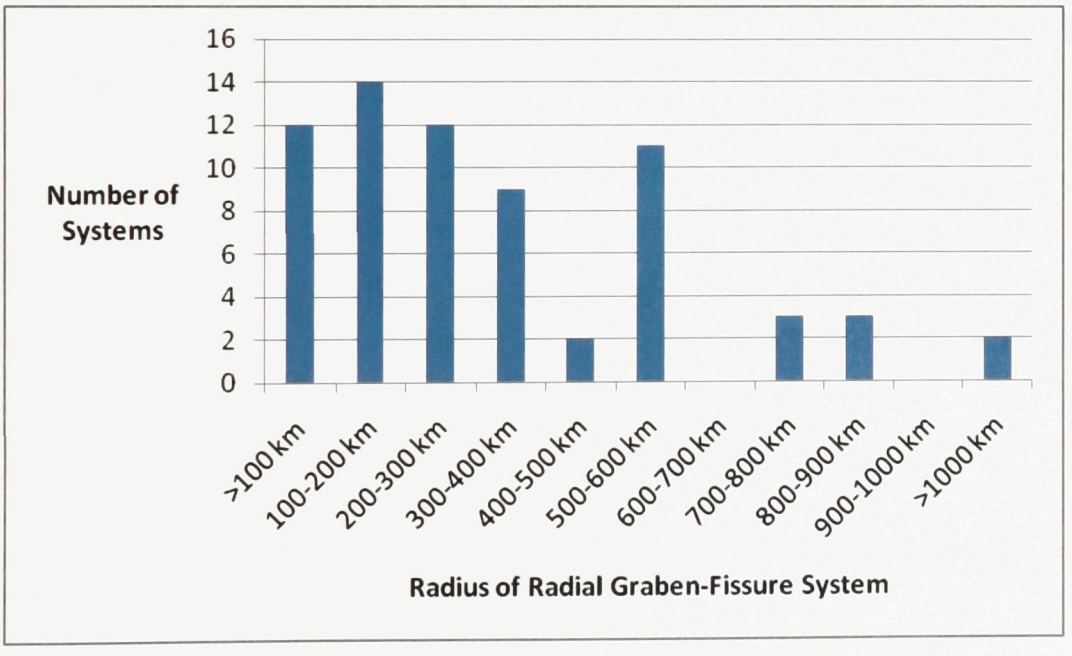

Figure 2.6. Size distributions of identified radiating graben-fissure systems.

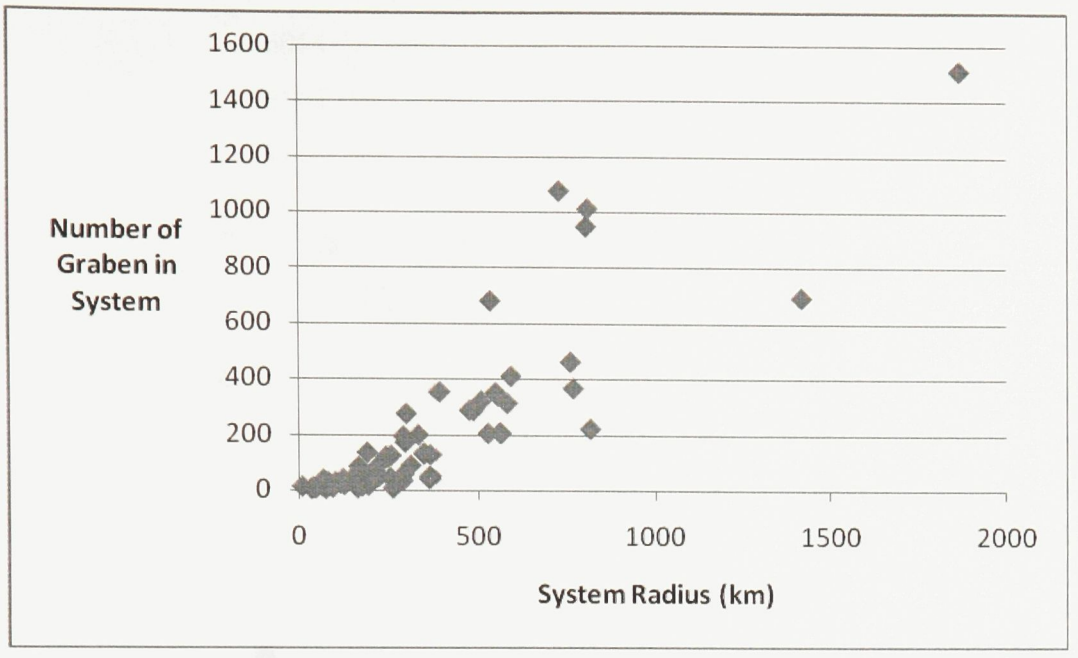

Figure 2.7. Populations of mapped graben within radiating systems.

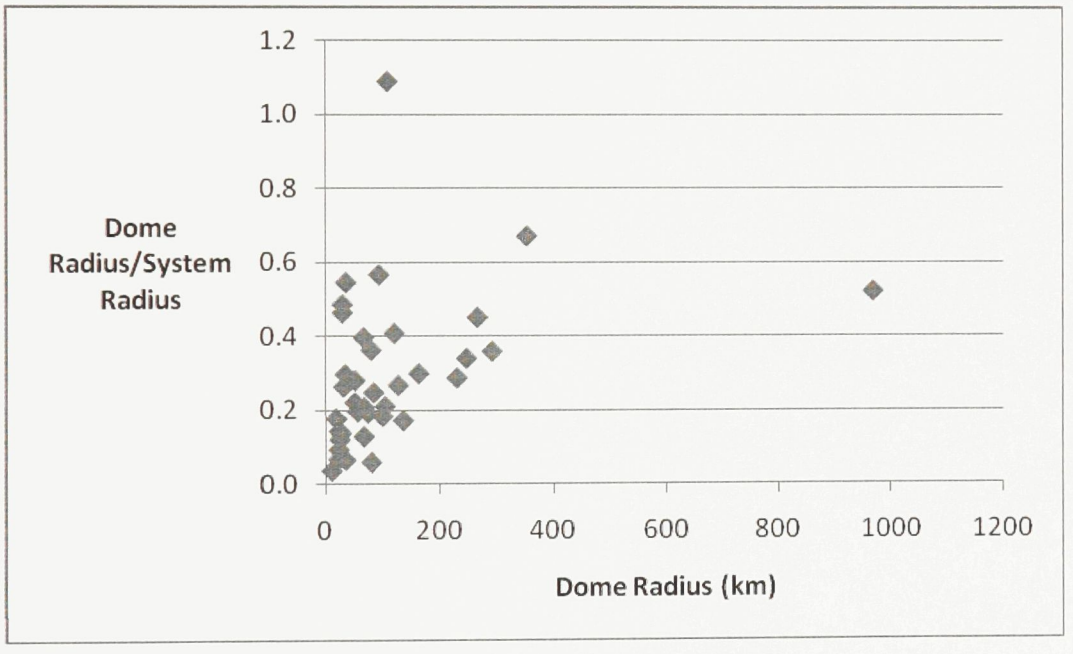

Figure 2.8. Plot relating the radii of the radiating graben-fissure systems to the radii of their related central topographical uplifts, where observed.

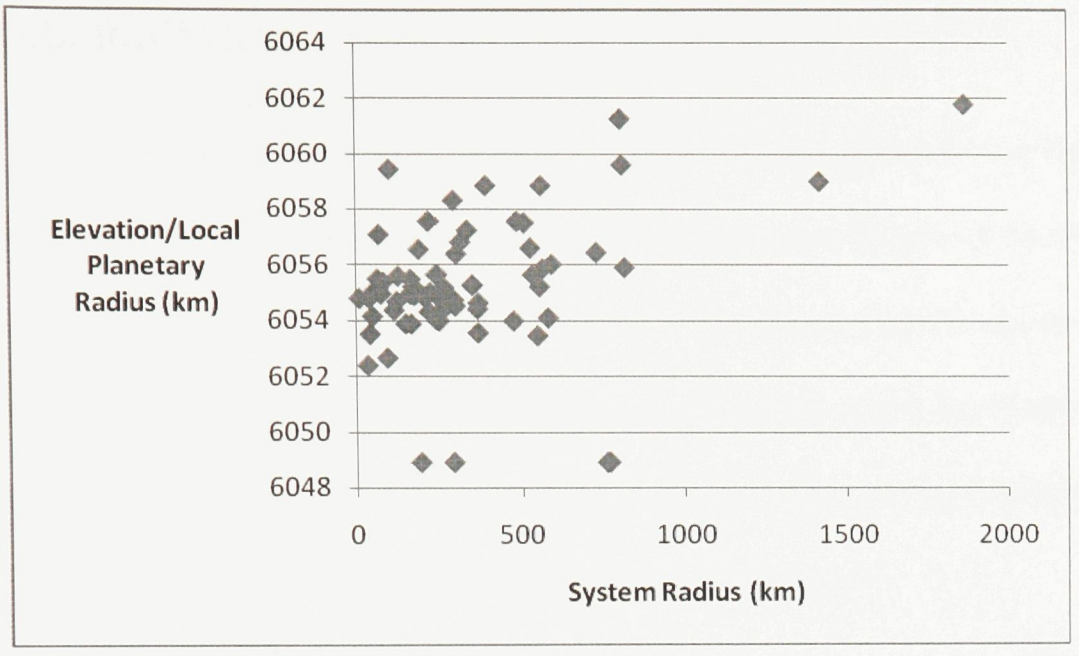

Figure 2.9. Plot relating the radius of radiating systems to the elevations of related central topographical uplift, where observed.

3.0. Radiating Graben-Fissure Systems

Within the study area, 66 radiating graben-fissure systems have been identified, mapped, and analyzed. Herein, detailed descriptions and analysis of 22 of these centres are presented. The focus of these analyses is the nature of cross-cutting relationships between individual systems. These data are aggregated and examined in Section 3 of this thesis. A summary of properties of all these centres can be found in Appendix 1. The centres were numbered in the order they were mapped.

Two examples are provided of the manner of cross-cutting relationships used and how they are interpreted in this study.

Interaction between graben in system 3 – which is centred at Nazit Mons – and lobate lava flows emanating from Pani Corona (Figures 3.1 and 3.2). The interaction takes place 350 km northwest of the centre of system 3 and 450-500 km northwest of the centres of systems 4 and 9, on the rim of Pani Corona. Graben in system 3 can be seen cutting lobate lava flows that emanated from Pani Corona. This is interpreted as meaning that the lava flows were emplaced first, before the graben were created and crossed the lava flows. Graben associated with systems 4 and 9 are mostly obscured by the same lava flows. From this, it is inferred that activity at Nazit Mons – system 3 – occurred more recently than at Pani Corona – systems 4 and 9. It follows that system 3 is younger than systems 4 and 9.

Four radiating systems (23, 36, 40, and 64) interact in and near Zisa Corona (12°N, 221°E) and are displayed in Figures 3.3-3.6. Cross-cutting relationships between

these systems are herein presented as an example of such relationships discussed throughout this section.

Systems 23 and 36 interact along the eastern margin of the corona (Figure 3.4). System 23 (15°N, 221.5°E) is centred near the northern end of Zisa Corona, and system 36 (9°N, 219°E) is centred near the south end of the structure. Southeast-trending graben in system 23 very clearly cut northeast-trending graben in system 36. This is corroborated by the lava flooding that fills and obscures some graben in system 36, but is itself cut by the graben in system 23. From this, system 23 is inferred to be younger than system 36.

System 23 and 64 (13°N, 219.5°E) meet within Zisa Corona (Figure 3.5). Within the region of intersection, it is clear that the trend of system 23 is cut by system 64. Individual graben in system 64 also overprint graben in system 23. System 64 is likely younger than system 23.

System 40 is centred south of Zisa Corona at (7.5°N, 217°E). Graben from system 36 cross the centre of system 40 cutting both graben in system 40 and the lava field at the centre (Figure 3.6). It is likely that system 36 is therefore younger than system 40.

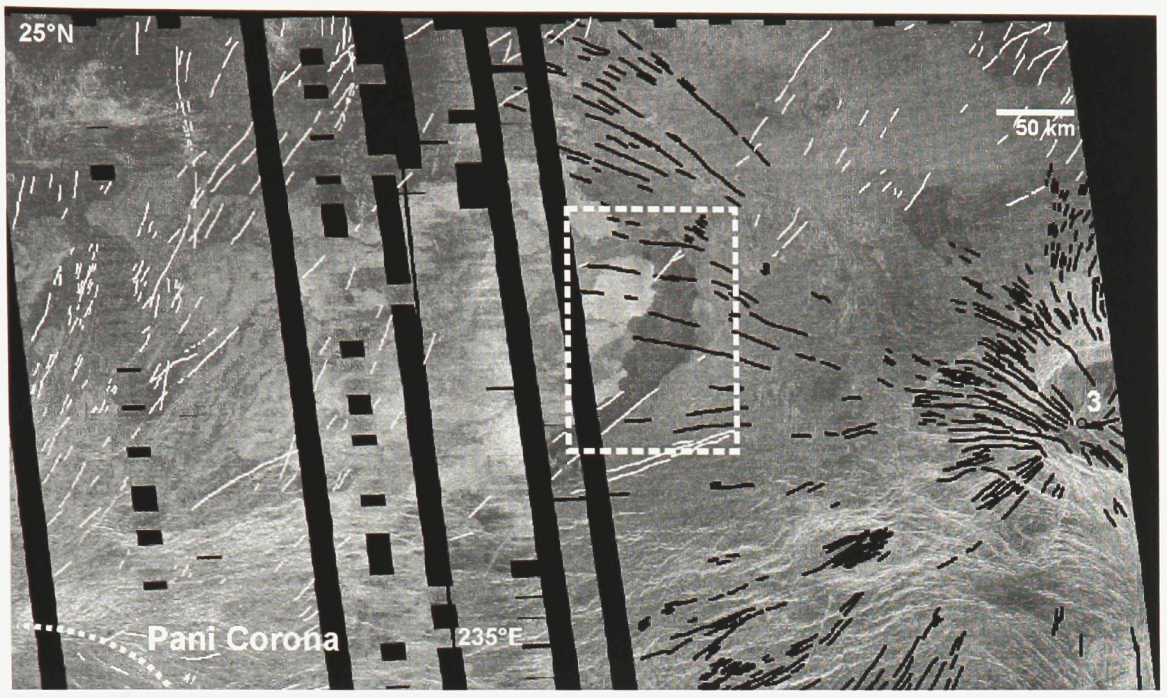

Figure 3.1. Cross-cutting relationship between the radiating system associated with Nazit Mons and volcanism associated with Pani Corona. Black lines show graben in system 3, white lines show graben in other systems. Dashed box shows the location of Figure 3.2.

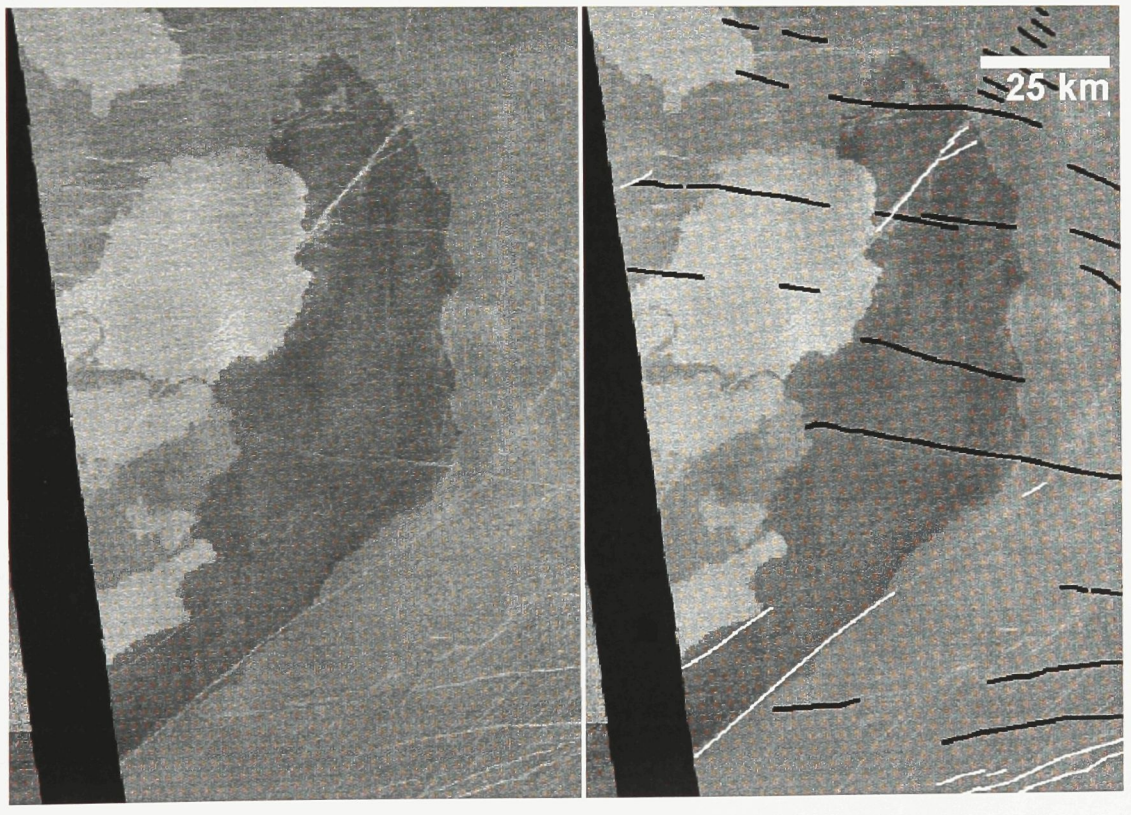

Figure 3.2. Cross-cutting relationship between graben of system 3 and lobate flows associated with systems 4 and 9. Images are identical, with mapped graben shown on the right as per Figure 3.1. The radar-bright flow obscures the radar trace of the graben, but they are visible cutting the darker flows.

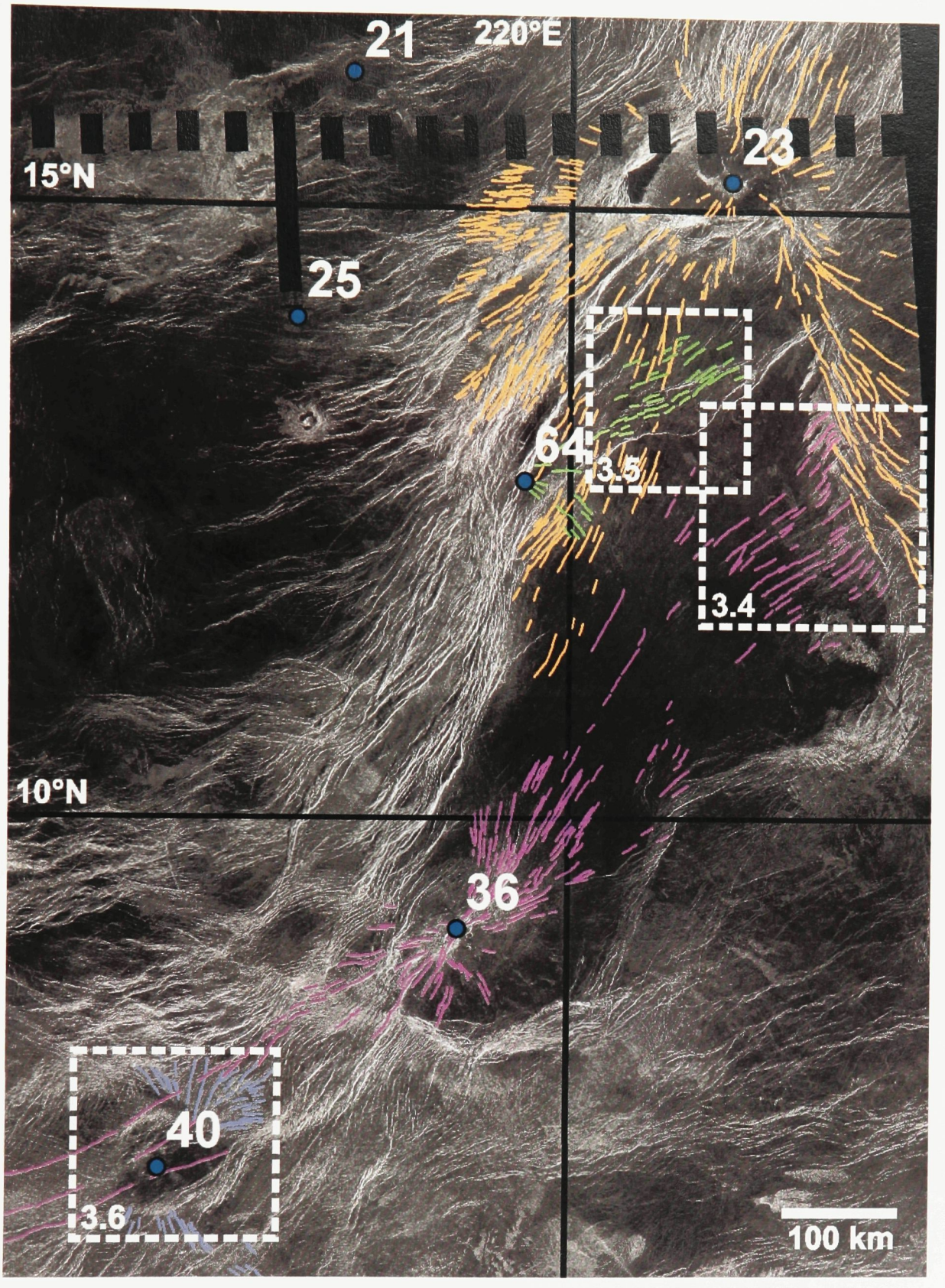

Figure 3.3. Graben from systems 23, 36, 40, and 64, centred in and near Zisa Corona, interact. Dashed boxes indicate the location of Figures 3.4, 3.5, and 3.6.

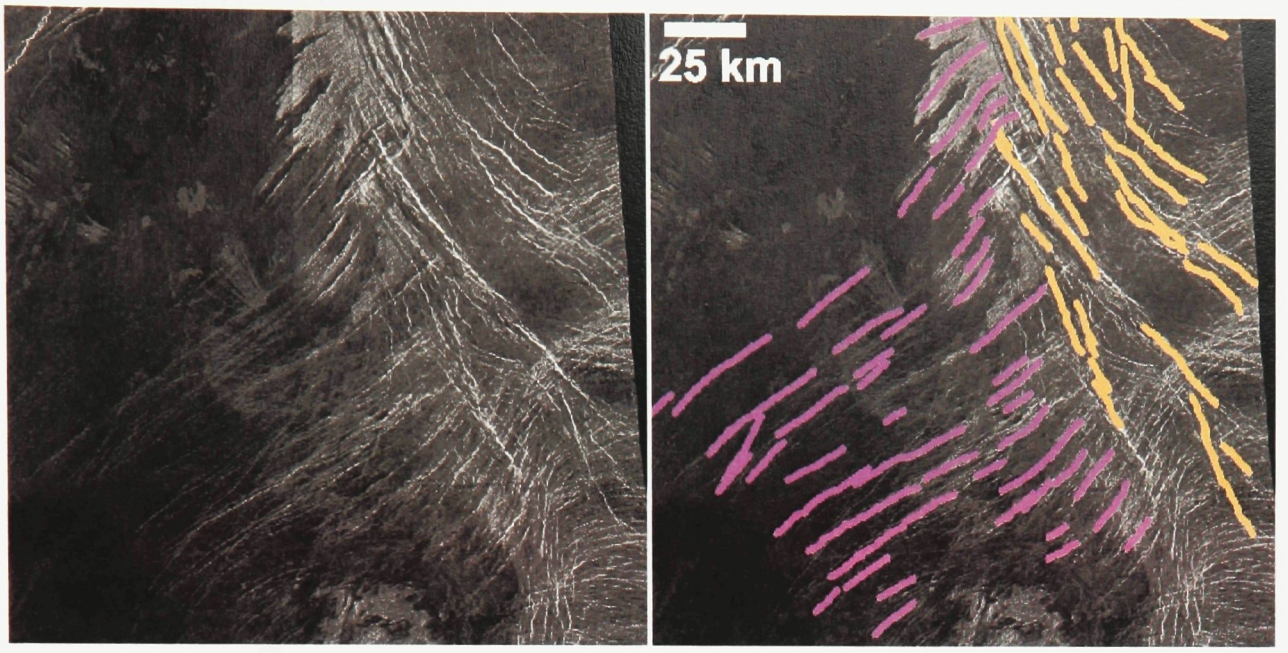

Figure 3.4. Close-up of cross-cutting relationship between systems 36 and 23; image repeated on the right with mapping overlaid. System 23 is represented by orange lines, 36 by purple.

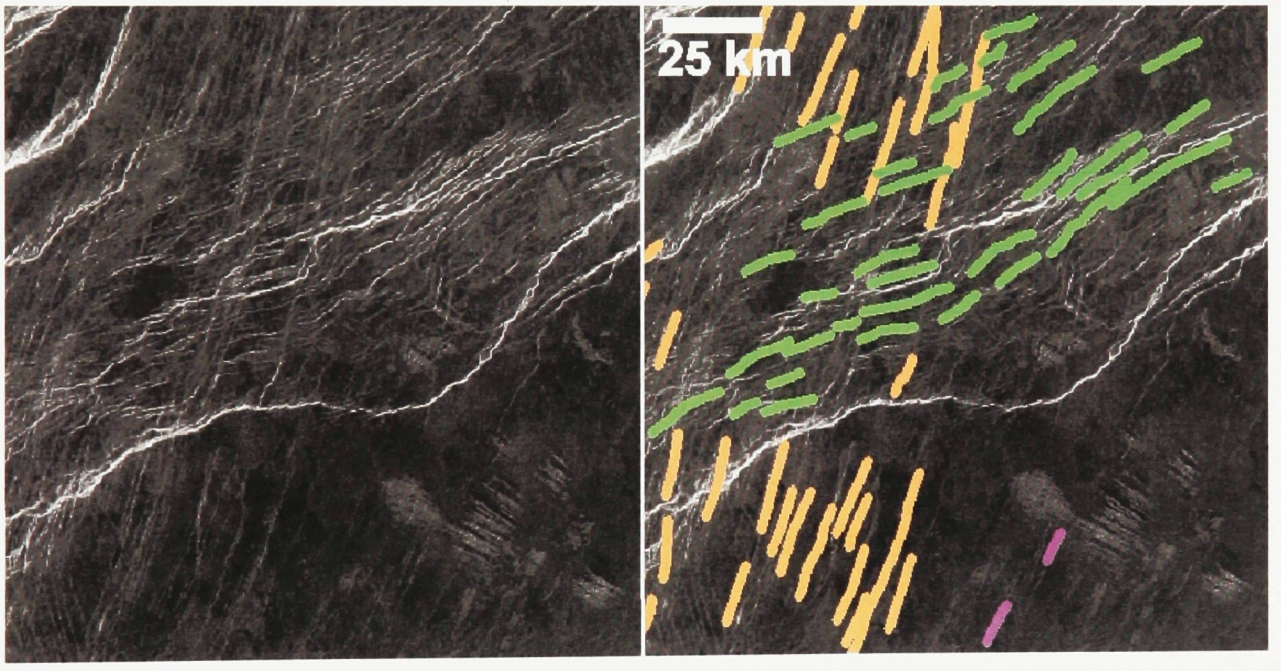

Figure 3.5. Close-up of cross-cutting relationship between systems 23 and 64; image repeated on the right with mapping overlaid. System 23 is represented by orange lines, 64 by green.

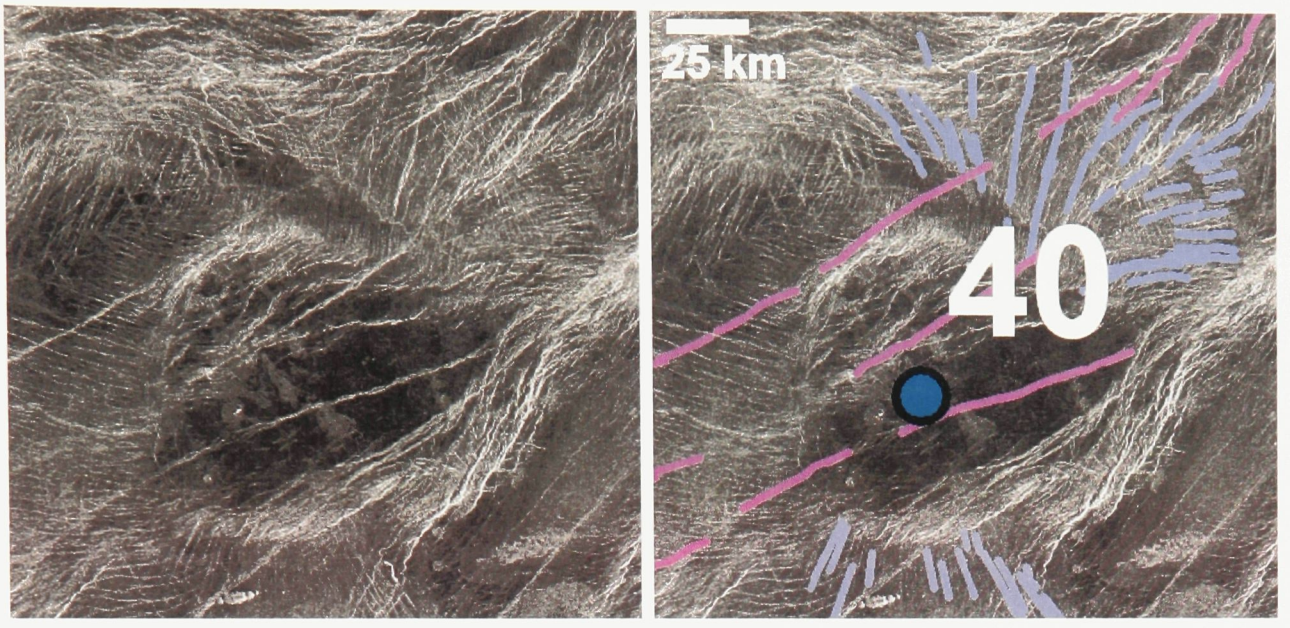

Figure 3.6. Close-up of cross-cutting relationship between systems 36 and 40, with mapping overlaid on the right. Graben from system 36 (purple) can be seen cutting across lava flows which cover the centre of system 40 (blue).

3.1. System 2: Perchta Corona (17°N, 234.5°E)

This is a very well defined radiating system with an easily identified centre (Figures 3.7, 3.8, and 3.9). The centre is within Perchta Corona, which has a poorly defined corona rim and sits along an arm of the Hecate Chasma rift zone, which has an E-W orientation at this location. The system is centred on the corona's central plateau, which has a maximum radius of 165 km and a central elevation of 6055.2 km, 3.4 km above the planetary mean. Perchta Corona is officially listed as having a diameter of 500 km[7]. The graben of this system have a maximum radius of 555 km, with 339 individual features mapped, extending out in all directions.

While the corona rim is poorly-defined, there is a significant trench surrounding the corona plateau. The plateau slopes upwards towards the southern rim, where the trench is deepest. To the south and east, the corona rim does appear to cut the graben in the radiating system, which would indicate that corona formation at least partially post-dates the formation of the radiating system.

To the north of the centre, graben of system 2 intersect with graben of system 8. The latter graben appear to be cut by and less well defined than those of system 2. I believe this to indicate that centre 2 was more recently active.

Further north, system 8 intersects system 4 (which is associated with Pani Corona). It is clear in that region that the graben of system 8 are continuous and cut

---

[7] http://planetarynames.wr.usgs.gov/jsp/SystemSearch2.jsp?System=Venus

across those of system 4. It is probable that centre 8 is thus younger than system 4. A likely corollary of this relationship is that Pani Corona is older than Perchta Corona.

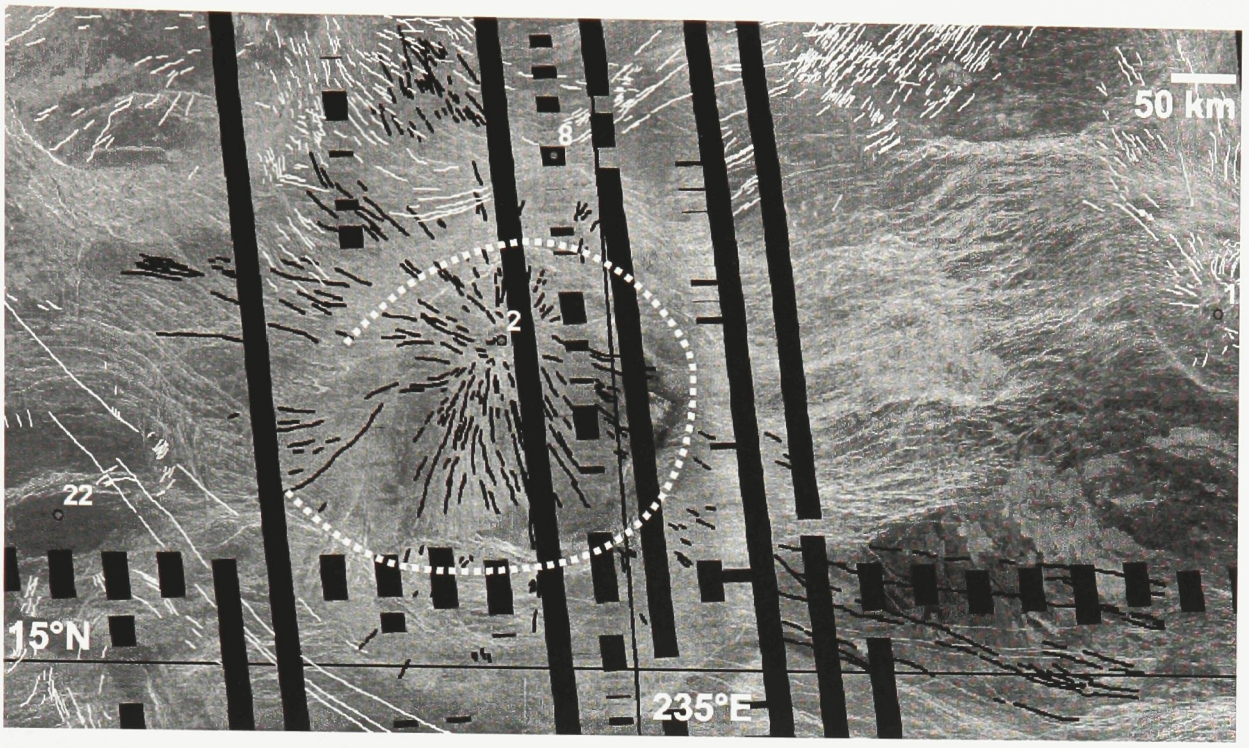

Figure 3.7. Mapping of radiating system 2 overlain on SAR image. System 2 is mapped with thick black lines, and other systems with thin white lines. The rim of Perchta Corona is indicated by the dashed white line.

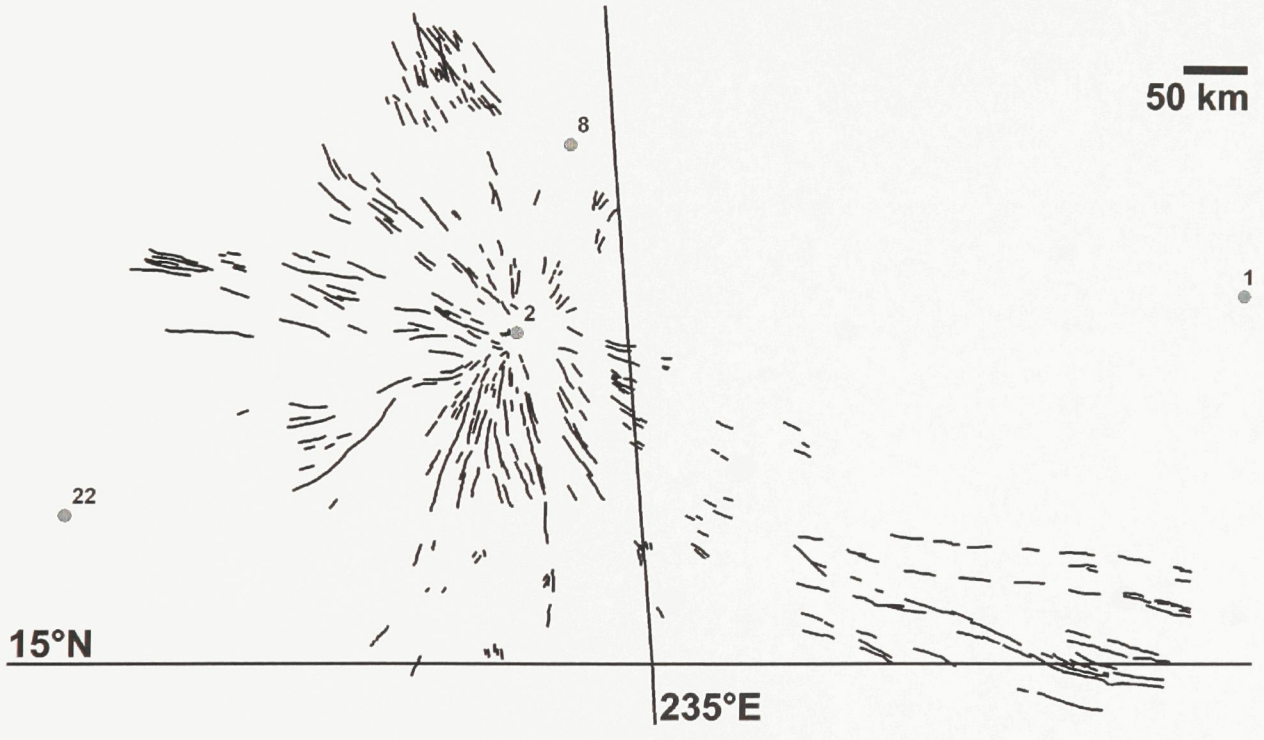

Figure 3.8. Mapped graben related to system 2.

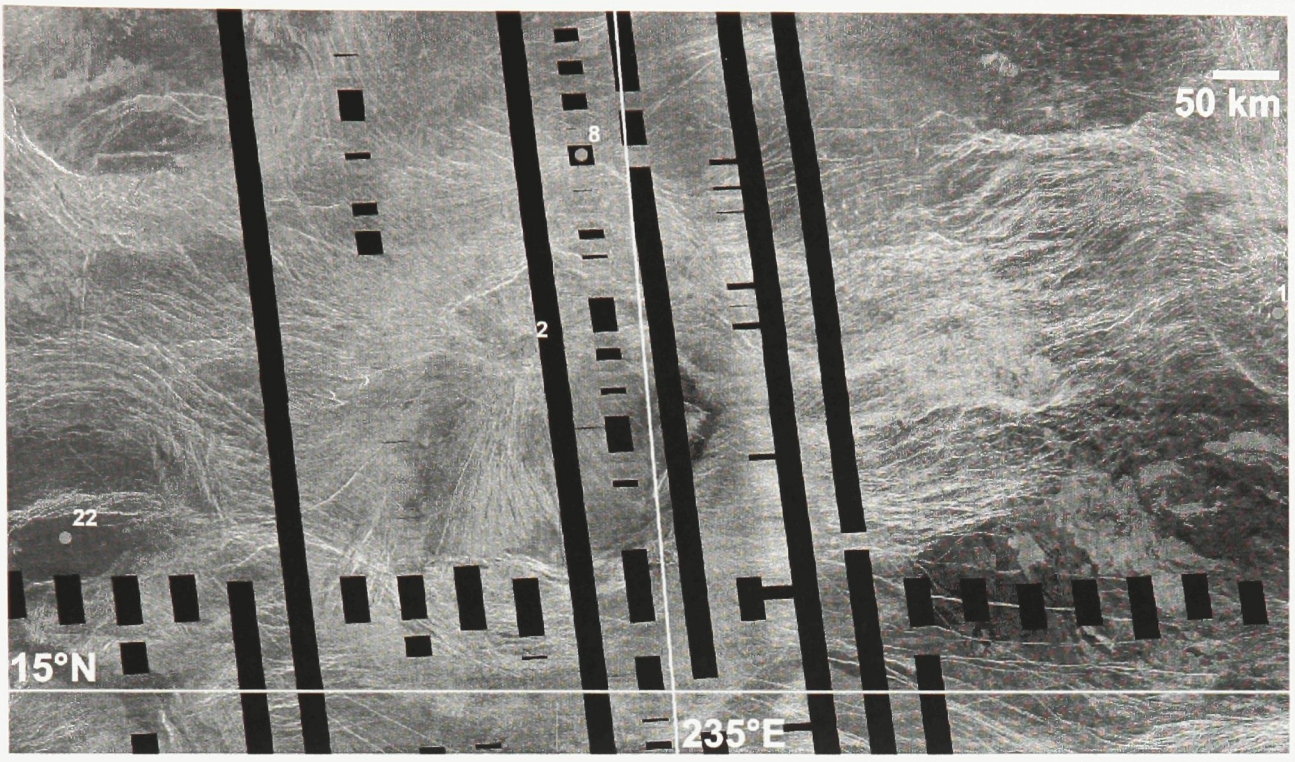

Figure 3.9. Magellan SAR image of system 2.

3.2. System 3: Nazit Mons (22.5°N, 240°E)

Radiating system 3 is centred at Nazit Mons, a large volcano on the northeastern edge of the study area (Figures 3.10, 3.11 and 3.12). It sits on the north side of an arm of the Hecate Chasma rift system. Nazit Mons is located near the eastern margin of the study area; for this project we will only consider it in relation to other features within the study area.

The system as mapped includes 680 graben extending up to 534 km from the centre. This is a partial total, as Nazit Mons is found on the very edge of the study area, and many more features probably exist to the east. The volcano features a corona rim structure surrounding an elevated plateau. The altitude of the centre is 6055.6 km, 3.8 km above the planetary mean radius. Small regions within the rim appear to have been filled with lava postdating the creation of the graben-fissure system.

West northwest of the centre, graben in system 3 appear to be obscured by a lava flow which is interpreted to emanate from Pani Corona (Ivanov, 2008). While this would appear to indicate that the lava flow is younger than the graben (and therefore that Nazit Mons is older than Pani Corona), other intersections provide a different interpretation. Graben in system 4, which is associated with Pani Corona, clearly cut the lobate flow in question, but are also cut by graben in system 3. System 9 is also associated with Pani Corona, and further north there are graben in that system that can be seen to be cut and offset by narrower graben in system 3. According to these observations, Nazit Mons is younger than Pani Corona. I favour this interpretation as it

is possible that it is the high albedo of the lobate lava flow that is obscuring any radar return from the relatively narrow linear graben of system 3, rather than the graben being filled in by a younger flow.

To the southwest, graben from system 3 intersect with graben from system 8. While direct cross-cutting relationships are difficult to interpret, both systems can be seen to intersect a linear feature which is unattributed to any radiating system. A graben from system 8 clearly cuts this lineament, while several graben in system 3 appear in turn to be cut by the same lineament. This indicates that system 8 is likely to be younger than system 3.

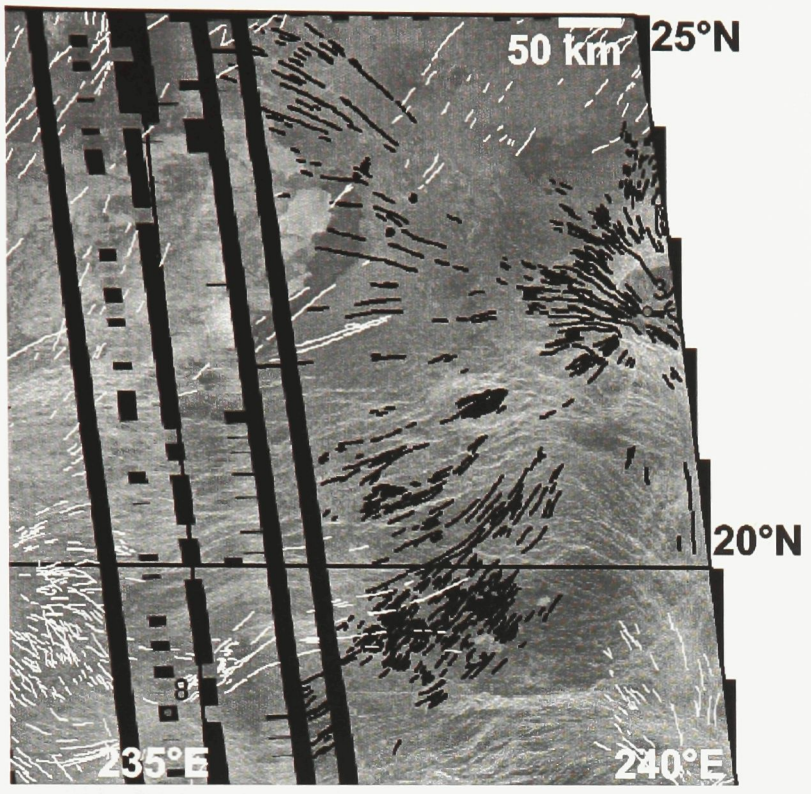

Figure 3.10. Mapped radiating graben-fissure systems overlain on a Magellan SAR image. System 3 is indicated by thick green lines, other systems by thin lines of other colours.

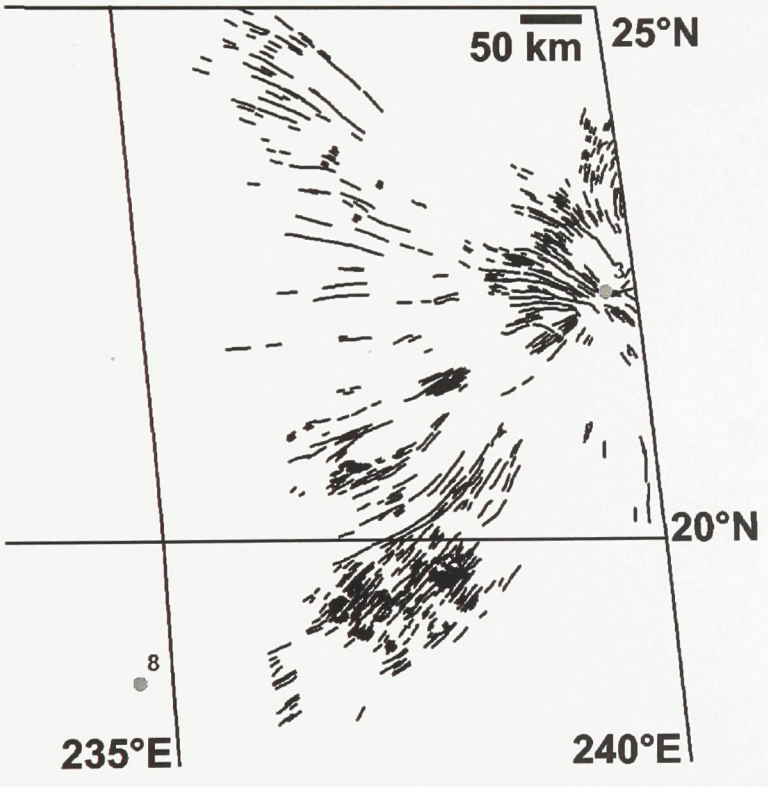

Figure 3.11. Graben mapped as belonging to system 3.

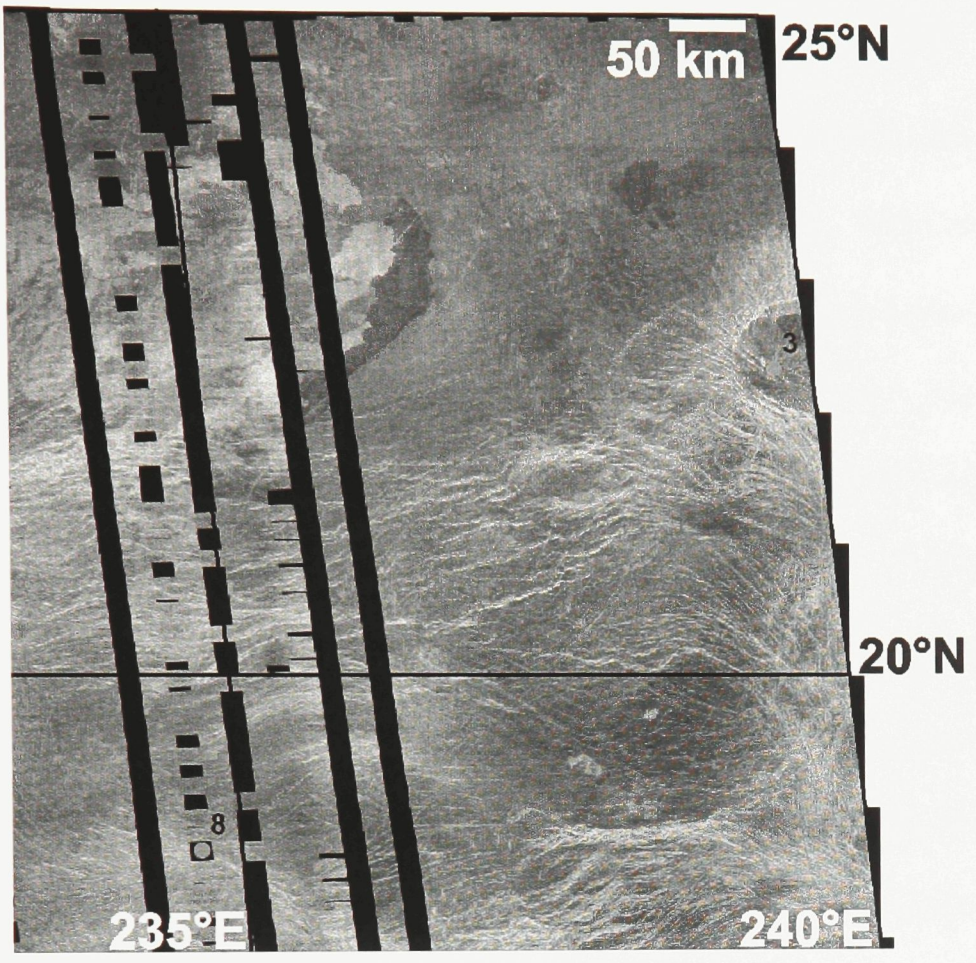

Figure 3.12. Magellan SAR image of the region around Nazit Mons.

3.3. Systems 4 and 9: Pani Corona (19.9°N, 231.5°E)

Radiating systems 4 and 9 (Figures 3.13, 3.14, and 3.15) are both centred on the rim of Pani Corona, a 320 km diameter circular structure. Pani Corona sits on the same arm of the Hecate Chasma rift system as system 6. The corona has an elevated rim surrounding a bowl that at its lowest point is still higher than the surrounding terrain. From Magellan altimetry, the rift chasm is known to cut across the northern portion of the corona. Aittola and Kostama (2005) noted that this can also be seen in the SAR image and inferred that Pani Corona was older than the rifting events. System 4 (21°N, 231.5°E) is centred on the northern rim of Pani Corona, just on the northern edge of the cross-cutting rift. As mapped, system 4 includes 410 graben which extend up to 592 km from the centre. System 9 (20°N, 233°E), on the eastern rim of the corona, is composed of 221 graben and has a maximum radius of 816 km.

Northeast of Pani Corona, graben from both systems 4 and 9 intersect with graben from system 3 (Nazit Mons), where it appears that system 3 cuts both 4 and 9. This is discussed in detail in the section on that centre.

South of the corona, graben in system 4 intersect with graben from system 2 (Perchta Corona), where it is apparent that they are cut by the latter set. System 8 also intersects with and appears to cut system 4 in this area.

From the mapping completed in this project, it appears that systems 4 and 9 are older than all other systems which they interact with, and therefore Pani Corona is the

oldest of the major tectono-magmatic features in the northeastern portion of the study area.

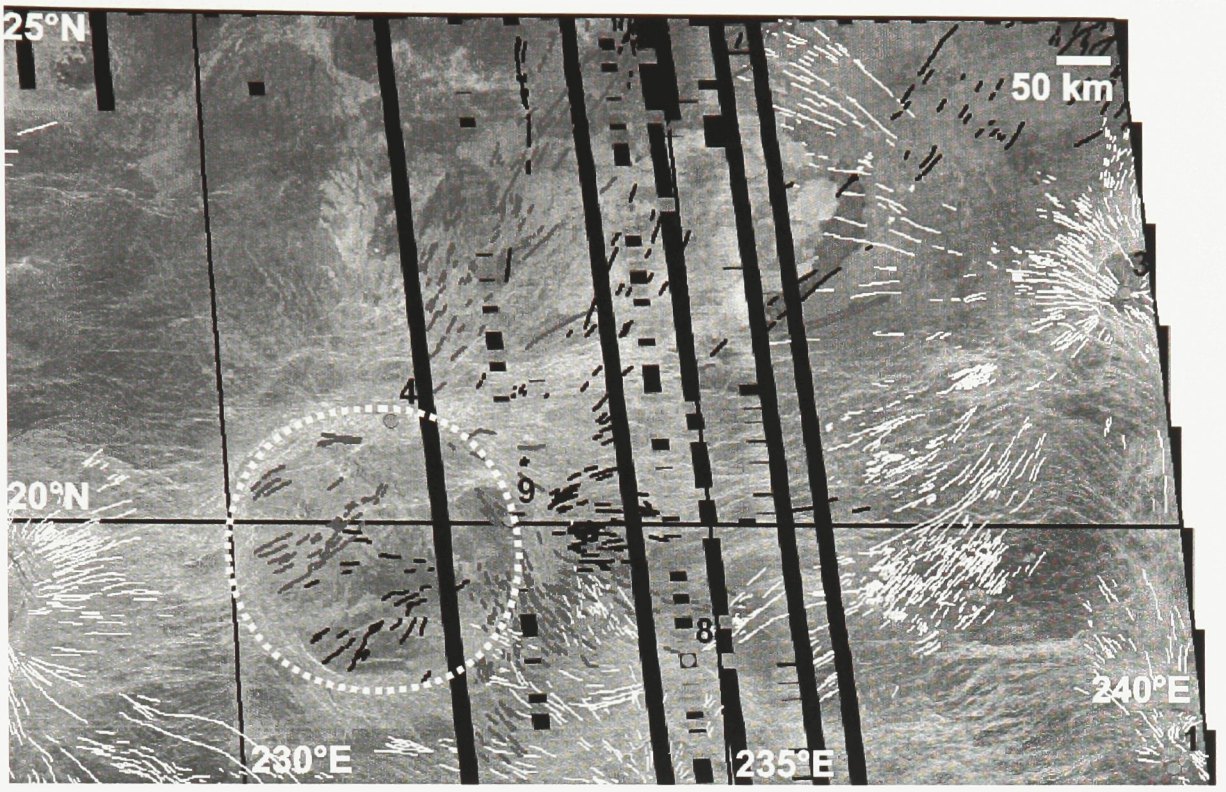

Figure 3.13. Mapped radiating systems in the Pani Corona region, overlain on Magellan SAR images. Black lines show graben belonging to system 9, grey lines show system 4, and thin white lines show other radiating systems. The rim of Pani Corona is shown by the dashed white line.

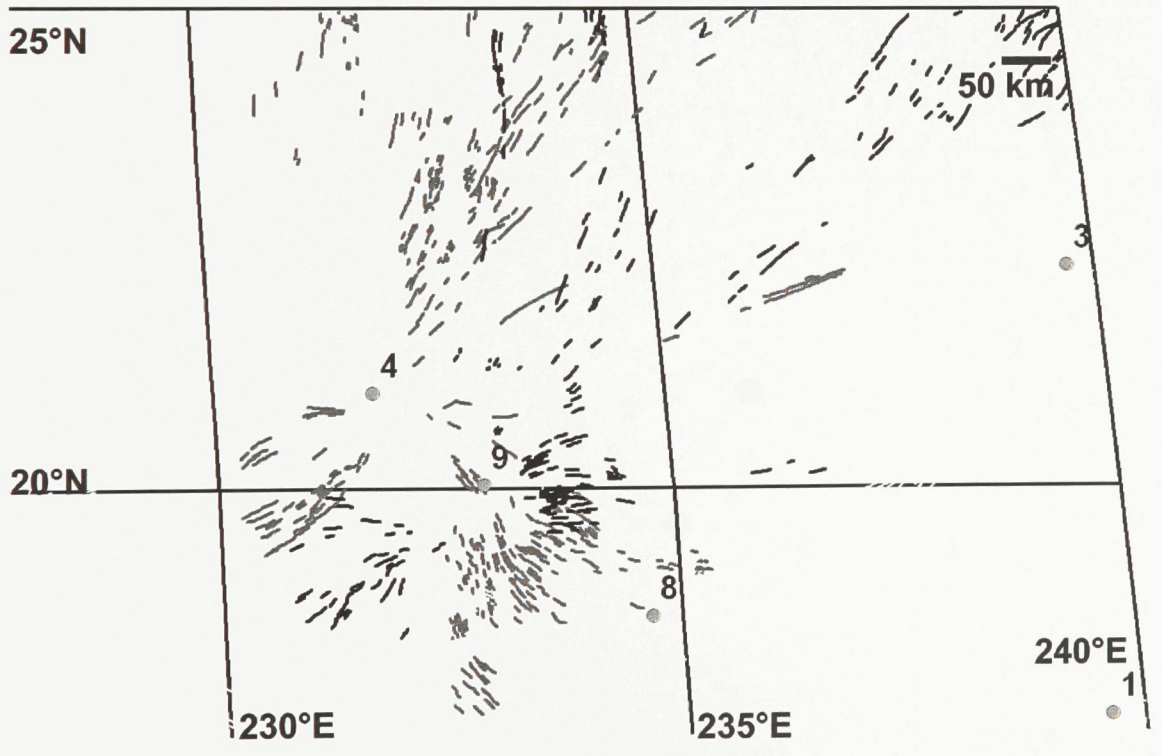

Figure 3.14. Mapping of graben and fissures belonging to radiating systems 4 (grey lines) and 9 (black lines).

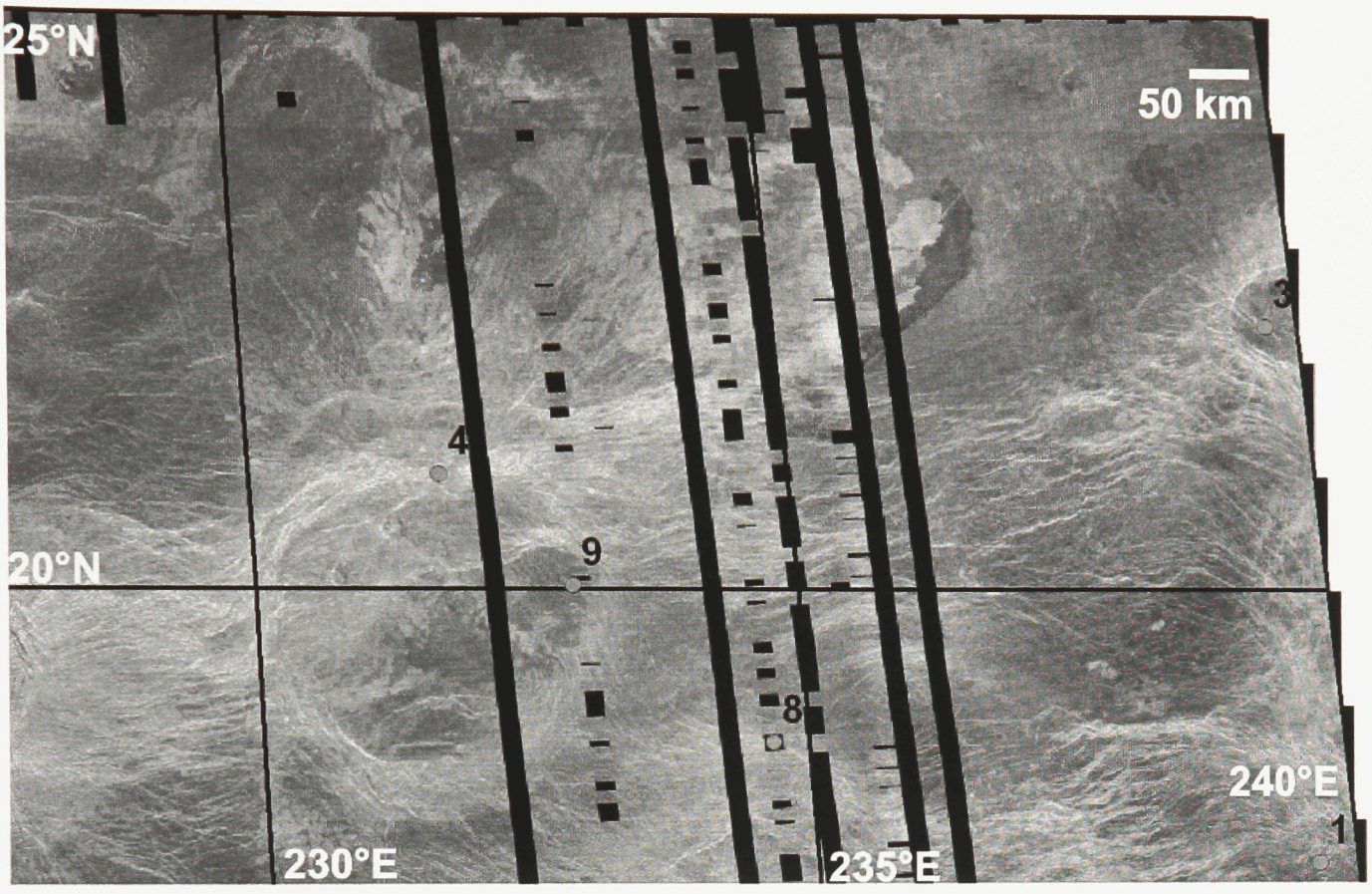

Figure 3.15. Magellan SAR image of the region around Pani Corona.

3.4. System 5 (22.5°N, 224°E)

This is a very well defined radiating system with a clearly defined centre. The centre is within a partial corona rim which can be seen to the north and east (Figures 3.16, 3.17, and 3.18). It also sits along an arm of the Hecate Chasma rift zone, running in an NNE-SSW direction. The centre sits on a topographic rise, with a maximum radius of 138 km and a central elevation of 6059.6 km, 7.8 km above the planetary mean. The graben-fissure system related to this centre has a maximum radius of 809 km, with 1011 individual features mapped, extending out in all directions.

Examining direct cross-cutting between the radiating system and the fissures of the corona rim, the two features appear to be concurrent in age. Radiating graben both cut through the corona rim and are broken themselves by circumferential fissures within the rim. Lava has pooled within the corona rim to the north and east of the radiating centre and is uncut by graben. Neither volcanic edifices nor vents are discernable within the area of lava flows, and therefore, it seems likely that the flows emanated from the radiating graben.

To the east of the centre, radiating graben curl around a dome-like topographic rise that is crossed by few graben. To the north and south, the radiating system is intermixed with the Hecate Chasma rift. To the west, beyond the rift zone, the graben fissure system generally has a western trend into and across a low albedo plain for 800 km to within 100 km of centre 14 (215°E, 22°N). The very end of a graben from centre 5

appears to both cut and be cut by graben from centre 14, suggesting concurrent ages of formation.

415 km to the southeast is centre 6, another well-defined, major radiating system. Directly between the two centres, the respective graben-fissure systems curve away from their initial orientations to become parallel to each other, and appear to be formed in the same event or time frame. To the west of centre 6, and south of centre 5, the south-trending graben related to system 5 are both better-defined and more continuous than those of system 6. From these observations, it is inferred that while system 5 was formed concurrently with system 6, system 5 was also active more recently than system 6.

Centre 7 is found 580 km WNW of centre 5. Where the two radiating systems intersect, approximately 425 km from centre 5, the graben of system 5 are continuous and uncut by those of system 7. It is inferred that system 5 is younger than system 7.

A shield field at (24°N, 227°E) is clearly overprinted by a graben in system 5, implying that the volcanic region is older than the radiating centre and system.

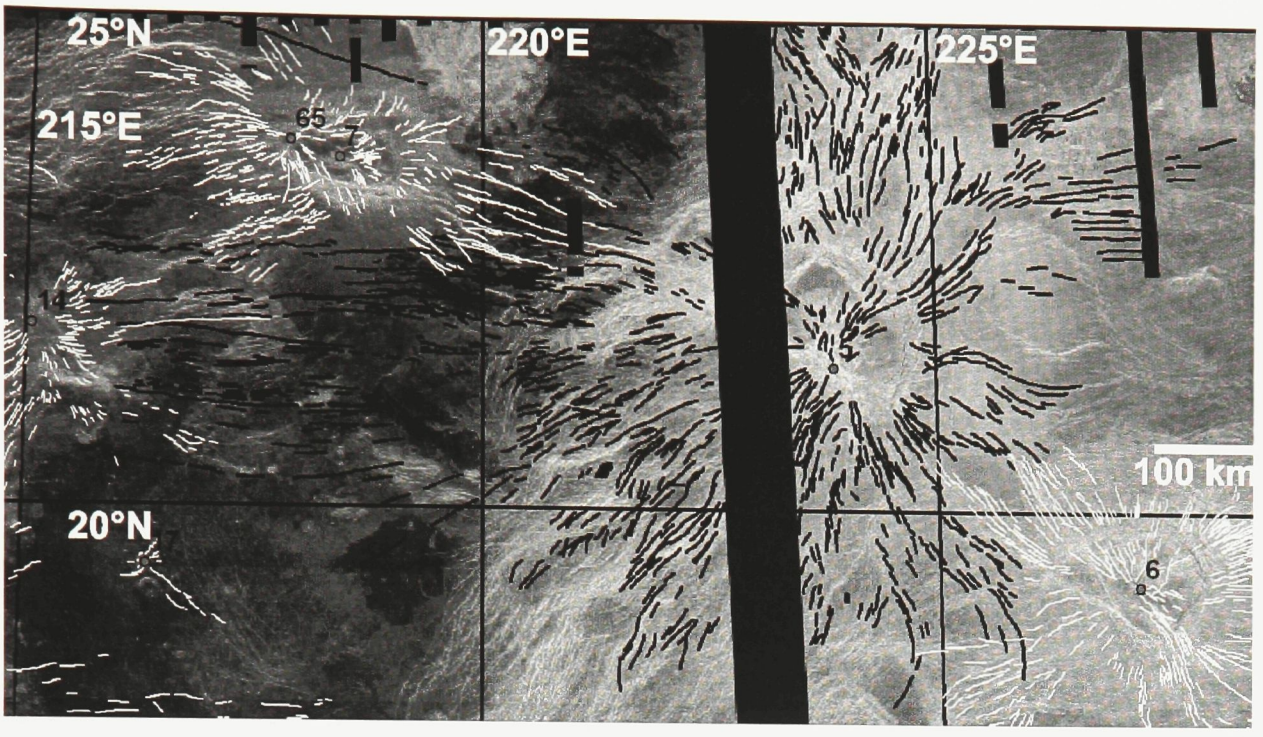

Figure 3.16. Mapping of radiating system #5 overlain on a Magellan SAR image. System #5 is mapped with thick black lines, thinner white lines represent other radiating systems.

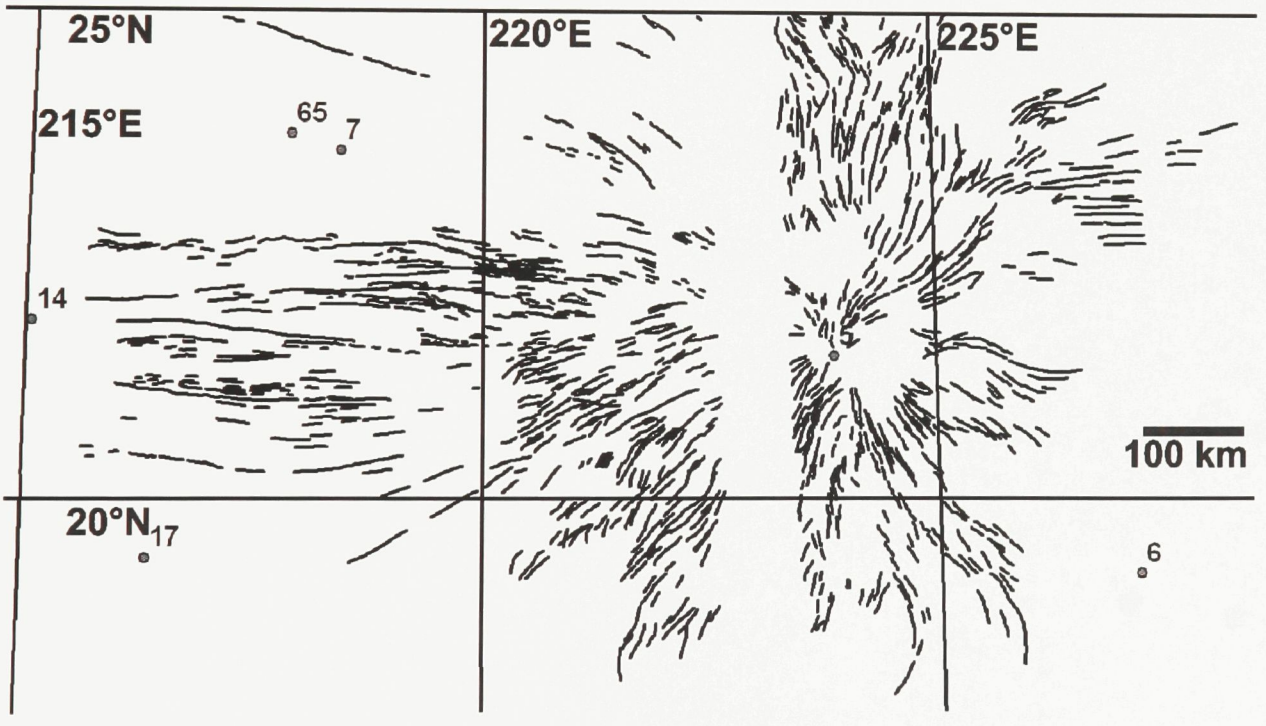

Figure 3.17. Mapped graben related to centre #5.

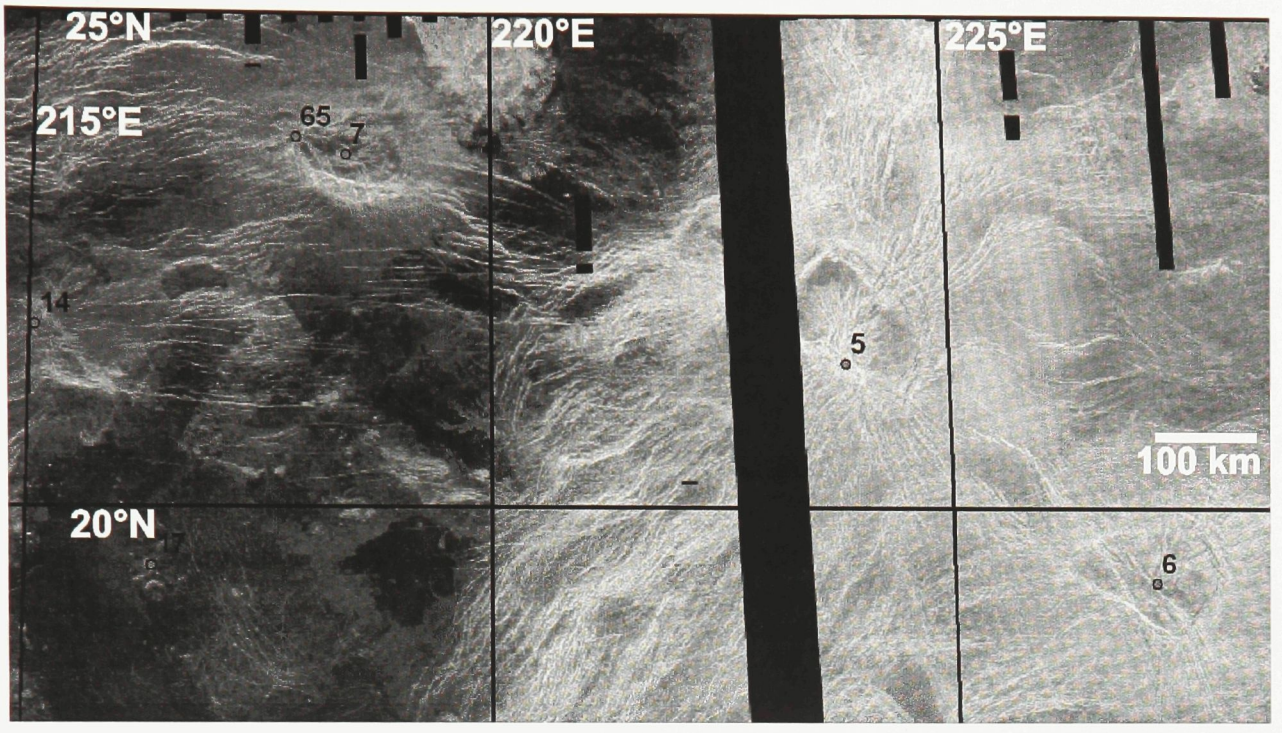

Figure 3.18. Magellan SAR image of centre #5 region.

3.5. System 6 (19°N, 227.5°E)

System 6 (Figures 3.19, 3.20, and 3.21) is an extensive system with an easily identified central point. It sits within a partial corona rim, which is visible from the northwest clock-wise around to the southeast. The centre sits on a minor arm of the Hecate Chasma rift system and is 300 km directly west of Pani Corona. The system converges on a dome-like topographic rise 82 km in diameter; the central point sits at an elevation of 6059 km, 7.2 km above the planetary mean radius. The majority of the system extends to no more than 550 km from the centre, with one set of well-defined graben reaching far beyond that distance to the southeast. Graben extend out up to 1418 km from the centre and 693 individual graben are mapped. While occasionally broken, their trends are continuous and they have no likely source other than system 6.

Interaction between graben in this system and Pani Corona to the east is difficult to interpret; the graben are within the Hecate Chasma rift, and I am uncertain which are part of the rift and which are related to the radiating systems. While the rift itself appears to continue into the corona, the graben are not traceable. It seems possible that there has been lava flooding within the corona, as it shows a much lower degree of deformation than the surrounding territory. Assuming that the flooding is associated with Pani Corona, then a plausible interpretation is that Pani Corona is younger than system 6.

To the south, graben can be traced for up to 550 km, until they meet deformation related to a cluster of coronae (which includes radiating systems 27 and

28). In this region, they are also flooded by lava flows which emanate from system 22 to the east and system 28 to the south, as mapped by Ivanov (2008). In my interpretation, it is also possible that some of these flows are sourced from fissures and graben in system 6, suggesting that volcanism occurred late in the history of the centre.

To the west of system 6, associated graben are quickly merged with and/or obscured by the rift zone. The most distal graben in this direction associated with this system is 260 km from the centre. Similarly, graben to the northwest are obscured by graben from system 5. Sets either trend towards and into sets emerging from the centre of system 5, or are completely overprinted, as discussed in the section focussing on that system.

Graben to the north and northeast do not appear to extend beyond the limits of the rift zone.

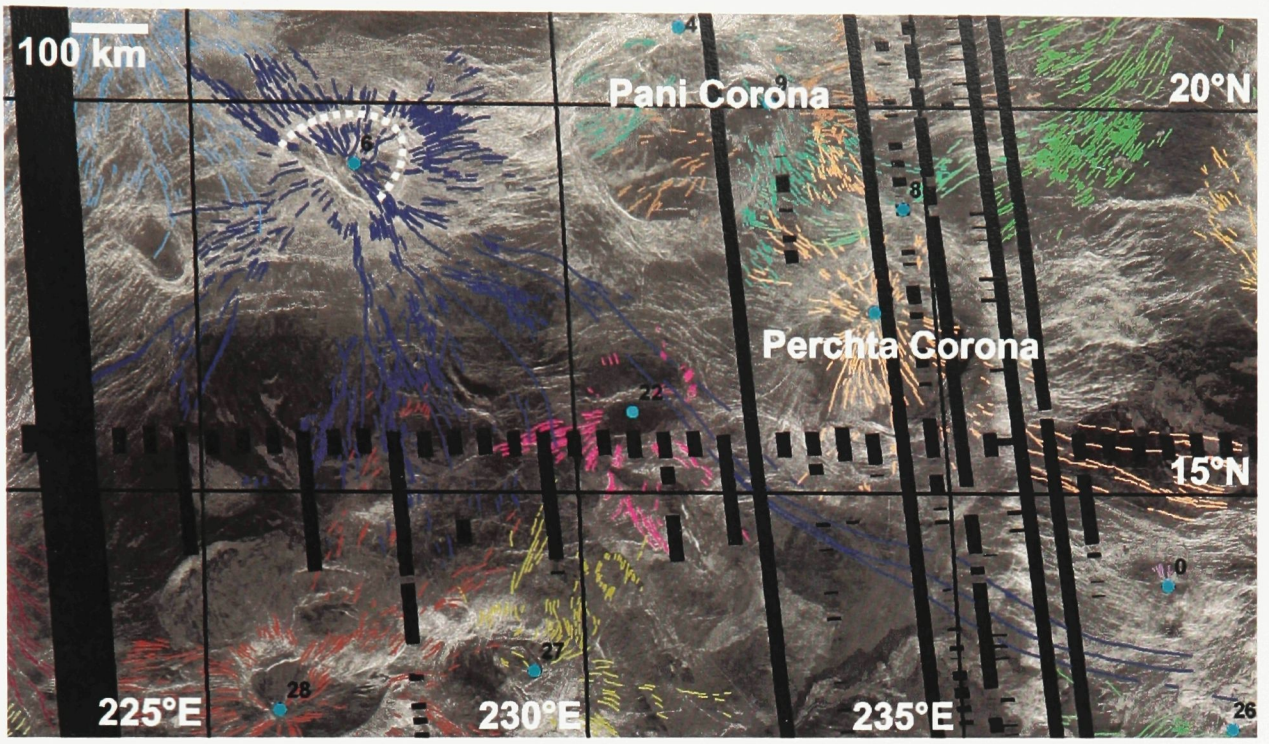

Figure 3.19. Mapped radiating graben-fissure systems overlain on Magellan SAR images. Dark blue lines represent system 6; other centres are represented by thin lines of other colours. The dashed white line represents the corona rim.

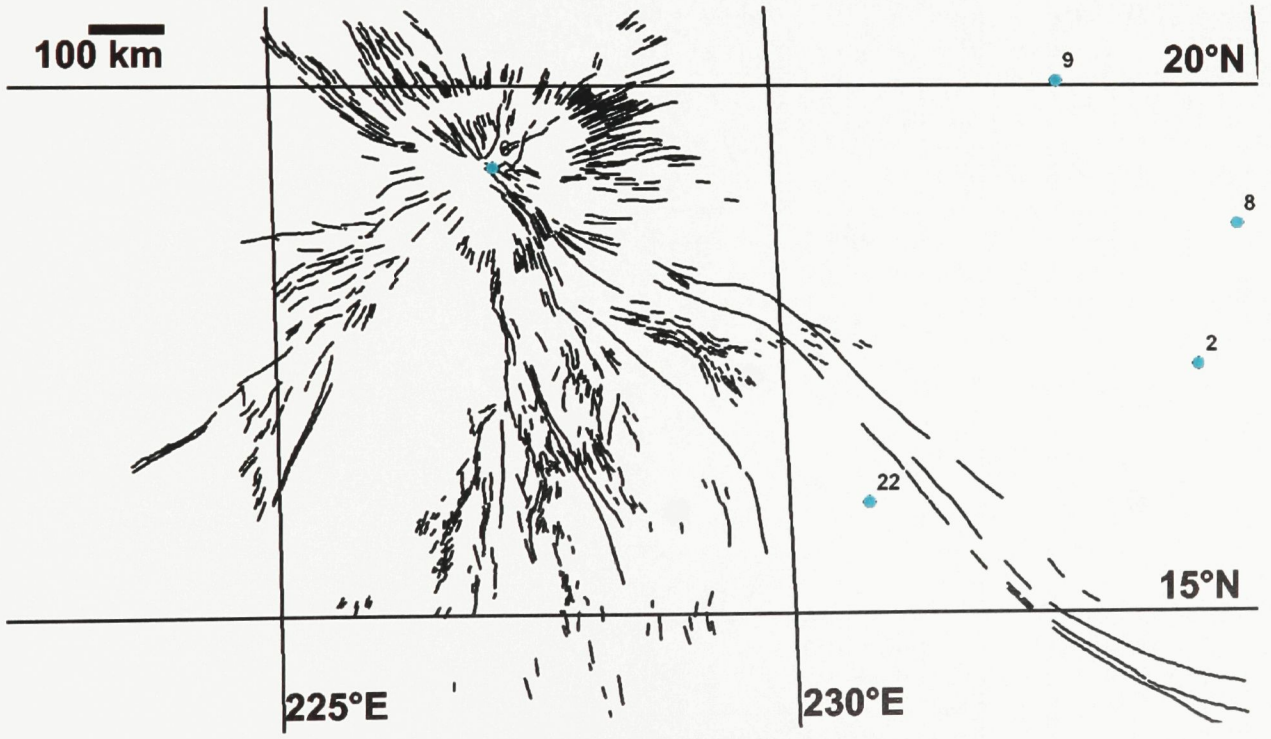

Figure 3.20. Mapped graben belonging to radiating system 6.

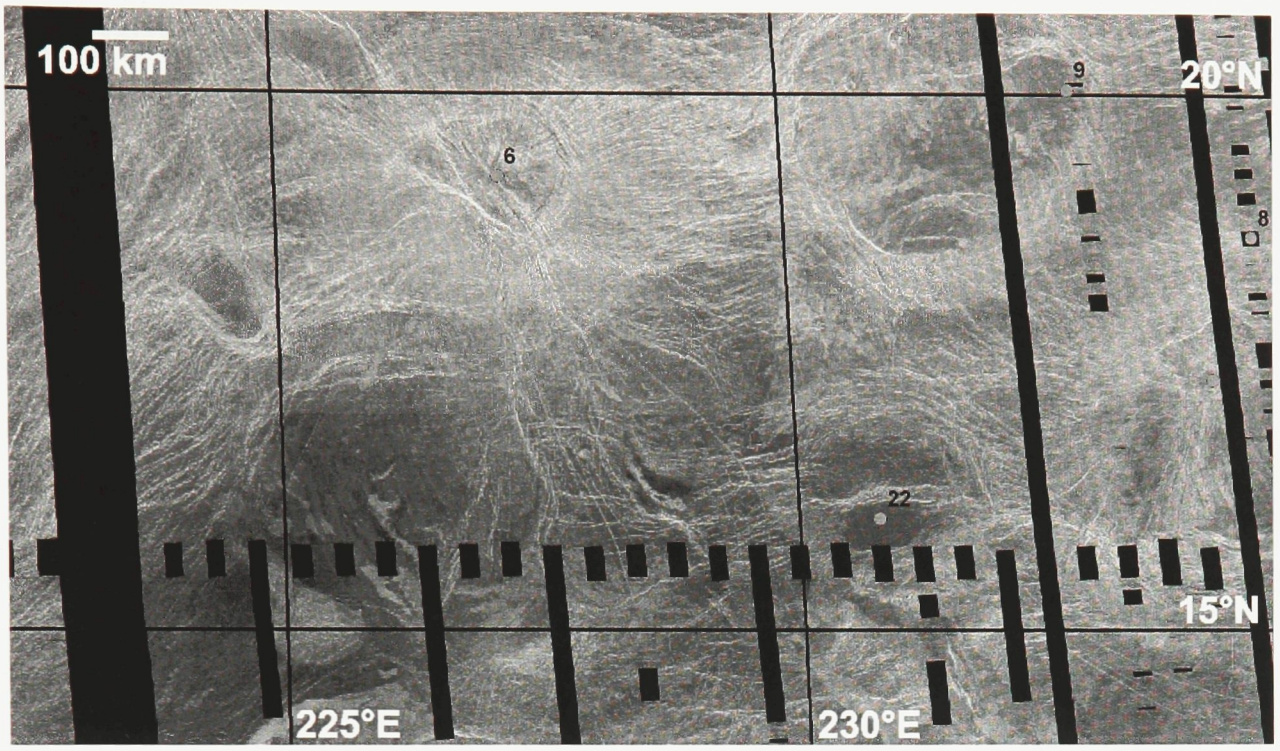

Figure 3.21. SAR image of the region around radiating system 6.

3.6. Systems 7 and 65, Minona Corona, (23.5°N, 218.5°E)

The two radiating systems 7 and 65 are centred within the rim of Minona Corona (Figures 3.22, 3.23, and 3.24). The corona rim is not complete and is open to the west. Minona is in the north of the study area, 400 km west of the Hecate Chasma rift zone where system 5 can be found. The systems sit on a topographic rise (the corona plateau) with a radius of 157 km. The centre of system 7 has an elevation of 6057.2 km while system 65 is centred at an elevation of 6056.6 km, altitudes that are 5.4 km and 4.8 km above the planetary mean radius, respectively.

System 7 has a maximum radius of 334 km and is comprised of 199 graben. System 65 has a maximum radius of 190 km and is comprised of 135 graben. The two systems are largely separated, with little interplay between them, aside from two local intersections. At the first, in the north, system 65 appears to be better defined and more continuous, however at the second, southern, intersection system 65 is less sharply defined and appears to be overprinted by graben in system 7. It is inferred that the two centres formed at the same time, over the same duration of activity.

To the north of Minona Corona and west of the crater Boleyn, both systems are flooded by a plains lava flow. This flow is crossed by a well-defined graben attributed to system 5, which is believed to be younger than systems 7 and 65.

The southern and eastern portions of the rim of Minona Corona are strongly defined and obscure radial graben related to the two systems. The northern portion of

the rim, however, is seen to be crossed by the radiating systems. It is thus apparent that ages of formation of the corona and the radiating systems are congruent.

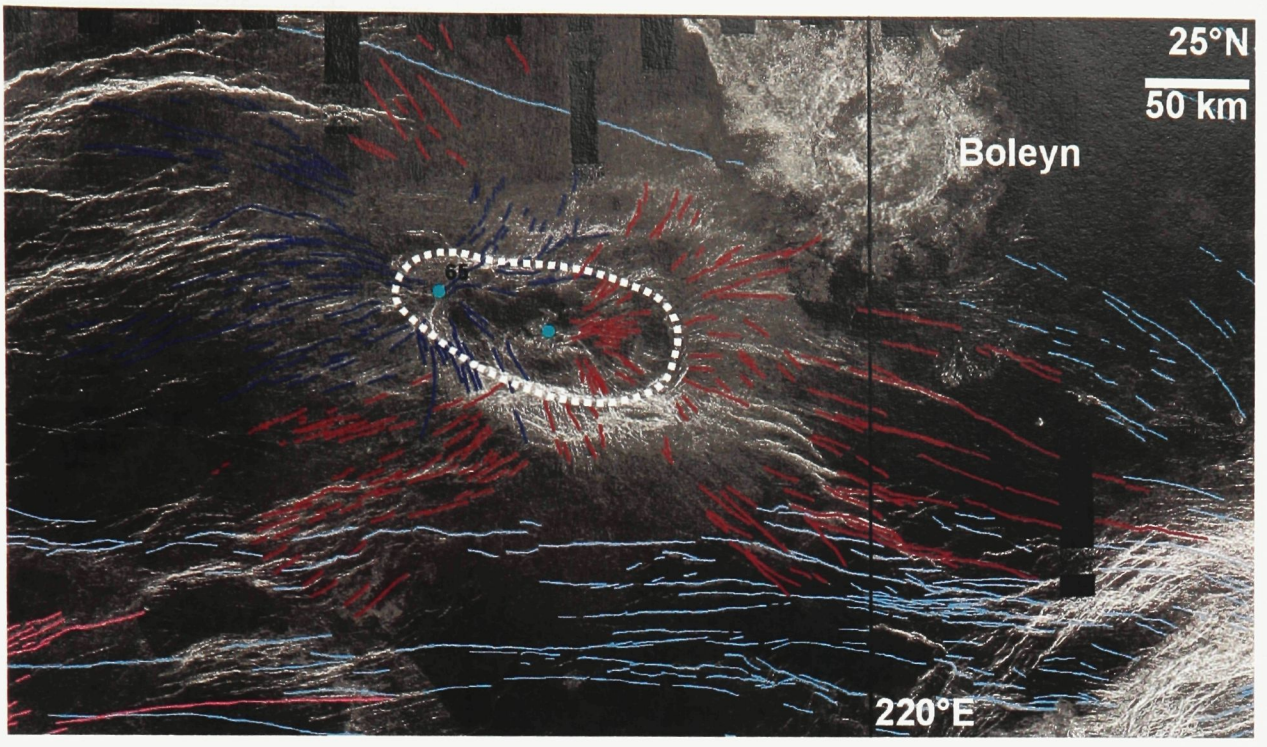

Figure 3.22. Mapping of radiating systems overlain on Magellan SAR image; system 65 in thick dark blue lines, system 7 in thick reddish lines, other systems in thin lines of other colours. The Minona Corona rim is shown as a white dashed line.

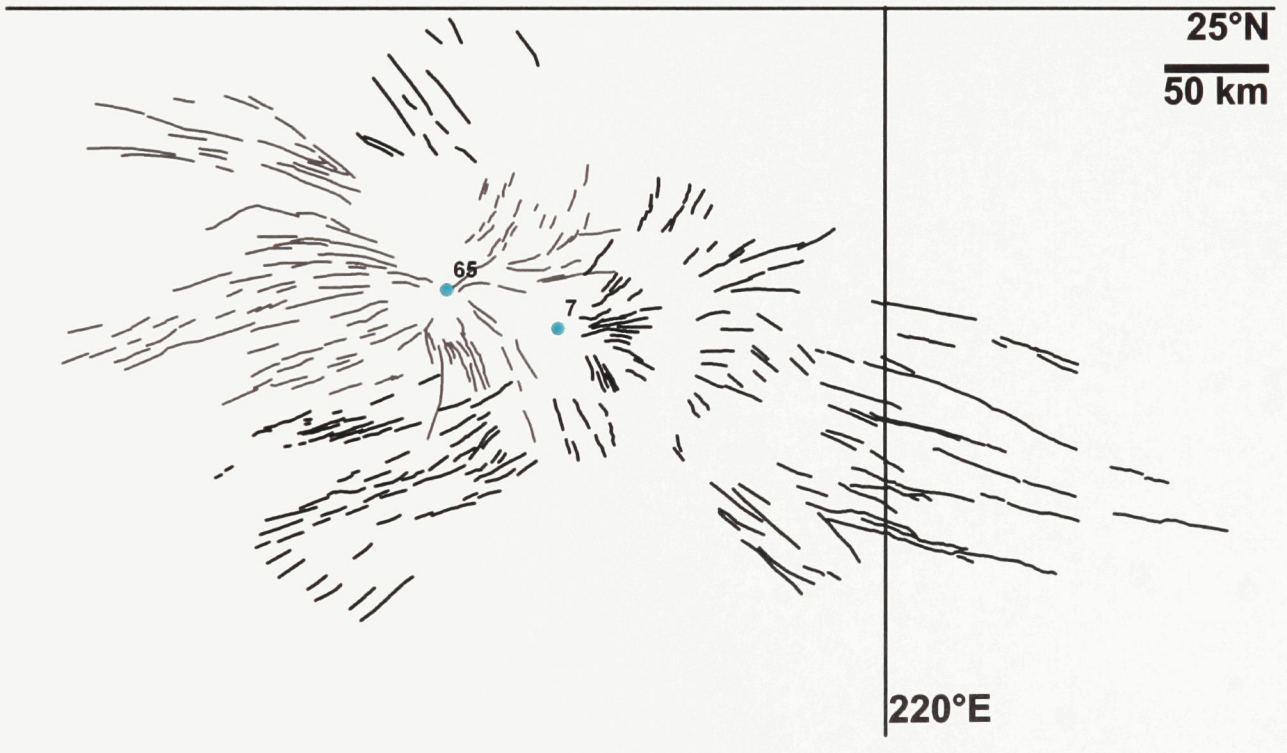

Figure 3.23. Mapped graben in the radiating systems 65 (grey) and 7 (black).

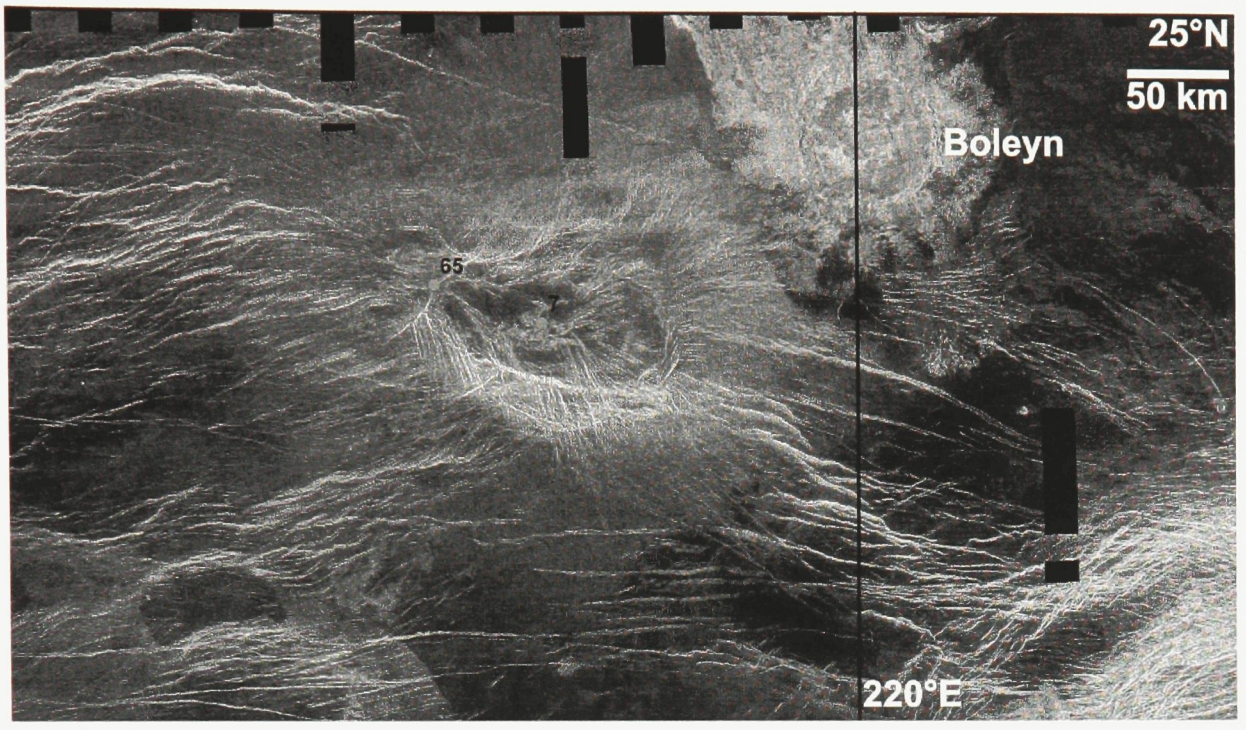

Figure 3.24. Magellan SAR images of the region around Minona Corona.

3.7. System 10 (25°N, 207°E)

Radiating graben-fissure system 10 (Figures 3.25, 3.26, and 3.27) is centred just above the north edge of the study area. Herein we only evaluate the interactions between system 10 and other features within the study area. System 10 consists of 367 mapped graben and has a maximum radius of 768 km. The centre of the system is just off the edge of the study area; there is a slight rise in association with the system and the elevation at the centre is 6055.0 km, 3.2 km above the planetary mean radius. While there are some lineaments with a circumferential orientation, there is not a clearly defined corona rim associated with the centre of system 10.

Towards the southern end of system 10, there is an area of intersection with system 15. In this region, direct cross-cutting relationships are unclear. There are places where the graben in system 15 are not present (likely obscured by later volcanic activity), but in these same areas the graben in system 10 are abundant. This implies that system 15 is older than system 10.

To the east, there are interactions with graben from systems 11, 12, and 13 – a closely packed group of radiating graben-fissure systems. In most interactions, it appears that system 10 is cut by and is older than the other three systems. These interactions are discussed in more detail in the section on systems 11, 12, and 13.

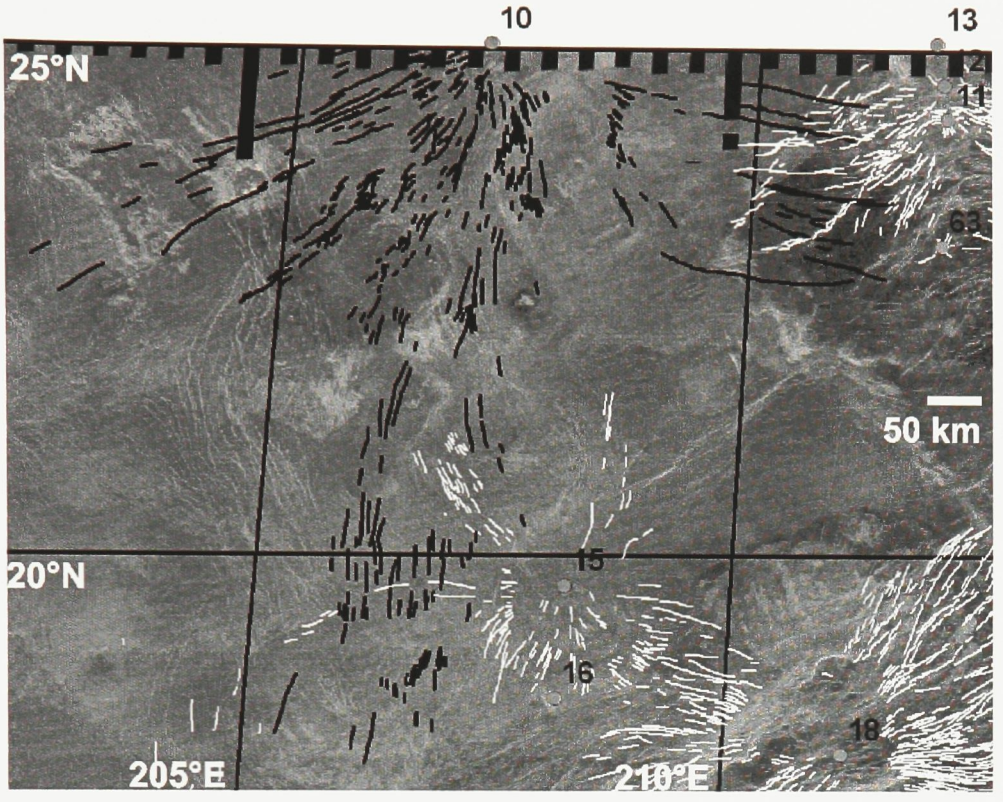

Figure 3.25. Mapped radiating graben-fissure systems overlain on Magellan SAR images; thick black lines represent system 10, thin white lines represent other radiating systems.

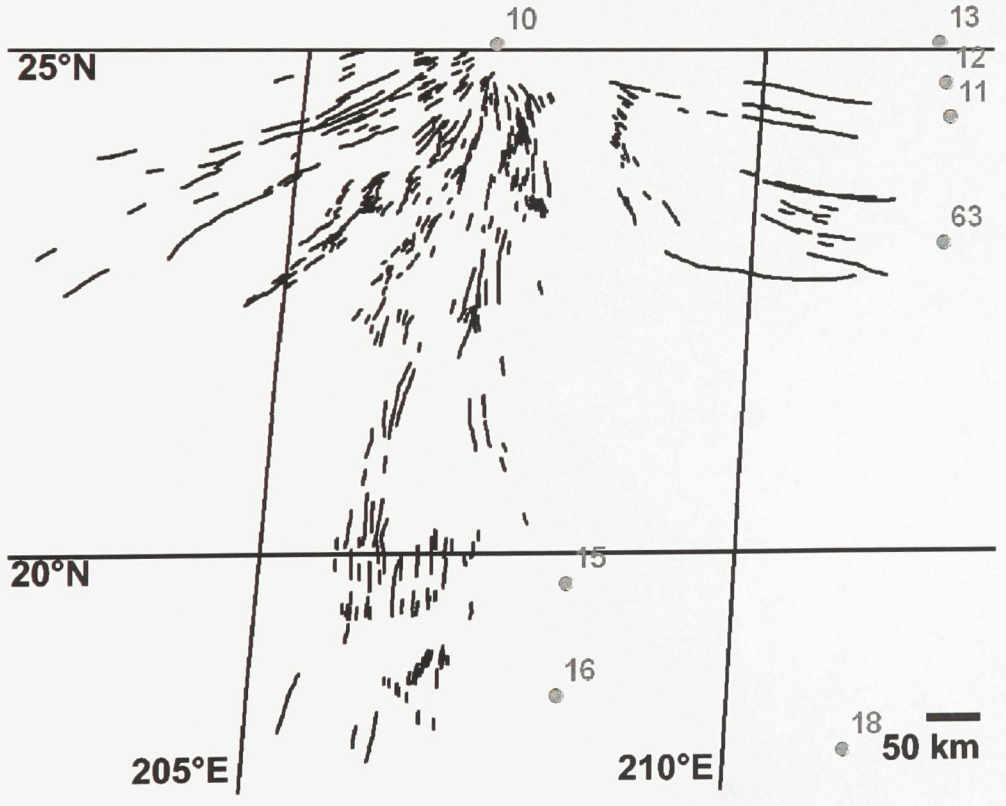

Figure 3.26. Mapped graben of radiating graben-fissure system 10.

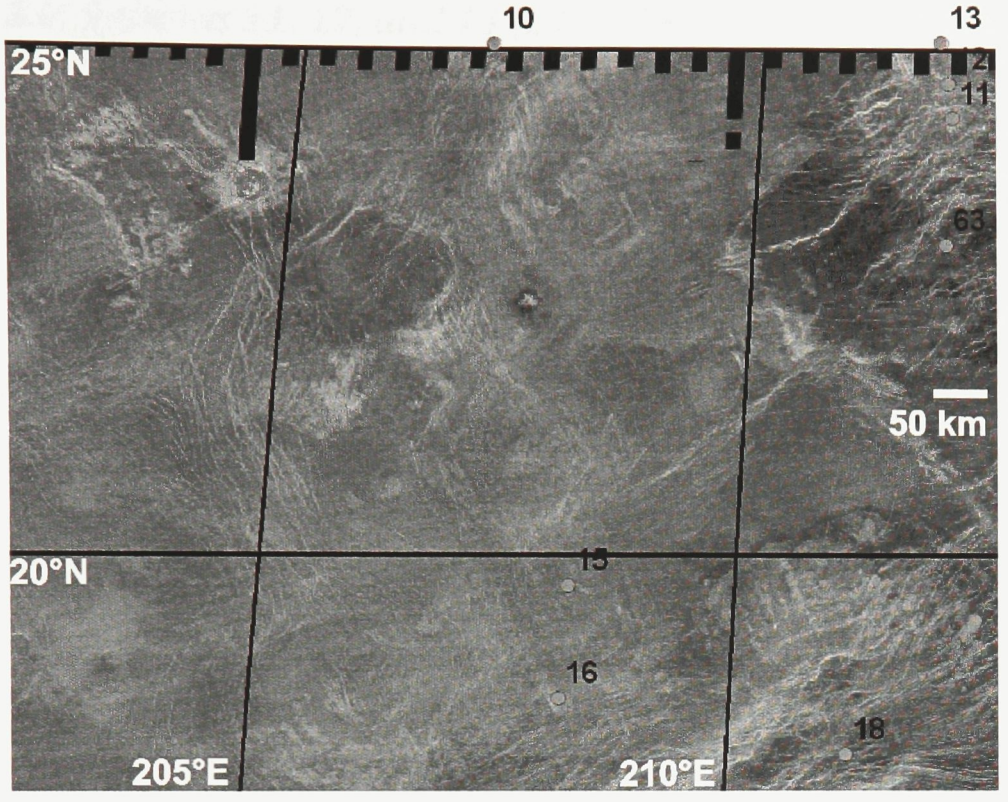

Figure 3.27. Magellan SAR images of radiating system 10.

3.8. Systems 11, 12, and 13 (24-25°N, 212°E)

Systems 11, 12, and 13 are aligned along a north-south line at the northern edge of the study area. This study will only take into account interactions between these systems and other features within the study area. System 11 consists of 41 mapped graben and has a maximum radius of 122 km (Figures 3.28, 3.29, and 3.30). System 12 consists of 130 mapped graben and has a maximum radius of 149 km. System 13 consists of 35 mapped graben and has a maximum radius of 290 km. The centre of system 13 is just off the edge of the study area; the elevation at the centre is 6054.7 km, 2.5 km above the mean planetary radius. There is a noticeable topographic rise near the centres of system 11 and 12; system 11 is on the southern slope of this rise, and system 12 is on northern edge. Systems 11 and 12 have elevations of 6054.7 km and 6055.3, altitudes of 2.5 km and 3.3 km above the planetary mean radius, respectively. None of the systems are associated with corona rim structures.

Systems 11 and 12 have most of their intersections west and south of their centres. Just to the west of the centre of system 11, it appears that a graben from system 11 cuts one from system 12. To the southwest, in one intersection it appears that first one set then the other is more continuous (and therefore younger). Further from the centres, an intersection sees a graben from system 12 cutting system 11.

Systems 12 and 13 likewise have most of their intersections to the west and south of their centres. There is one intersection to the east of the centre of system 12, where a graben from system 12 clearly cuts one from system 11. West of the centre of

system 12, system 12 is again seen cutting graben from system 10. Further from the centre, an intersection sees a graben in system 13 cutting 3 graben in system 12.

Systems 11 and 13 do not meet. Given the contradictory nature of the observed cross-cutting relationships, the most likely interpretation gives the three systems the same age of formation.

There are 11 observed interactions between system 10 and systems 11, 12, and 13, and in all but one, it is clear that system 10 is cut by and is older than the other systems. In the final intersection, the graben from system 10 appears continuous across a meeting with a graben from system 13. The same graben from system 10 is then cut by another graben in system 13, 30 km to the east. The overwhelming evidence of cross-cutting relationships indicates that system 10 is older than systems 11, 12, or 13; the single outlier gives evidence of a slight overlap in ages of formation between system 10 and 13 and may also indicate that system 13 is slightly older than 11 or 12.

Figure 3.28. Mapped radiating graben-fissure systems overlain on Magellan SAR images; systems 11, 12 and 13 are represented by red, green, and yellow lines, respectively. White lines represent other radiating systems.

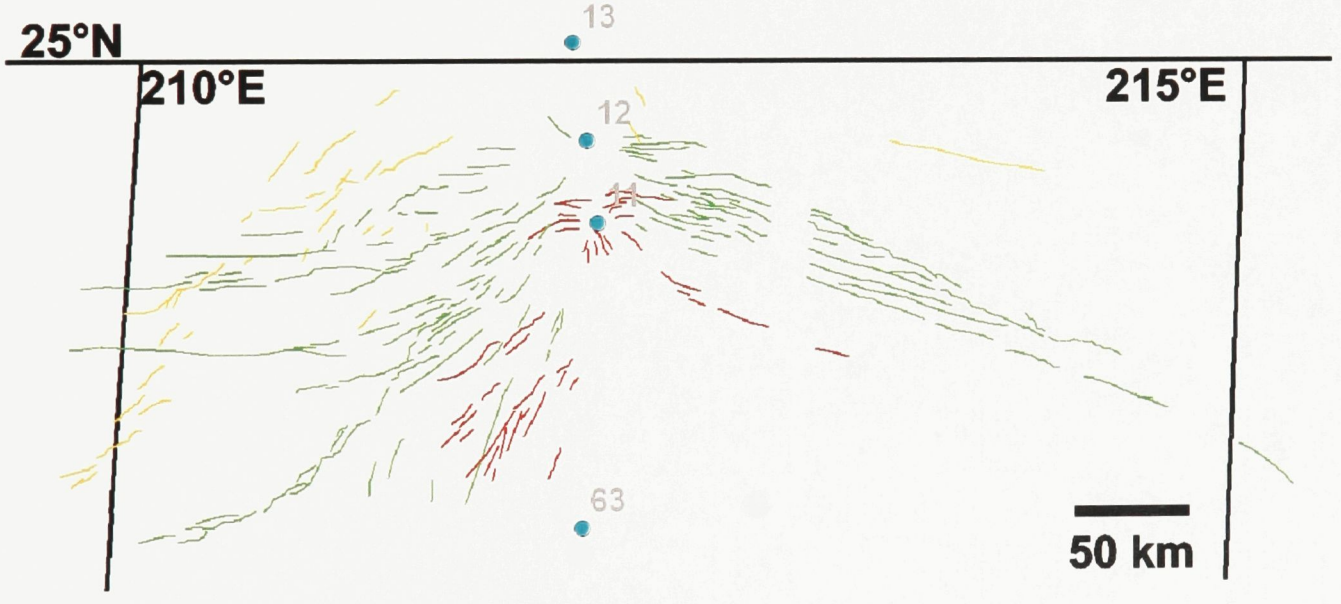

Figure 3.29. Mapped graben of radiating graben-fissure systems 11, 12, and 13 in red, green, and yellow, respectively.

Figure 3.30. Magellan SAR images of radiating systems 11, 12, and 13.

3.9. System 18 (18°N, 211.5°E)

This is an extensive radiating graben-fissure system, sitting on an arm of the Hecate Chasma rift system. The system converges on a topographic rise with a maximum radius of 247 km; the central point sits at an elevation of 6056.4 km, 4.6 km above the planetary mean radius. Graben extend up to 729 km from the centre and 1075 individual graben are mapped (Figures 3.31, 3.32, and 3.33).

There is a circumferential structure to the south of the centre, but the extent is not sufficient to label it a corona. It cuts all other graben it touches, and so appears to have formed more recently than the radiating system in that location. The topographic rise associated with this radiating system is cut by structures of the Hecate Chasma rift arm, an interaction that is clearly visible in both the SAR and topographic data. This indicates that system 18 is older than the rifting activity.

System 15 is centred 340 km northwest from system 18. There do not appear to be any direct intersections between the systems. In the region directly between the two centres, there are many graben attributed to system 15, and comparatively few attributed to system 18. Since system 18 is otherwise a larger and more dominant system than system 15, it is probable that since system 15 is more prevalent between the two systems it is the younger of the two.

To the northeast, system 18 intersects with the southern end of system 14. In this case, it appears that a graben of system 14 that crosses several graben from system 18 is the more continuous, and thus system 14 is likely younger.

To the east, system 18 intersects with system 21, northwest of that system's centre. There, the graben in system 21 are more continuous and therefore system 21 is likely younger.

The southernmost graben mapped in system 18 ends at its point of intersection with a graben in system 33. The graben is very faint and poorly defined as well. This makes it very likely that system 33 is younger than system 18.

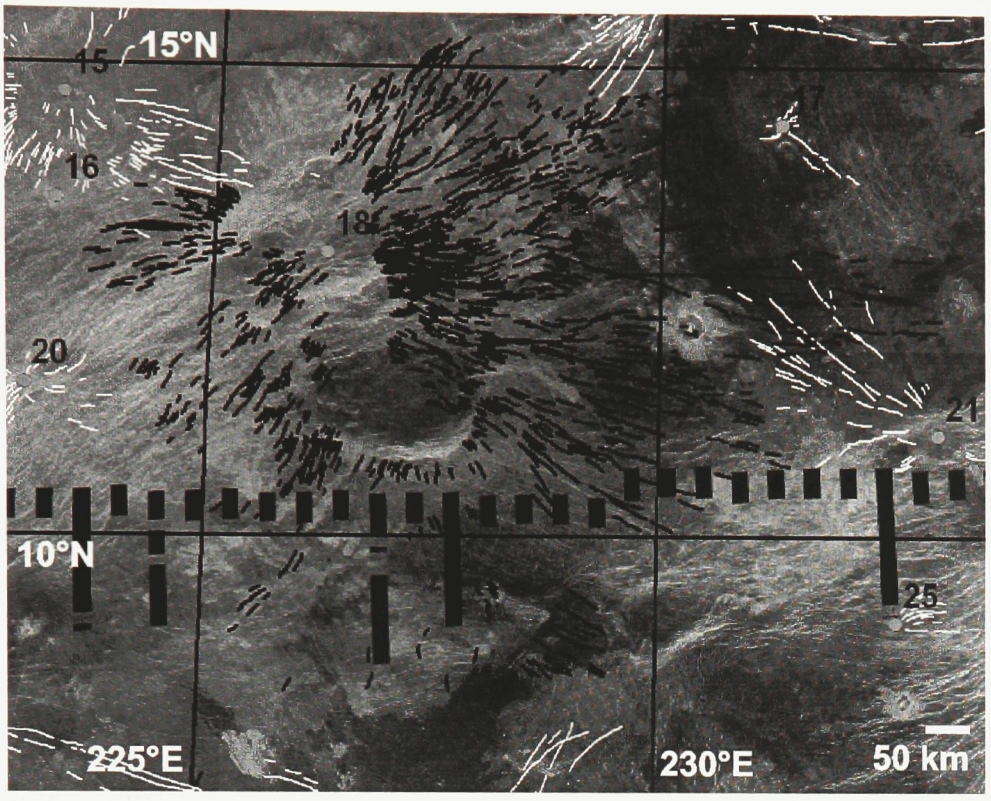

Figure 3.31. Mapped radiating graben-fissure systems overlain on a Magellan SAR image; thick black lines represent system 18, thin white lines represent other radiating systems.

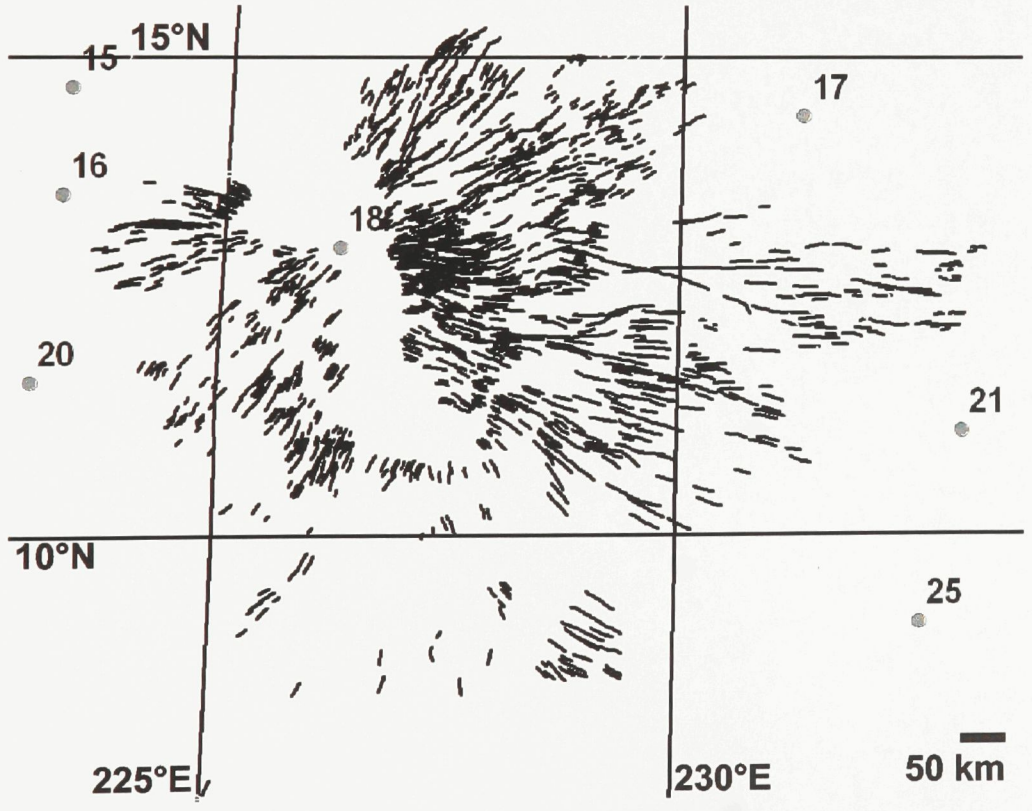

Figure 3.32. Mapped graben of radiating graben-fissure system 18.

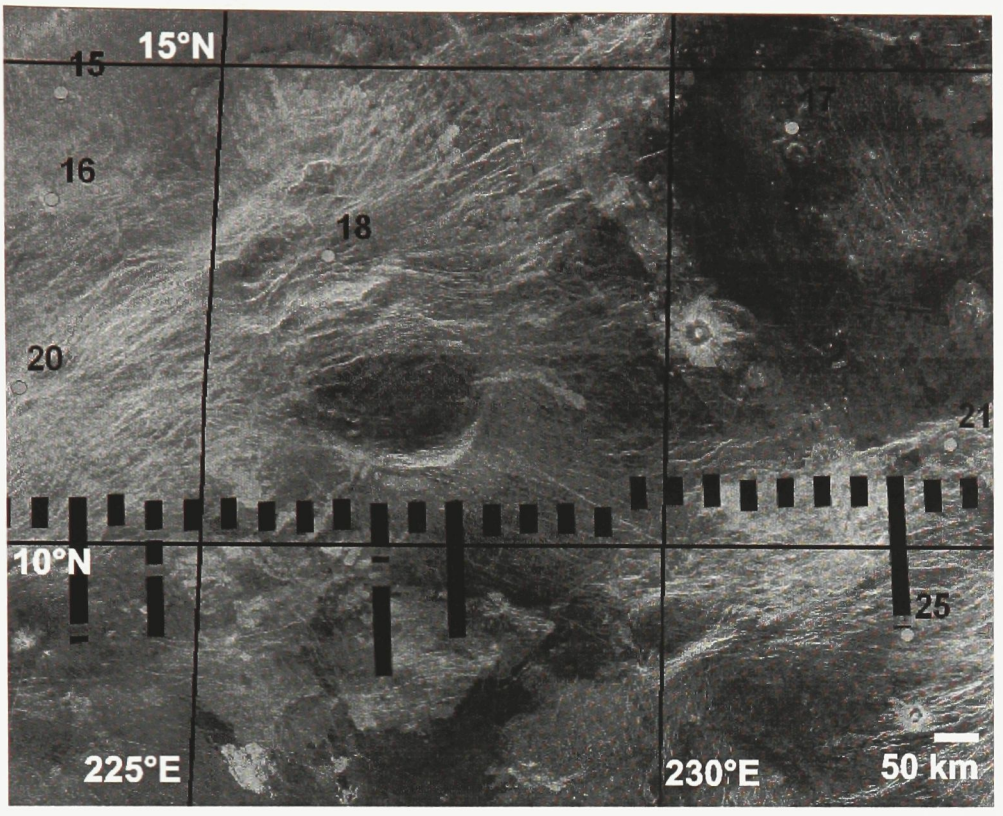

Figure 3.33. Magellan SAR image of radiating system 18.

3.10. Systems 23, 36, 40, and 64: Zisa Corona (12°N, 221°E)

Zisa Corona is an elongate corona structure approximately 800 km in diameter along its long north-south axis. Radiating systems 23 and 36 are both centred within the rim of Zisa Corona, at its north and south ends, respectively (Figures 3.34, 3.35, and 3.36). An arm of the Hecate Chasma rift system runs up the entire western margin of the corona. The corona rim is elevated at the northern and southern ends, along the western margin, and at a point midway along the eastern rim. System 23 (15°N, 221.5°E) is centred in elevated terrain at the northern end of Zisa Corona, while system 36 (9°N, 219°E) is similarly elevated at the southern end. System 23 has a maximum radius of 391 km and includes 353 individual graben. System 36 consists of 260 graben and fissures and has a maximum radius of 560 km. Also in the vicinity, there is system 64 (13°N, 219.5°E), a small radiating system found within the corona rim, midway up the western side.

On the northwest edge of Zisa Corona, systems 23 and 26 intersect. The direct cross-cutting relationships are difficult to interpret. However, the northeast trending graben of system 36 are flooded by lava flows while the southeast trending graben of system 23 are not, except where they overlap the system 36 graben. This suggests that system 36, and hence its associated magmatic centre, is older than system 23 and its centre. In this region, the graben of system 23 appear to form the rim of Zisa Corona, suggesting that system 23 and the corona rim formed simultaneously.

At the southern end of the corona, graben of system 36 clearly cut the corona rim, suggesting that they are younger.

On the western edge of the corona, system 64 clearly cuts graben of system 23, suggesting that centre 64 is younger than centre 23. However, system 64 is not continuous across the corona rim.

These contradictory observations suggest that the structures (systems 23, 36, 64, and Zisa Corona) all formed over a similar span of time. It is likely that system 36 may have started forming first of the three centres, system 64 finished forming last, and the corona rim may have formed over the entire time span of the three systems.

Southwest of Zisa Corona, system 36 intersects with the radiating system and corona associated with system 40 (7.5°N, 217°E). As system 40 also sits within an arm of the Hecate Chasma rift system, the region is densely packed with linear features and difficult to interpret. It does appear that system 36 cuts system 40 in certain instances, but more tellingly the graben of system 36 cross through the corona structure associated with system 40. This would indicate that system 36 is younger than system 40. This set of graben in system 36 was initially attributed to system 47, but upon review was attributed to system 36. It was also suggested that the graben were part of the rift system, however the trends differ by approximately 30° and the graben morphology is more typical of radiating systems than rifting in the region.

The location of the Hecate Chasma rift zone along the western side of Zisa corona and its absence within the corona rim suggests that the corona is younger, being unbroken by the rifting.

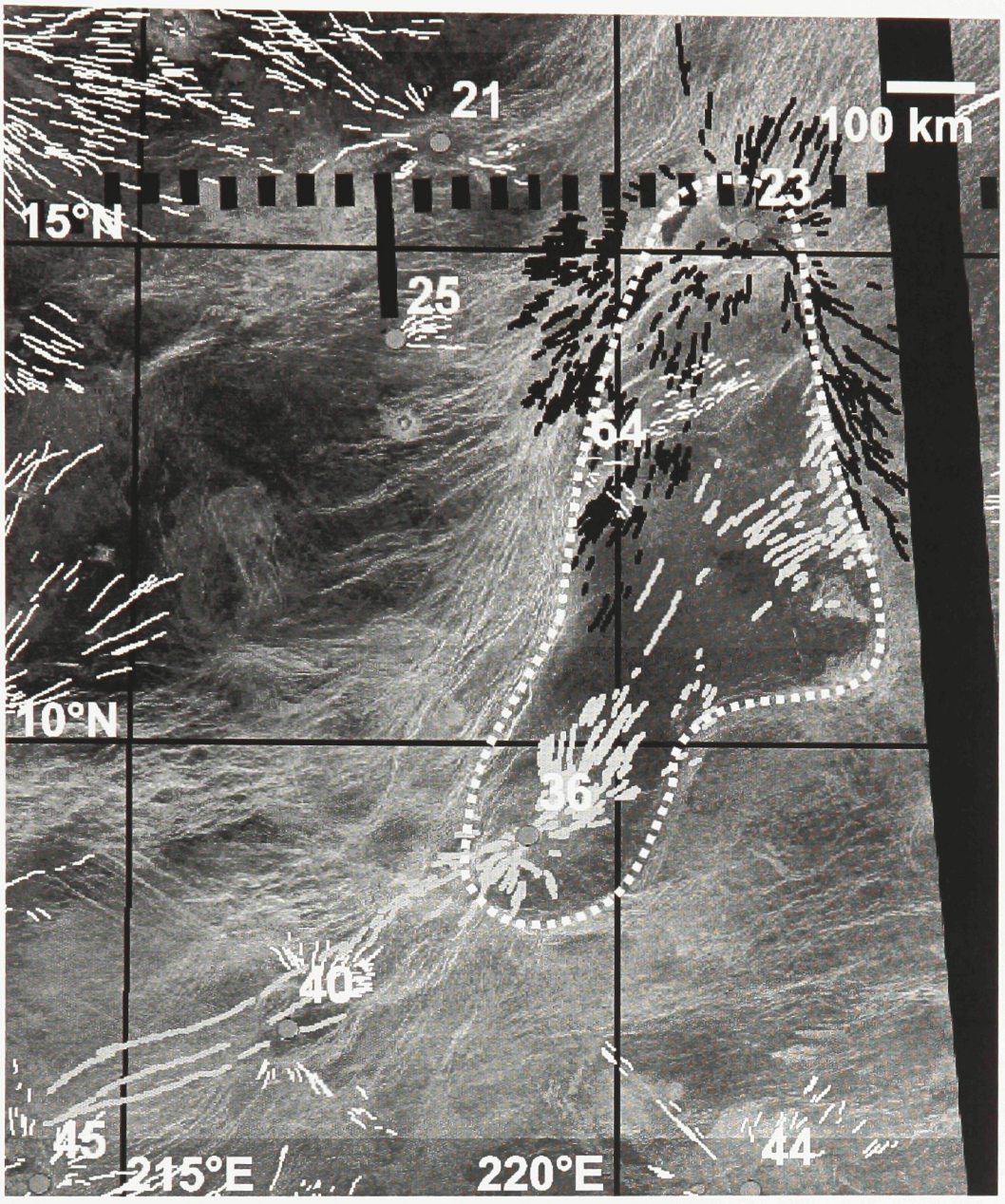

Figure 3.34. SAR image and mapping of radiating systems associated with Zisa Corona. System 23 is shown by thick black lines, system 36 by thick grey lines, and other systems by thin white lines. The dashed white line shows the corona rim.

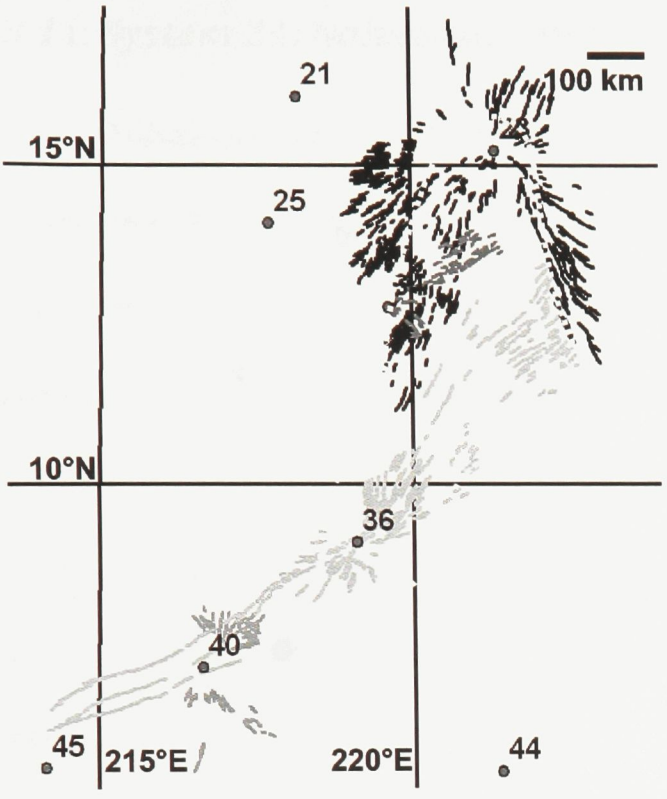

Figure 3.35. Mapped graben and fissures related to radiating systems 23 (black), 36, 40, and 64 (in progressively lighter shades of grey).

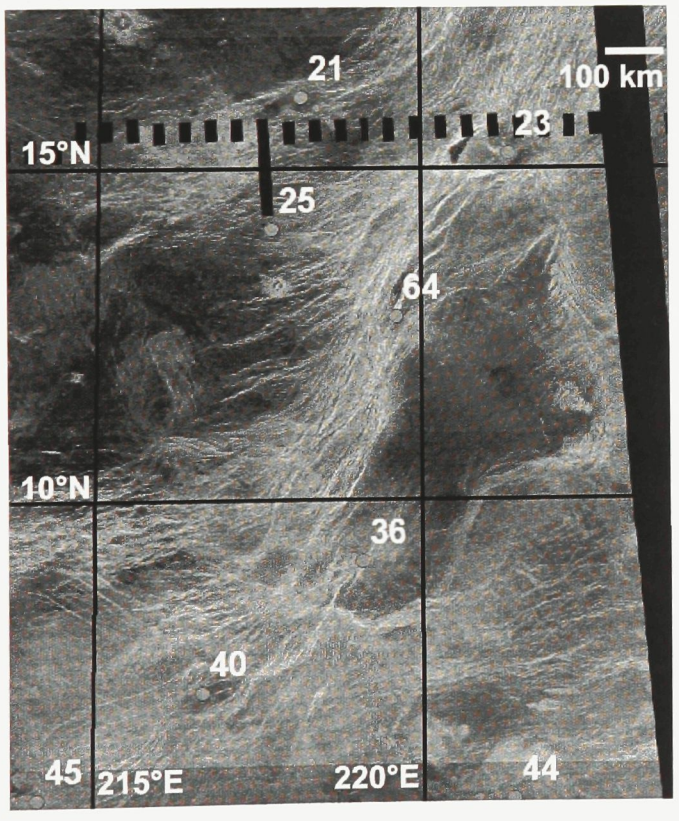

Figure 3.36. Magellan SAR images of the Zisa Corona region.

3.11. System 24: Nahas-tsan Mons (14.5°N, 204.5°E)

Nahas-tsan Mons is a large volcano within a corona in the western portion of the study area. It has an officially listed diameter of 500 km[8] (Figures 3.37, 3.38, and 3.39). During this project, a central elevation of 6057.5 km, 5.7 km above the planetary mean radius, and a maximum radius of 240 km were identified. The wide central plateau inside the corona rim structure has a maximum radius of 106 km. The radiating system consists of 321 graben extending up to 508 km from the centre. The volcano sits on the western edge of the Hecate Chasma rift system, extending north-northeast from Ozza Mons.

The corona rim structure is well defined to the northwest and southeast, and overprinted by the radiating system to the southwest and northeast, suggesting equivalent times of formation. There is a single graben from the radiating system identified within the rift belt, which would indicate that the centre predates the rifting event. In addition, lobate lava flows emanating from the volcano can be seen to be overprinted by lineaments in the rift belt.

At a distance of 400 km southwest of the centre of system 24 lie systems 29 and 30, themselves separated by 50 km. They are both small volcanoes with small radiating graben-fissure systems, and cross-cutting relationships cannot be determined between their radiating systems nor with system 24. A graben from system 24 appears to cross the topographic structure of system 30, and is well defined even on what appear to be

[8] http://planetarynames.wr.usgs.gov/jsp/SystemSearch2.jsp?System=Venus

associated lava flows. It appears then that system 30 is older than system 24. Lobate flows which appear to originate from the centre of system 29 do obscure graben in system 24, indicating that the centre has at least been volcanically active more recently than when radiating system 24 was formed.

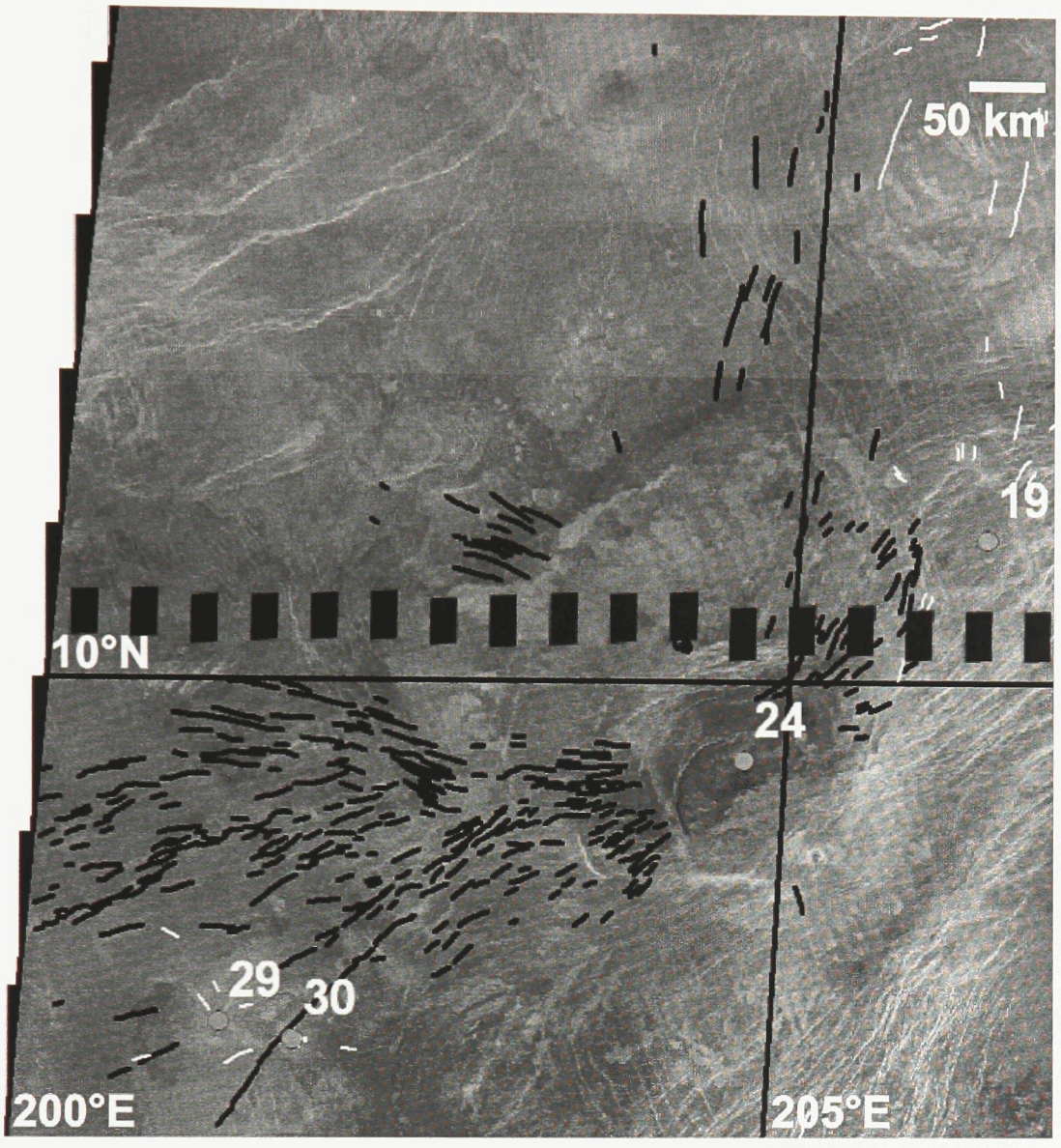

Figure 3.37. SAR images and mapping of radiating system 24 (thick black lines) and other nearby radiating systems (thin white lines).

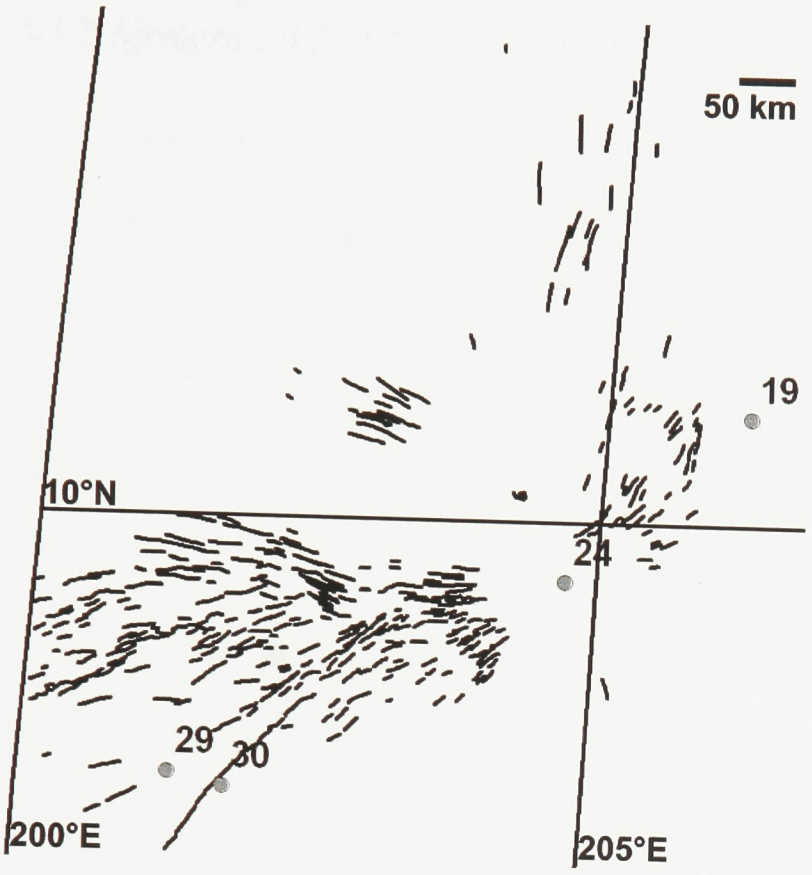

Figure 3.38. Mapped graben and fissures belonging to radiating system 24.

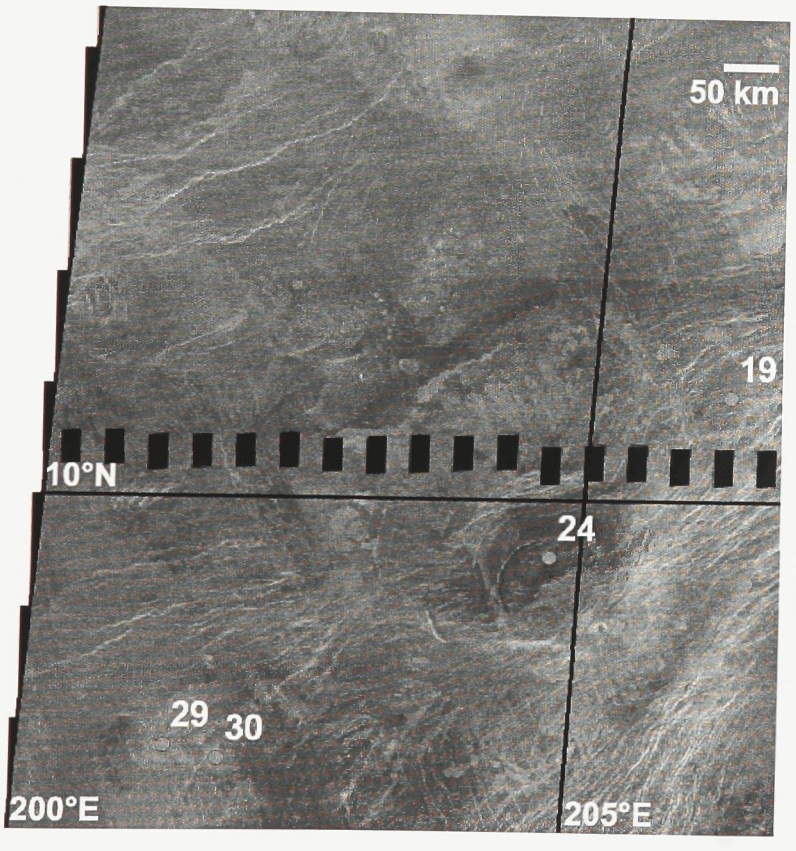

Figure 3.39. Magellan SAR images of the region around system 24.

3.12. System 28 (12.5°N, 226°E)

Radiating graben-fissure system 28 (Figures 3.40, 3.41, and 3.42) is within a cluster of systems to the east of Zisa Corona, sitting on an arm of the Hecate Chasma rift system. System 28 consists of 205 mapped graben and has a maximum radius of 527 km. The centre of the system is partially surrounded by a corona rim structure (to the north and south), which is accompanied with topographical depressions. Within the rim is an elevated plateau, which continues to the east towards another corona and radiating system 27. To the west the plateau has a gradual drop off. The centre of system 28 is slightly elevated above this plateau, and has an elevation of 6057.6 km, 5.8 km above the planetary mean radius.

The corona rim structure is largely defined by dense radiating fractures. Since these radiating fractures are not broken by circumferential structures, it suggests that the rim formed first, and was then overprinted (but not altered topographically) by the radiating system. The rim and associated circumferential depressions are somewhat parallel to the direction of the arm of the Hecate Chasma rift system in which the system is centred. It is also possible that the radiating system and corona formed concurrently with the rifting, leading to the formation of corona rims and trenches parallel to the rift lineaments and gentle downward slopes dipping parallel to the those same rift lineaments. The radiating system appears to cut across rift structures beyond the corona rim, suggesting that it may be at least partially younger than the rift arm.

To the east of its centre, radiating system 28 both cuts and is cut by the corona rim lineaments associated with system 27. Some graben of system 28 are found within the corona of system 27; in addition graben from system 28 appear to form the southwest portion of system 27's corona rim. This might indicate that system 28's activity ceased at a later date than that of system 27.

Northeast of the system's centre, graben in system 28 meet south-trending graben associated with system 6. Here, 450 km from the centre, the graben are poorly defined and are clearly cut by well defined graben from system 6, confirming that system 6 is younger than system 28.

Southwest of the system's centre, graben from system 28 intersect graben from system 35. Here system 28 is better defined and cuts across graben of system 35, and is likely the younger of the two.

There are lobate lava flows associated with system 28 arrayed primarily to the north and south of the centre, outside the corona rim (figure 3.39). In those regions with these flows, there are comparatively few radiating graben. It seems likely from the flow directions and source regions of these flows that they are fed by and likely younger than the graben of system 28.

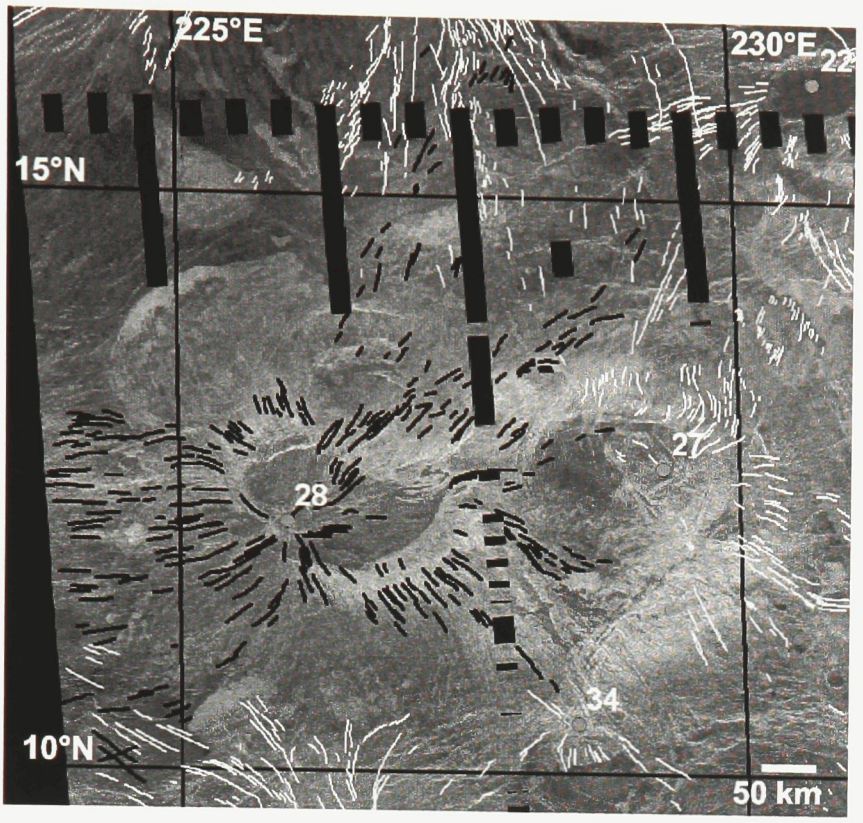

Figure 3.40. Mapped radiating graben-fissure systems overlaid on Magellan SAR image; thick black lines represent system 28, thin white lines represent other radiating systems.

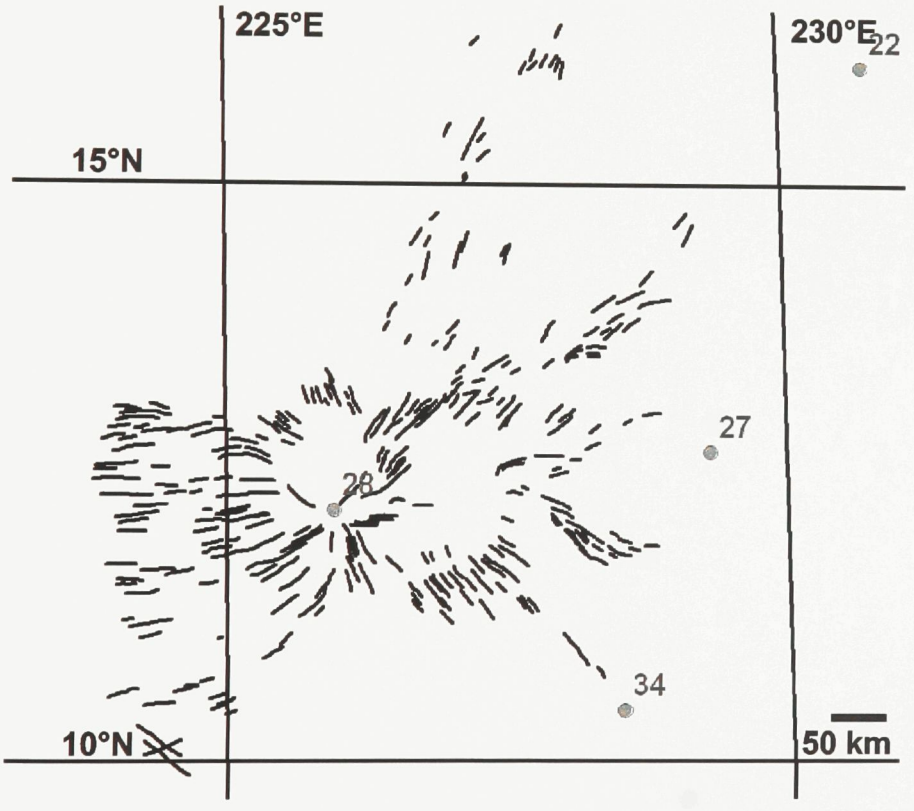

Figure 3.41. Mapped graben of radiating graben-fissure system 28.

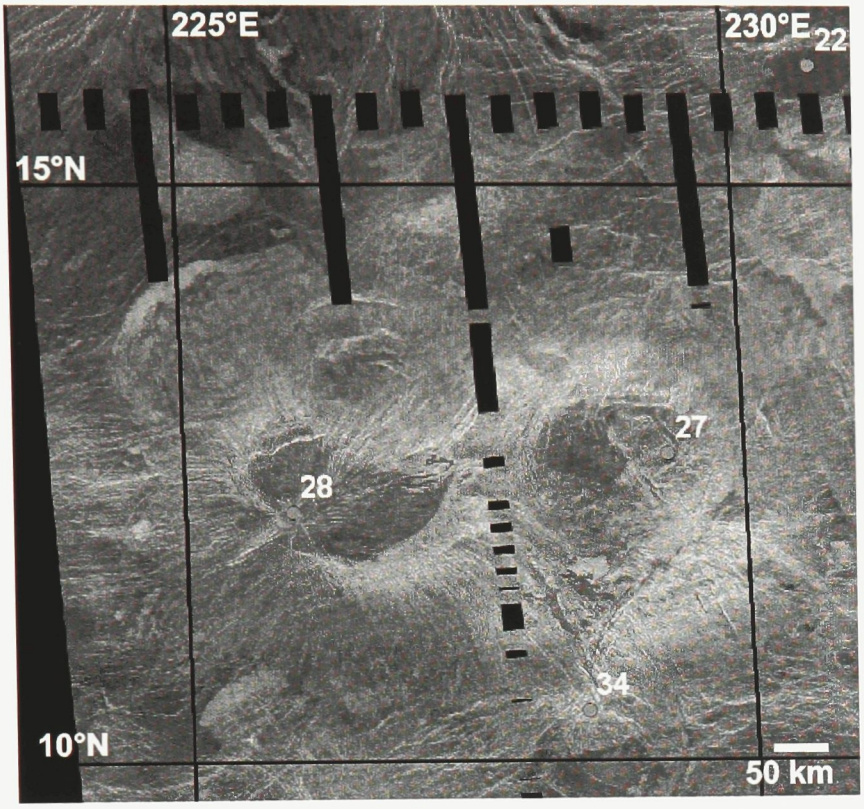

Figure 3.42. Magellan SAR image of radiating system 28.

3.13. System 33 (10°N, 212.5°E)

System 33 sits on an arm of the Hecate Chasma rift system which trends east-west in the vicinity of the radiating system centre (Figures 3.43, 3.44, and 3.45). It consists of 313 mapped graben and has a maximum radius of 581 km. System 33 has a central elevation of 6053.7 km, 1.9 km above the planetary mean radius. There is no significant topographical feature associated with system 33 other than the deep canyons of Hecate Chasma. While there are some circumferential lineaments associated with the system centre, there is no actual corona rim structure.

The topographic lows associated with Hecate Chasma extend through the centre of system 33, indicating that the system likely predates the rifting activity.

Graben from system 33 intersect graben from system 47 both to the north and south of the centre. In each area of intersection, the graben of system 33 can be seen cutting system 47. It is likely that system 33 is younger than system 47.

To the northwest of the system centre, there is an intersection with a graben from system 32. Here, it appears that the graben from system 33 is offset as it crosses the graben from system 32. This is a clear indication that system 32 is the younger of the two providing the offset is due to strike slip faulting along the graben and not a younger dyke intersecting and tracking along an older dyke before ultimately cross-cutting it.

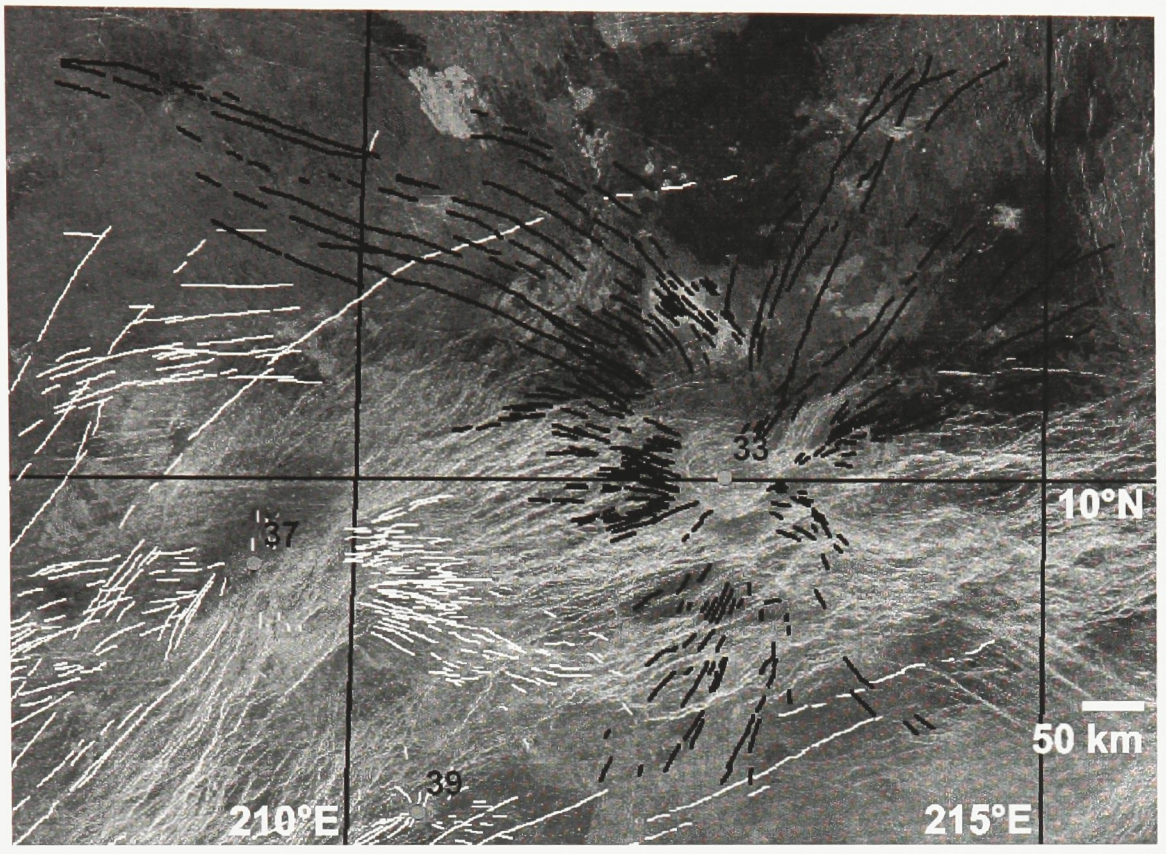

Figure 3.43. Mapped radiating graben-fissure systems overlain on a Magellan SAR image; systems 33 is represented by thick black lines. White lines represent other radiating systems.

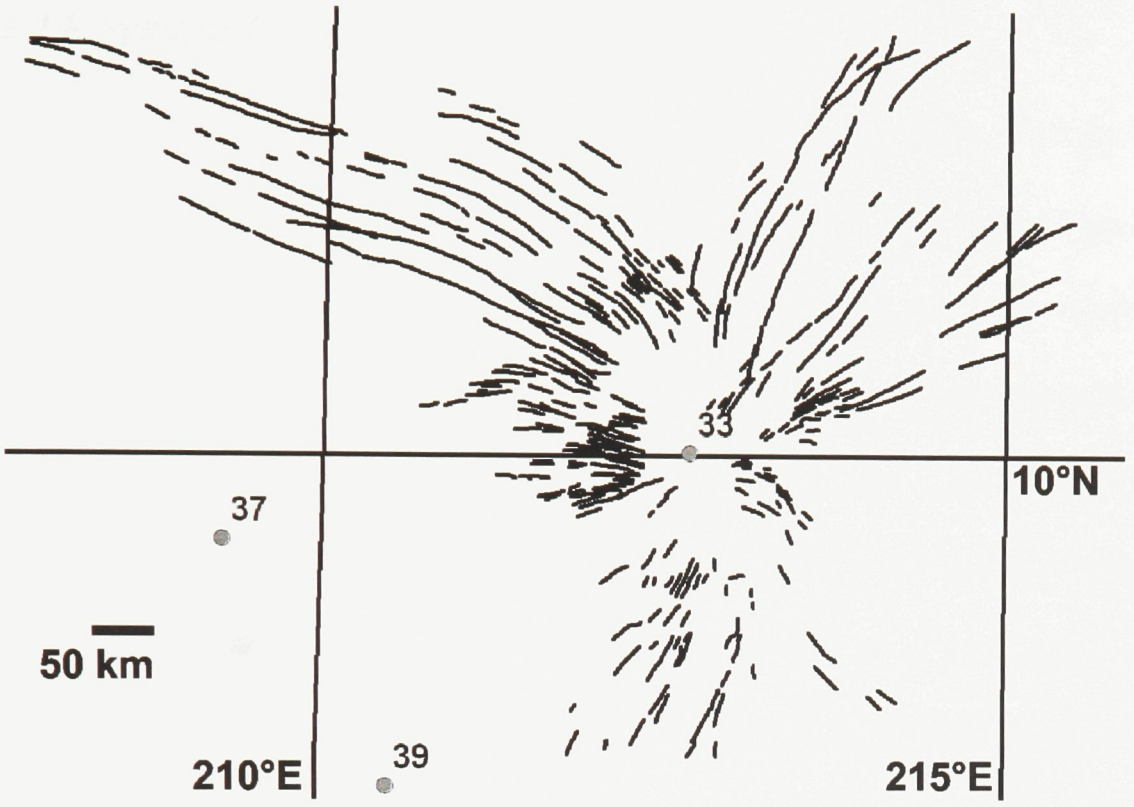

Figure 3.44. Mapped graben of radiating graben-fissure system 33.

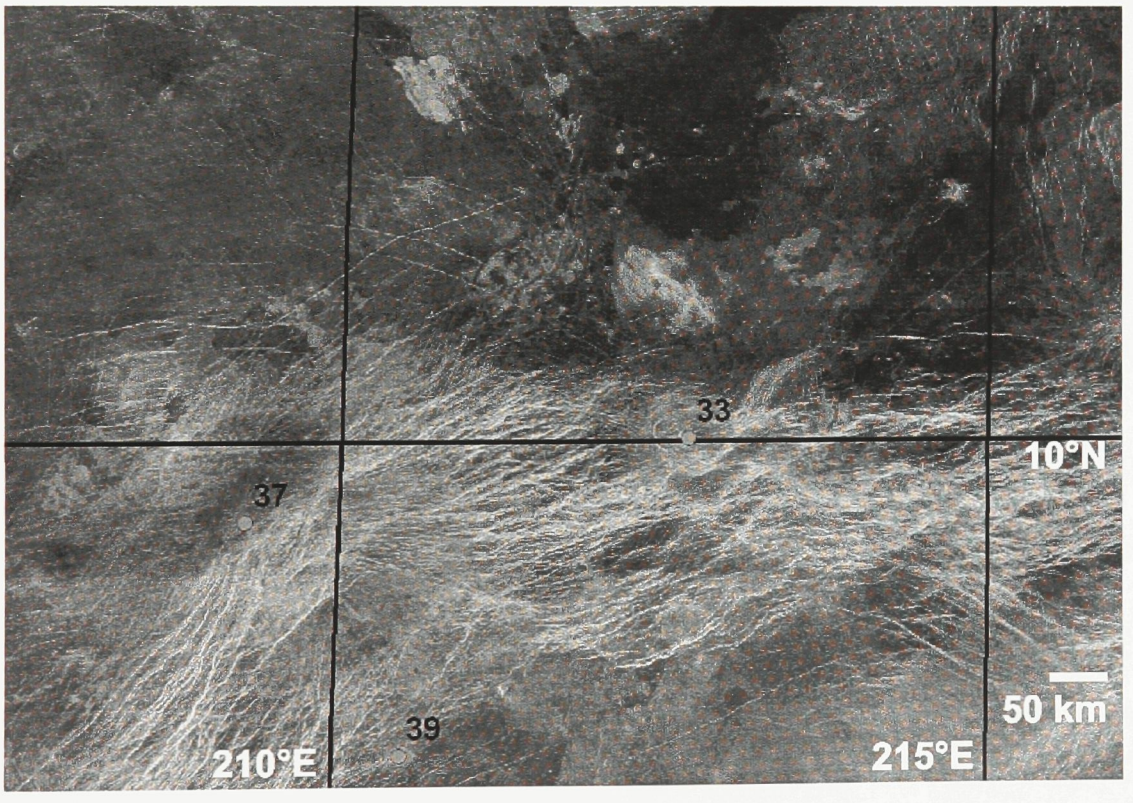

Figure 3.45. Magellan SAR image of radiating system 33.

3.14. System 47: Ozza Mons (4.5°N, 201°E)

Ozza Mons is a large volcano with an officially listed diameter of 500 km[9]. As mapped during this project, the central rise has a maximum radius of 300 km while the entire topographic rise associated with the volcano has a maximum radius of 970 km. System 47 (4°N, 199.5°E) is centred on Ozza Mons, and is the largest system in the study area, including 1508 individual graben extending up to 1985 km from the centre (Figures 3.46, 3.47, and 3.48). The elevation of centre region of system 47 is 6061.8 km, 10.0 km above the planetary mean radius. There does appear to be a central corona-like structure, which corresponds neatly with the plateau-like central topographic high. The centre of system 47 also sits just off the western edge of the study area, so only interactions with other systems and structures within the study area will be considered.

Many of the graben and fissures on the flanks of the volcano are either flooded by abundant lava flows or obscured by high albedo features. The majority of mapped graben in system 47 are at least 400 km removed from the centre; however, there is a clear radiating pattern to these distant mapped graben with trends that converge. Graben are continuous from the centre towards the north-northwest.

The Hecate Chasma rift zone has its western termination at Ozza Mons; there are two rift belts that approach the volcano from the northeast and north-northeast. Topographical depressions associated with the two rift belts only reach to within 600 and 730 km of the centre of system 47.

---

[9] http://planetarynames.wr.usgs.gov/jsp/SystemSearch2.jsp?System=Venus

At a distance of 617 km north of the centre of system 47, graben in the associated system intersect with system 31. In this area, it is clear that system 47 is obscured by graben and flows associated with system 31, the latter therefore being the youngest of the two systems. In particular, one graben in system 47 trends directly through the centre of system 31, and while being seen on either side of the centre, it is obscured for 43 km in the vicinity of the centre.

System 32 is centred 879 km north-northeast of the centre of system 47. It is located on the previously mentioned north-north-easterly rift belt. The interactions between the two radiating systems are difficult to interpret. It appears that in close proximity to the centre of system 32, to the west and north, system 32 cuts system 47 and is clearly more continuous. However, further removed from the centre, to the west and southwest, system 47 appears to be the better defined and more continuous of the two systems. It is probable that this contradiction indicates a simultaneous period of emplacement.

System 38 sits in the north western rift belt, 900 km from the centre of system 47. System 38 intersects with system 47 to the west of the centre. Where individual graben intersect, those of system 47 appear dominant and unbroken, and therefore system 47 is younger than system 38. This interpretation, however, may be somewhat influenced by the relative sizes of the graben in each system; graben in this part of system 47 are quite wide (1-1.5 km) and provide strong radar responses, while graben in system 38 are a fraction of the size (300-500 m) with comparatively weaker radar

responses. The same set of graben in system 47 also intersect with those of system 39.These intersections are more consistent with no graben from system 39 being continuous across any intersection with a graben from system 47. From these relationships it is clear that system 47 is younger than system 39.

System 37 is on the western edge of the same rift belt, 1158 km away from system 47. The two systems intersect to the west of the centre of system 37. While most individual intersections are ambiguous and difficult to interpret, there are two instances where the graben from system 47 are clearly offset on either side of an intersection with graben in system 37. This would indicate that system 37 is the younger of the two.

System 33 is centred 1505 km northeast of the centre of system 47; and their respective radiating systems intersect approximately 250 km northwest of the centre of system 33. In the region of intersection, there are 2 points where a graben from system 47 is offset by a graben in system 33. It is clear that here system 33 is the younger of the two.

System 46 is located 950 km east-northeast of the centre of system 47. The two radiating systems intersect to the southwest of the centre of system 46, where graben in system 47 appear to clearly cut across graben in system 46. System 47 was likely emplaced more recently than system 46. Further along the same set of graben in system 47, 1520 km from the radiating centre, the graben pass by the centre of system 45. The graben set appears to separate into two individual subsets which enclose the

centre of system 45. There is one single intersection between the two systems with an ambiguous interpretation, and therefore the relative timing is uncertain.

The centre of system 58 lies 510 km southeast of the centre of system 47, and just off the south edge of the study area. Where the systems intersect, northeast of the centre of system 58, the fracturing is too dense to interpret the cross-cutting relationships. However, within 200 km of the centre of system 58 there are abundant graben from system 47 but none from system 58. It seems likely then that system 58 is older and has been overprinted by more recent activity of system 47.

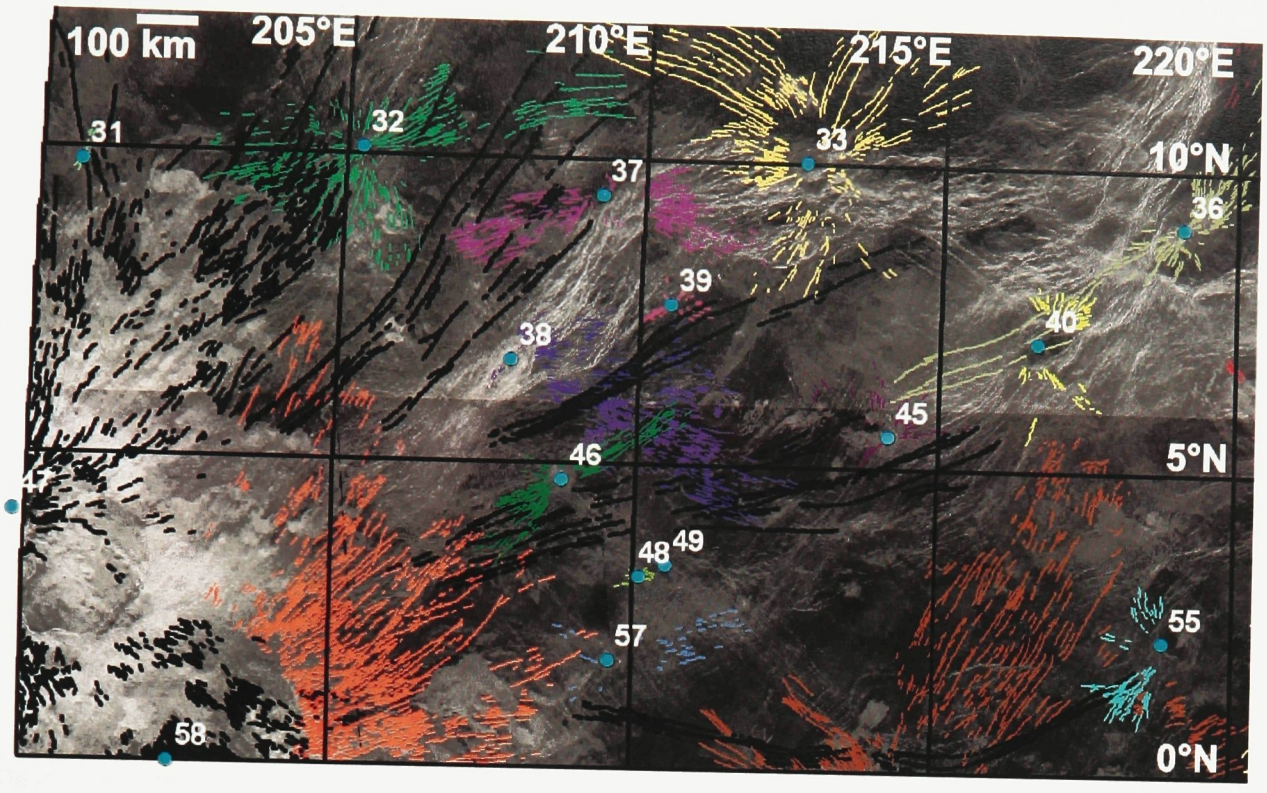

Figure 3.46. Mapping of system 47 and neighbouring systems overlain on Magellan SAR image. System 47 is in thick black lines, thin lines of other colours denote other radiating systems.

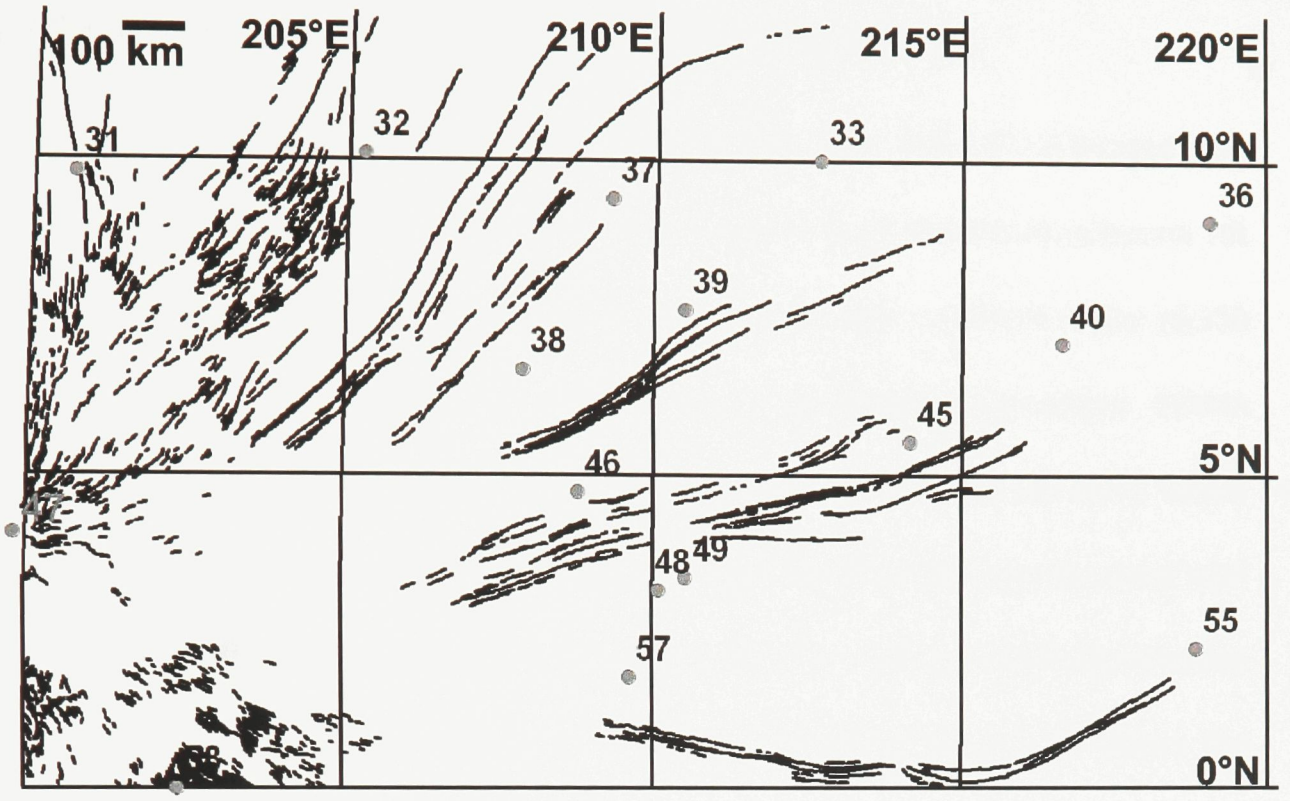

Figure 3.47. Mapped graben and fissures belonging to radiating system 47.

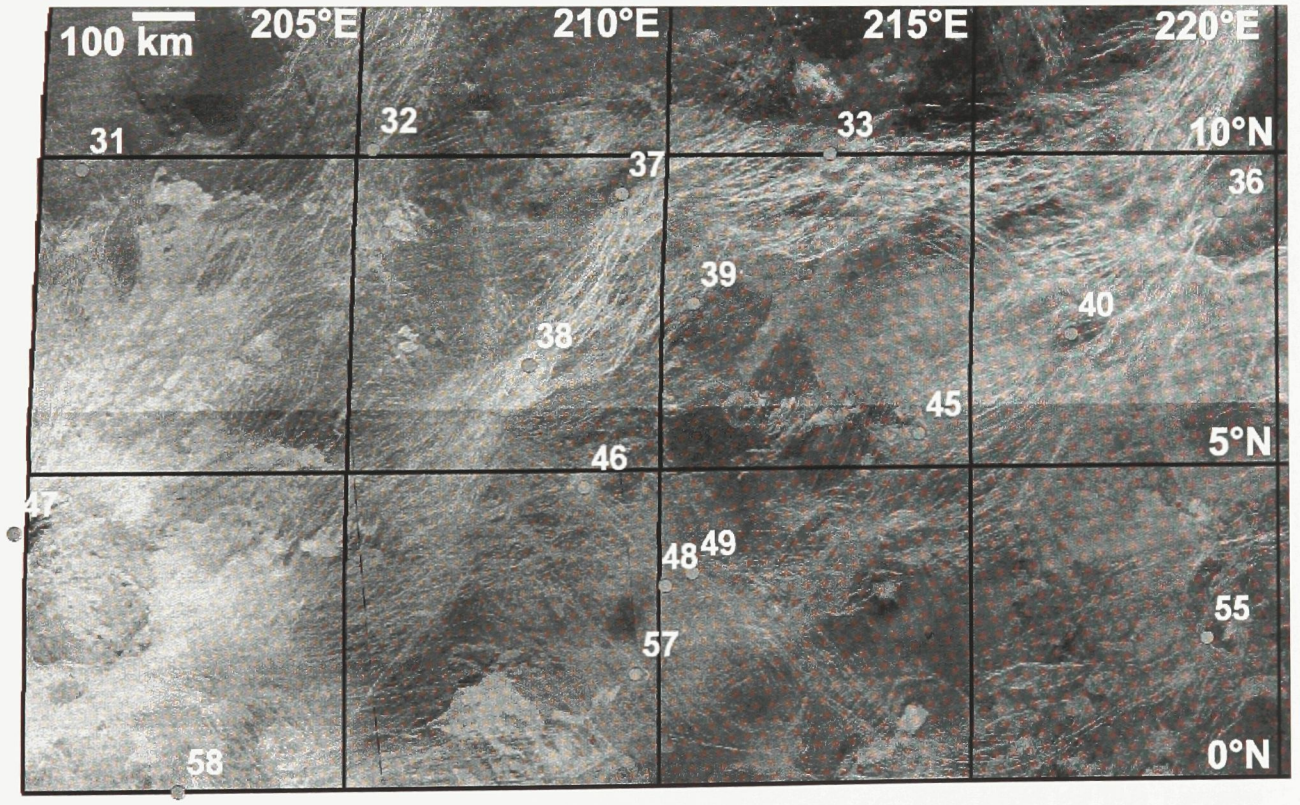

Figure 3.48. Magellan SAR images of the region around system 47.

3.15. Systems 52 and 62 (2.5°N, 236.5°E & 0°N, 237°E)

Radiating graben-fissure system 52 (Figures 3.49, 3.50, and 3.51) is located near the southeast corner of the study area. It is on an arm of the Hecate Chasma rift system. System 52 consists of 134 mapped graben and has a maximum radius of 350 km. The centre of the system is surrounded by a raised corona rim structure. Within the rim is a plateau, with a steep drop-off beyond the rim, except to the west, where there is a long downward slope. Stofan et al. (1992) classified this corona, along with the corona associated with system 62, as type "multiple" according to their classification scheme. The centre of the system has an elevation of 6055.3 km, 3.5 km above the planetary mean radius.

Radiating system 62 also has a corona rim structure. The rim is slightly elevated, but inside the rim the ground is noticeably depressed. It appears to be a caldera. The centre of the system has an elevation of 6053.6 km, 1.8 km above the planetary mean radius. The corona rim is fairly consistent in appearance around the centre. However, Its lineaments do turn outwards at the southwest – which coincides with the gentle slope mentioned previously. At the south side of the rim, it appears to be tangent to the rim structure associated with radiating system 62. The system 52 corona rim structure may also be partially formed by – or simply parallel to – radiating graben from system 62 along the southwest and southeast sides.

Systems 52 and 62 are centered in a location where two arms of the Hecate Chasma rift zone converge. Rifting is seen to the east and west of the system centres, as

well as to the northeast. Since none of the rift lineaments are seen to cross the centres of the systems within the corona rims, it is probable that systems 52 and 62 are younger than the rifting activity.

Systems 52 and 62 intersect to the east and southwest of the centre of system 52. At the east intersection, system 52 is better defined and does cut graben from system 62. At the southwest intersection, a zone of dense fracturing related to system 52 completely overprints graben from system 62. It is clear that system 52 is the younger of the two.

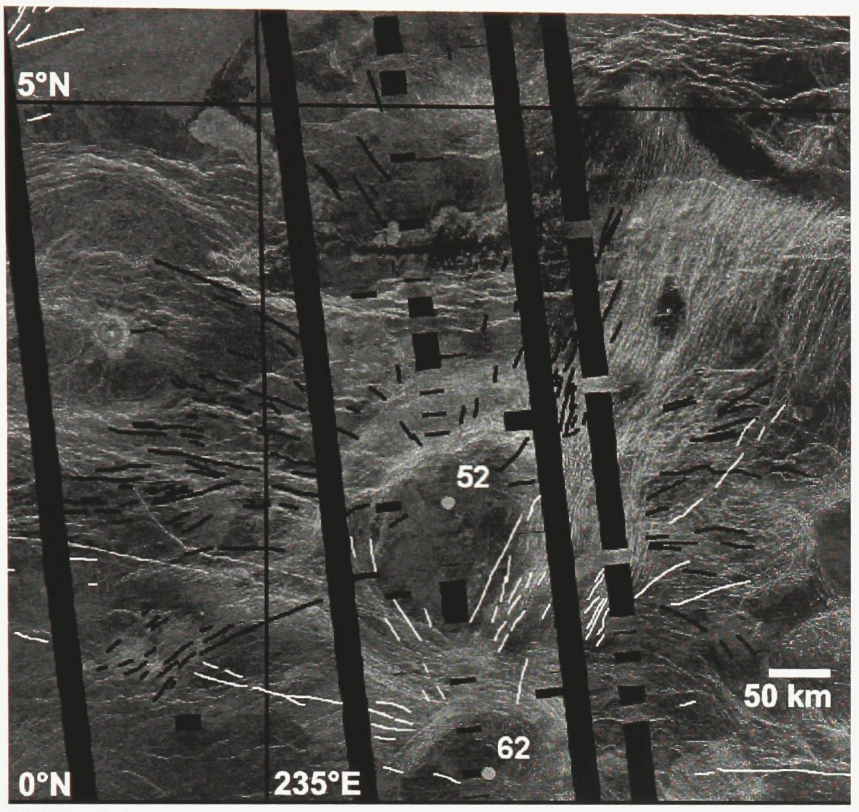

Figure 3.49. Mapped radiating graben-fissure systems overlaid on Magellan SAR image; thick black lines represent system 52, thin white lines represent other radiating systems, most particularly, system 62.

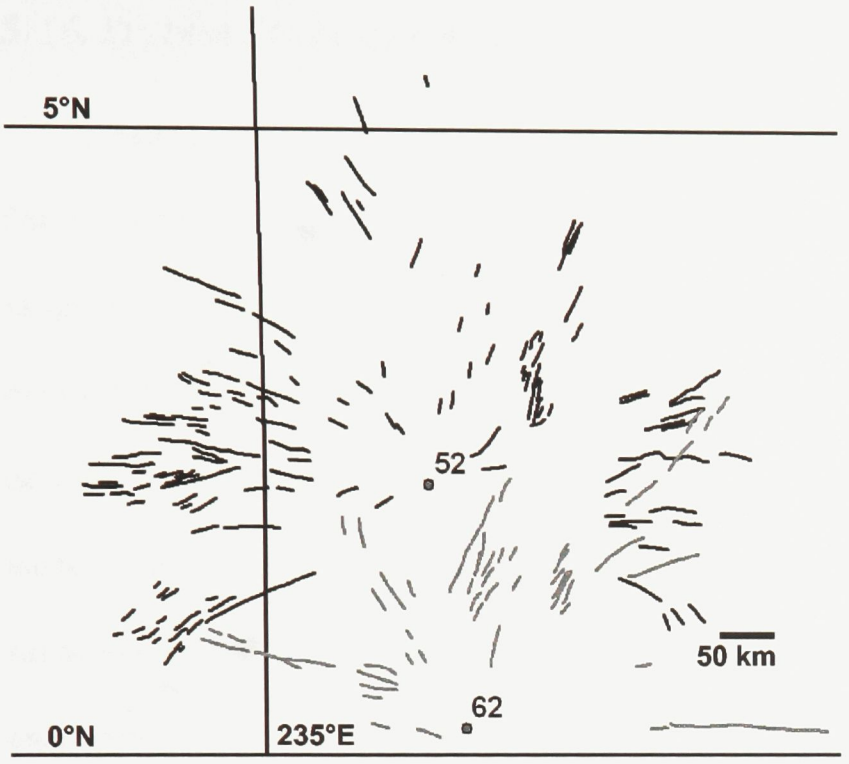

Figure 3.50. Mapped graben of radiating graben-fissure systems 52 (black) and 62 (grey).

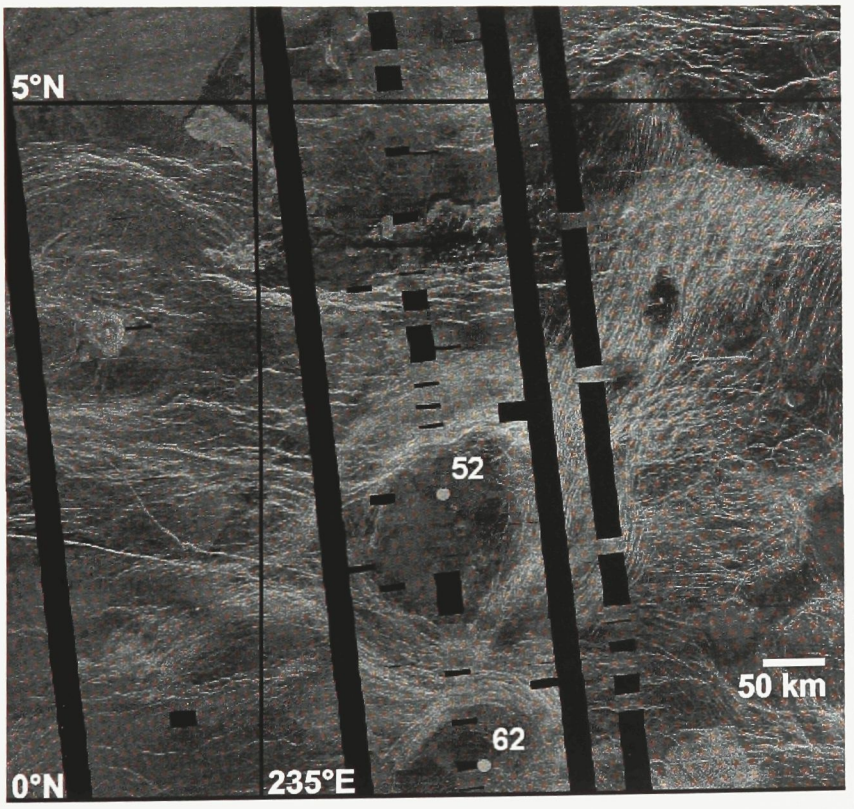

Figure 3.51. Magellan SAR images of radiating systems 52 and 62.

3.16. System 54: Lengdin Corona (2°N, 222.5°E)

Radiating graben-fissure system 54 is mostly contained within the rim of Lengdin Corona, near the southern edge of the study area (Figures 3.52, 3.53, and 3.54). Lengdin Corona is identified as having a diameter of 525 km[10]; 205 graben have been mapped in system 54, which has a maximum radius of 527 km. Lengdin Corona occupies a raised plateau, which is bordered by a steep-sided depression along the eastern side of the corona, and is bordered by a gentle slope along the western edge. According to the classification scheme of Stofan et al. (1992), Lengdin would be labelled an asymmetric corona. The centre of the system is elevated above this plateau, and has an elevation of 6056.6 km, 4.8 km above the planetary mean radius.

Lengdin Corona is surrounded by a well-defined rim structure, which largely appears to contain the graben of radiating system 54 except for in the south-western direction. A minor arm of the Hecate Chasma rift system crosses the north end of the corona. The corona rim can be followed across the set of rift lineaments that cross the corona. However there is a significant topographic drop associated with the rift structures and the northern extent of the corona rim sits 1-1.5 km below the rest of the structure. It appears that the rifting activity is more recent than the formation of Lengdin Corona.

System 54 is centred near the south-western edge of Lengdin Corona and it appears that the corona rim may have some effect on the ability of the radiating graben

[10] http://planetarynames.wr.usgs.gov/jsp/SystemSearch2.jsp?System=Venus

to propagate beyond the rim. It should also be noted that solitary graben have been mapped as belonging to system 54 beyond the corona rim to the northwest and northeast of the centre.

This is interpreted to suggest that the radiating system is younger than the corona rim, and that the corona rim provides a significant structural barrier to the propagation of the radiating graben. In this scenario, it is only where the extensional stresses relating to the formation of the radiating system are highest – near the centre – that they are strong enough to cross the corona rim barrier. However, the interplay between radiating systems and coronae rims is a subject that requires more in-depth study than could be completed during this project. Using the interpretation used for other corona-radiating system interactions within this project, the alternating cross-cutting relationships would indicate a more simultaneous period of formation for the corona rim and the radiating graben-fissure system.

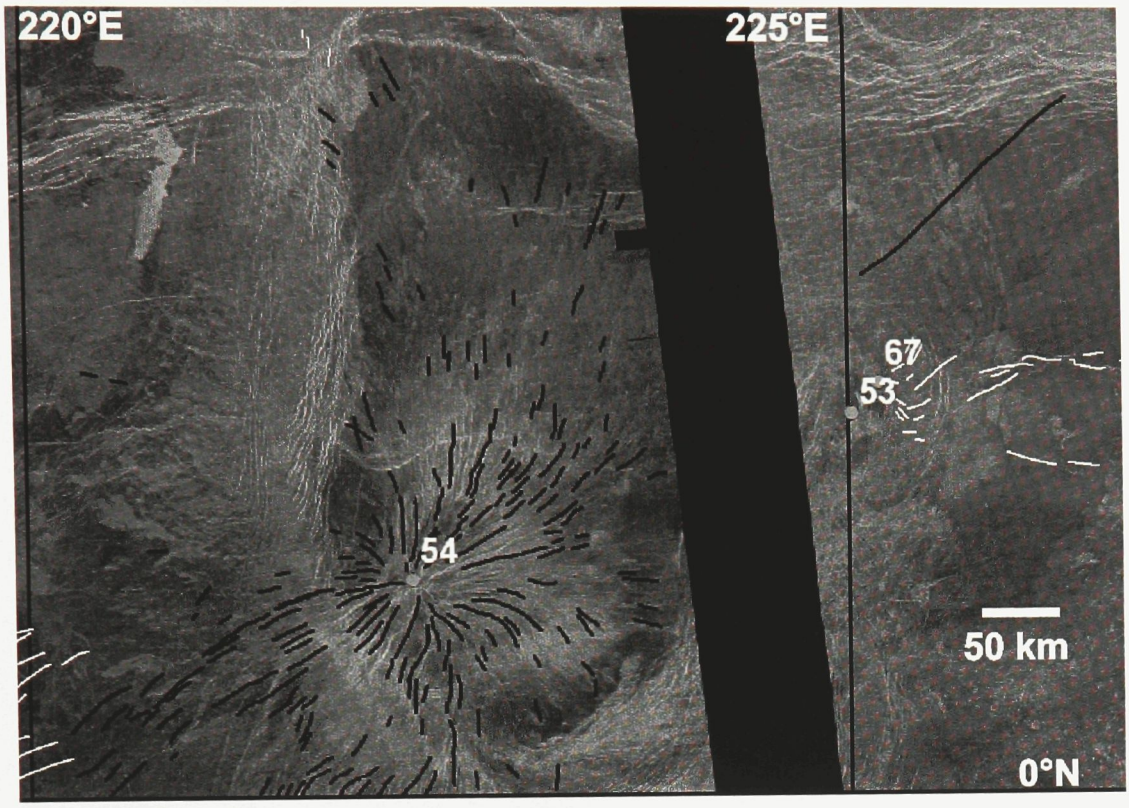

Figure 3.52. Mapped radiating graben-fissure systems overlain on a Magellan SAR image; thick black lines represent system 54, thin white lines represent other radiating systems.

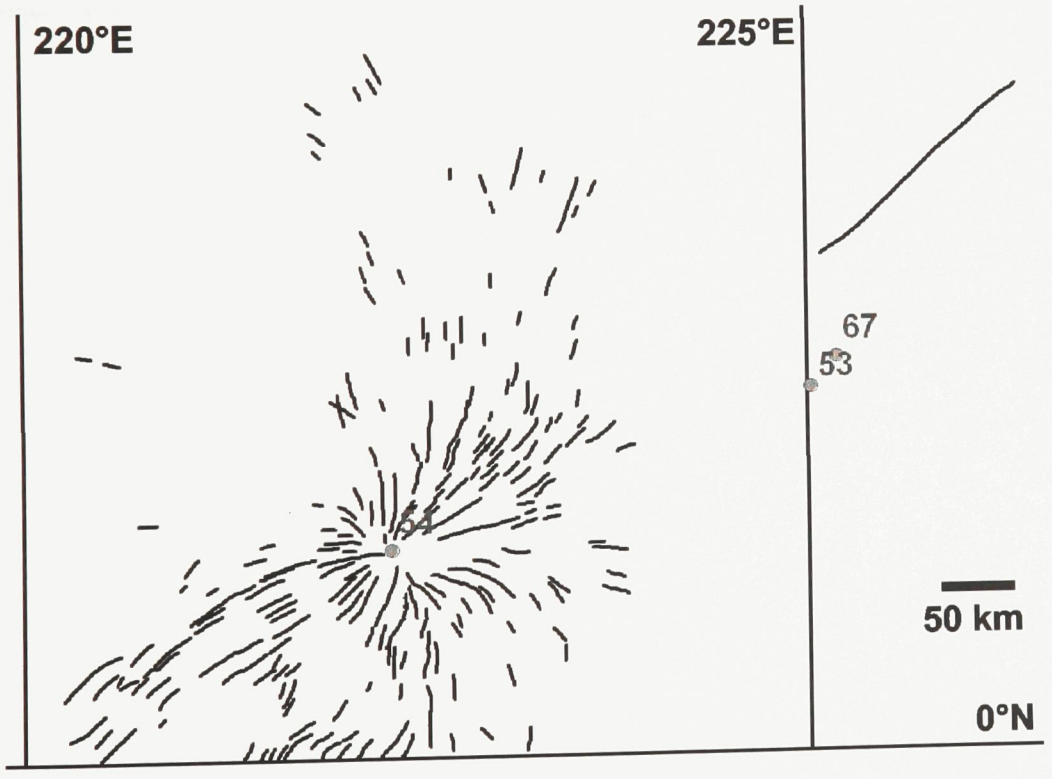

Figure 3.53. Mapped graben of radiating graben-fissure system 54.

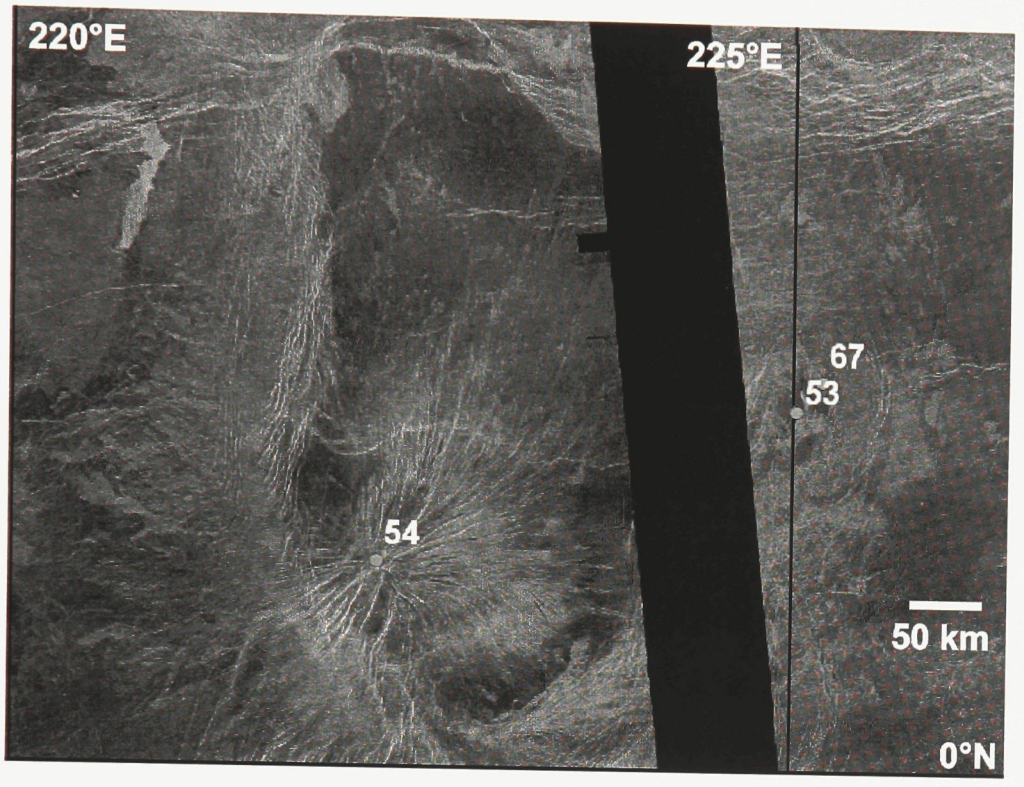

Figure 3.54. Magellan SAR image of radiating system 54.

3.17. System 58 (0°N, 202.5°E)

System 58 is centred just off the south edge of the study area, on the southeastern flank of Ozza Mons. There are 947 individual graben mapped in the system, extending out to a maximum radius of 805 km (Figures 3.55, 3.56, and 3.57). The centre of the system sits elevated above its surroundings (except towards the peak of Ozza Mons) at 6061.3 km, 9.5 km above the planetary mean radius. Due to the location of the system on the edge of the study area, only graben to the north and east of the centre are mapped.

System 47 is centred 510 km northwest of centre 58, and just off the south edge of the study area. Where the systems intersect, northeast of centre 58, the fracturing is too dense to interpret the cross-cutting relationships. However, within 200 km of the centre of system 58 there are abundant graben from system 47 but none from system 58. It seems likely then that system 58 is older and has been overprinted by more recent activity at centre 47.

System 57 is centred east-northeast of system 58. In the limited intersections between the two systems' graben, it appears that system 57 is the more continuous and younger of the two systems.

Graben from system 58 also intersect with those of system 46, northwest of system 58's centre. Here, too, it is apparent that system 58 is the older system, as graben from system 46 clearly cut several graben in system 58.

From these interactions with other radiating systems, it appears that system 58 may be one of the oldest in the study area.

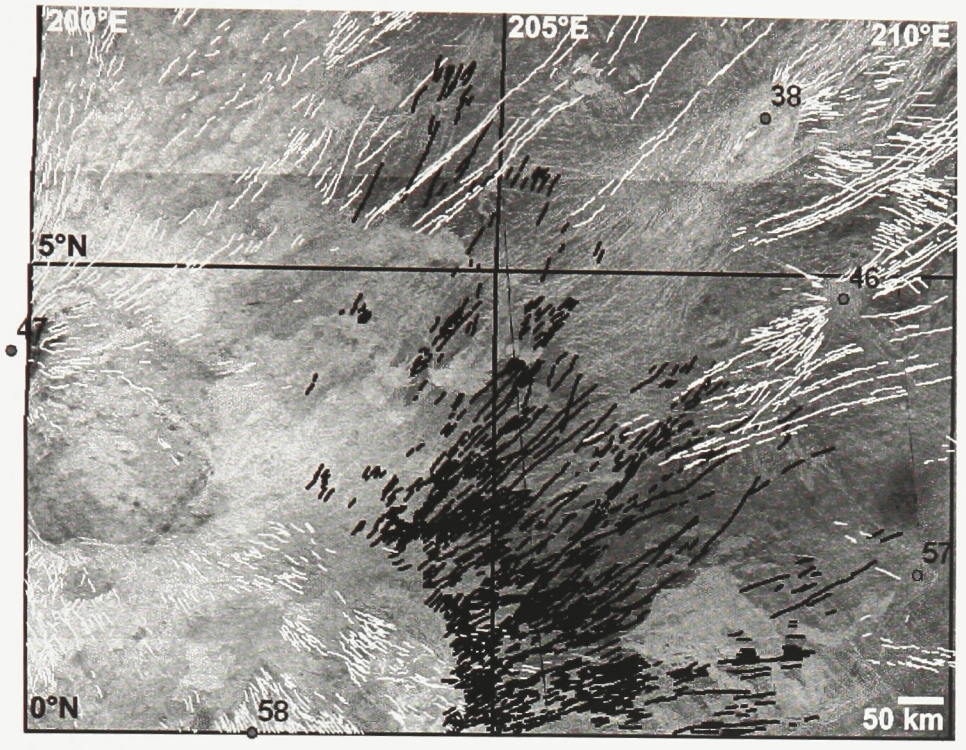

Figure 3.55. Mapping of system 58 and neighbouring systems overlain on a Magellan SAR image. System 58 is in thick black lines, thin white lines denote other radiating systems.

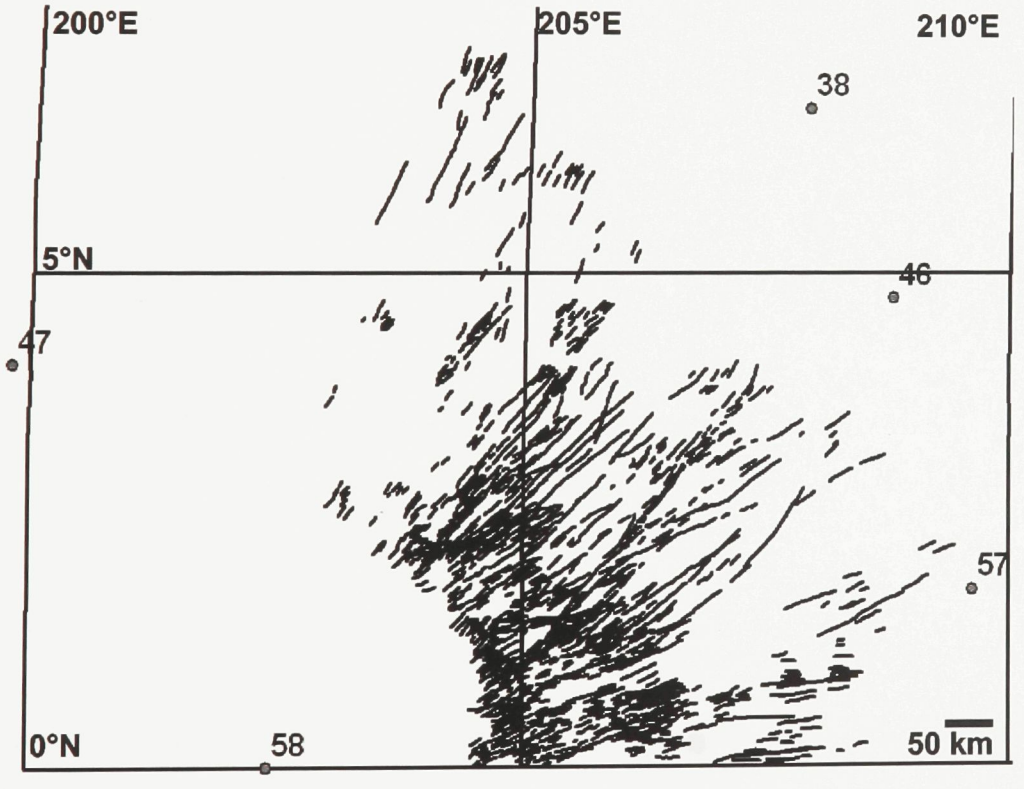

Figure 3.56. Mapped graben and fissures belonging to radiating system 58.

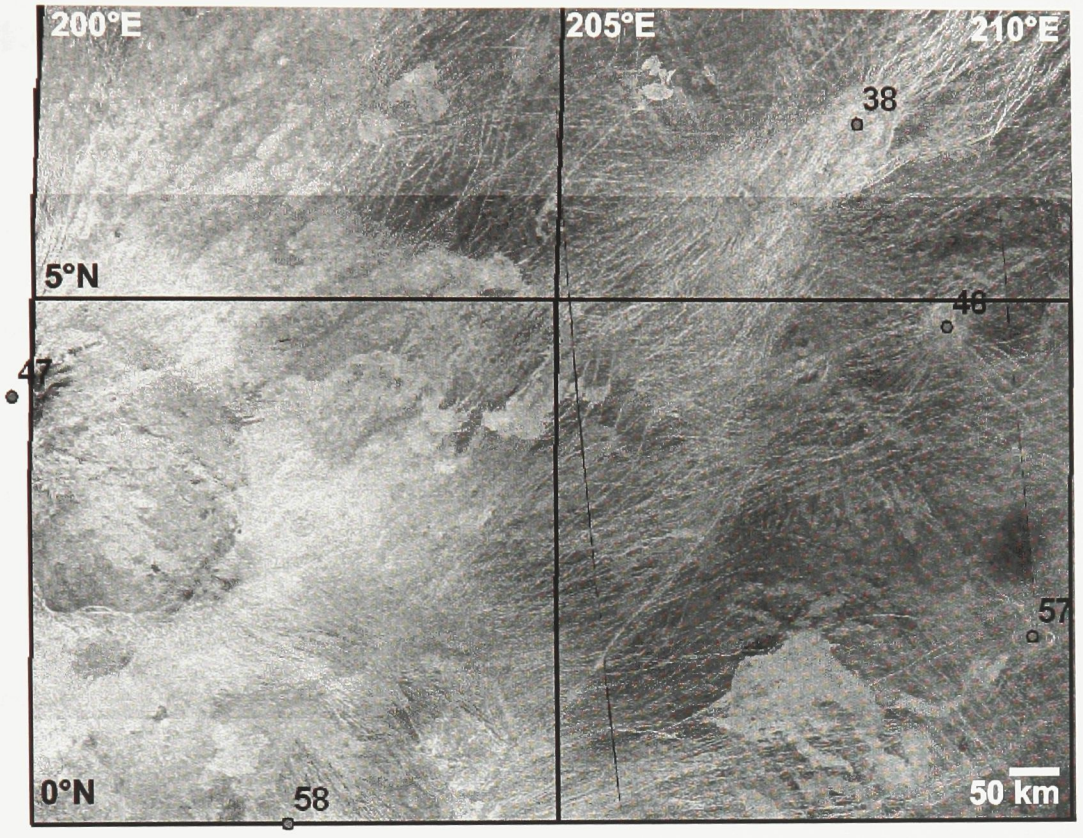

Figure 3.57. Magellan SAR image of the region around system 58.

4.0. Relative Ages of Radiating Graben-Fissure Systems

The cross-cutting relationships between radiating graben-fissure systems and their host geology can give us insight into the relative ages of the systems. The relative age relationships of individual systems are presented in the previous section, and below we provide an overview and regional synthesis of the age relationships in the study area.

It can be seen from the maps (Figure 2.5 and Appendix 2) that although many radiating systems are extensive they do not overlap enough to provide a complete chronology. The best coverage and estimates of relative ages are available for the northeast and southwest (those systems found in the first and largest grouping in Figure 4.1) portions of the study area. However, there are major gaps in coverage between these areas. Hecate Chasma, the rift zone that has deformed much of the study area, provides a useful reference from which we can compare ages of radiating systems from throughout the study area.

A preliminary assessment of relative ages is provided in Figure 4.1, with respect to Hecate Chasma, which is presented as a single point in time. While the rifting undoubtedly took place over an extended period of time; and activity in different arms of Hecate Chasma may have occurred at different times, there are only isolated local perspectives to base the age estimates on. For each radiating graben-fissure system that interacts with Hecate Chasma, I can only determine which feature is more recent or if the two are concurrent for that locale. Making the assumption that Hecate Chasma

has a similar age in all parts of the study area allows the production of a regional chronology between most of the radiating graben-fissure systems in the study area.

In Figure 4.1, each radiating system has been identified with a horizontal line representing their range of possible ages of formation. Time flows from left to right, that is, ages decrease towards the right edge of the figure. The systems were each initially assigned an arbitrary time span, which has been modified where evidence is provided. Where a radiating graben-fissure system has been interpreted to be younger or older than another feature, the representative line has been shortened or lengthened to meet that evidence. For example, system 32 is younger than system 33, so the line associated with system 32 begins at the end of the line associated with system 33. However, system 32 is also recognized to be concurrent in age but slightly older than system 31, therefore the youngest that system 32 could be is still older than system 32. The line depicting system 32's possible age is shortened appropriately. Some of the systems are unconstrained on either their oldest or youngest age and as such are extended to the edge of the figure. Systems in Figure 4.1 are grouped according to cross-cutting relationships. Each system in each group can be related to at least one other system within that group. The groups are separated in the figure by dotted lines. Relative ages between these groups are only comparable through comparison with Hecate Chasma, and therefore may not be reliable.

Systems 0, 1, 19, 20, 25, 26, 34, 41, 44, and 63 can only be related to Hecate Chasma. These systems are included at the bottom of Figure 4.1, separated from the others by a dashed line.

Systems 53 and 67 can only be related to each other and not to Hecate Chasma, the same is true for systems 59 and 68. Systems 48, 49, and 61 cannot be related to any other systems or Hecate Chasma. These systems are not included in Figure 4.1 as they cannot be assigned a relative age.

Projecting the information from Figure 4.1 onto the map of the study area (the map, which includes these data, can be found in Appendix 2) provides a new perspective on the area. A trend is found, with older activity prevalent in the southwest corner of the study area, around Ozza Mons and Atla Regio, and activity becoming younger towards the north and east. This trend is primarily defined by interrelated radiating systems, and is not dependent on ages defined relative to Hecate Chasma. Other systems, with relative ages dependent on the shared association with Hecate Chasma, do still tend to fit the trend. Pani Corona, in the northeast of the study area, is an outlier. It is surrounded by younger activity but its associated systems, 4 and 9, are interpreted to be among the oldest in the study area.

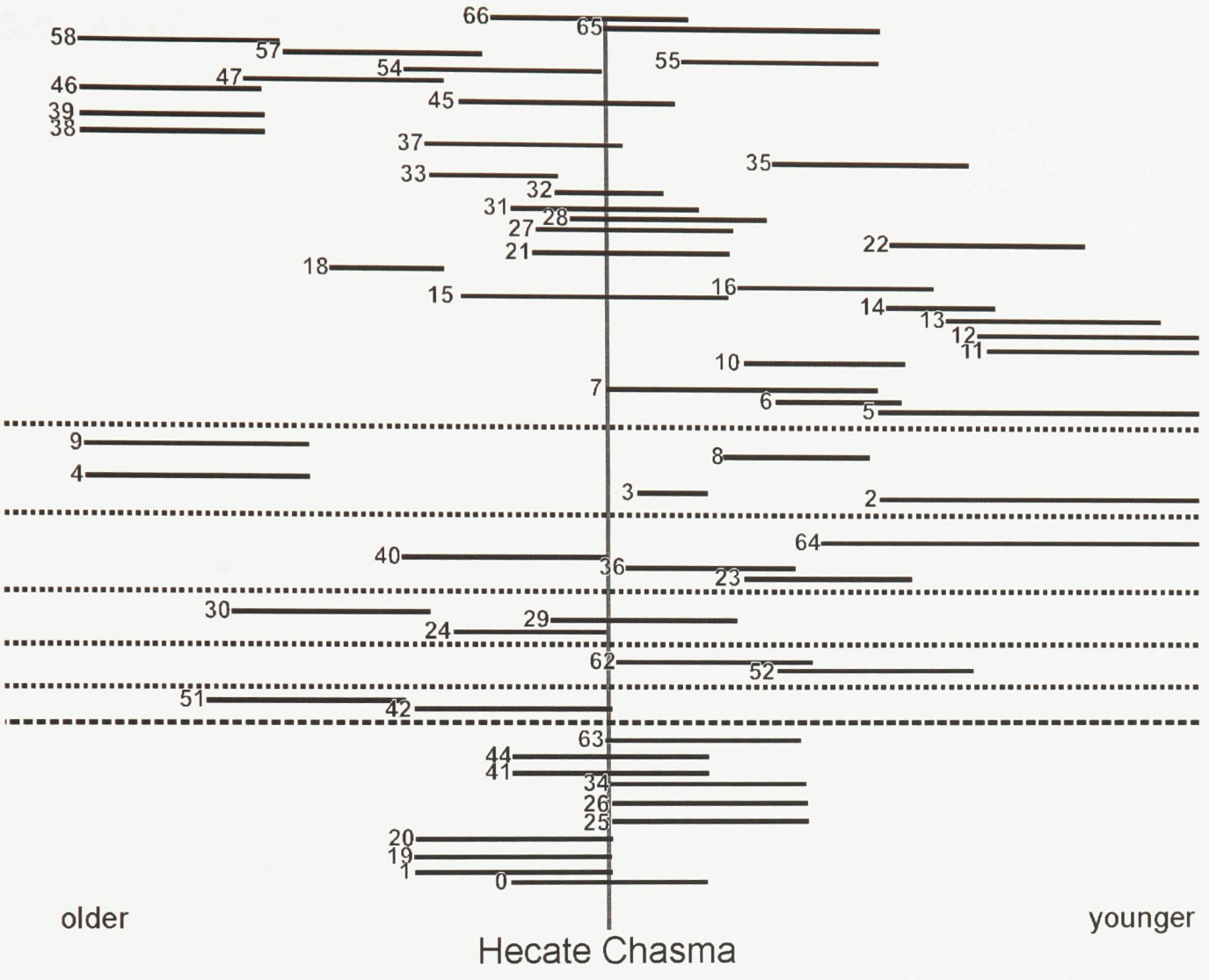

Figure 4.1. Estimated relative ages of radiating graben-fissure systems within the study area. Hecate Chasma is used a reference point to create a more cohesive picture over the entire study area. Radiating systems are identified by number; the range of possible ages of formation is represented by the horizontal lines. Dotted lines separate groups of related systems. Systems below the dashed line are related only to Hecate Chasma.

5.0. Ages of Radiating Centres With Respect To Surface Geology

An examination of the cross-cutting relationships has provided an estimate of the ages of radiating graben-fissure systems, relative to each other (chapters 3.0 and 4.0) and with respect to the faulting of Hecate Chasma (chapter 4.0). In this section we take a look at their ages from a third perspective. We examine the age relations of radiating graben-fissure systems with respect to their host geology.

The host geology is obtained from the global geological map of Venus produced by Ivanov (2008). The legend for this geological map can be found in figure 5.1. Of these units, ridged plains (pr), mountain belts (mt), and Artemis Chasma material (ac) are not found in the study area. Crater (c) and crater outflow (cf) material are found locally, but are largely irrelevant to discussions of geological age on Venus. The oldest units directly relevant to this study are tessera (t) and densely lineated plains (pdl). Tesserae are recognized as the oldest surface unit on Venus and are highly deformed and radar-bright. Densely lineated plains are the oldest of the volcanic plains units on Venus. Younger than these are the shield plains (psh), which are volcanic plains dotted with small shield volcanoes. Groove belts (gb) are interpreted as younger than the shield plains, and are regions of dense lineation. Younger than the groove belts are the lower (rp_1) and upper (rp_2) regional plains, which are volcanic plains typically crossed by multiple sets of lineations. The lower regional plains unit is more densely lineated than the upper unit. Rift zones (rz) are regions defined by large, densely packed graben and

are usually associated with areas of crustal rifting. Progressively younger than the rift zones are shield clusters (sc), smooth plains (ps), and finally lobate plains (pl). All three of these are volcanic plains units. Shield clusters are defined by volcanic plains featuring an abundance of small shield volcanoes, typically increasing in density towards the centre of the unit. Smooth plains are volcanic plains with smooth surfaces, without defining flow features or volcanic edifices. Lobate plains are volcanic plains with lobate flow morphologies. They typically emanate from single sources which can be identified by the flow directions within the unit.

This section investigates the interactions between radiating graben-fissure systems and the surface geology for selected systems, and presents the resulting ages and timeline for all systems in the study area.

5.1. System 54

System 54 is hosted by geological units that are quite common to the majority of radiating systems in this study area (Figure 5.2). The centre is found in a groove belt (gb) unit, which is surrounded by a lobate plains (pl) unit. This is unsurprising; the groove belt unit is defined by the dense lineations formed by the radiating graben of the system, and the lobate plains are likely fed from the same magma source that created the radiating system.

Within the lobate plains (pl) unit, the system's graben are much less dense. In many areas, the graben are obscured by lava flows, although faint traces of graben can

be seen in much of the lava plain. The unit is likely younger than the radiating system, with a small degree of concurrence in terms of ages.

To the northeast of the centre, a single graben crosses a lower regional plains (rp_1) unit. As the graben is clearly defined within the unit, it is likely that the system is younger than the lower regional plains unit.

To the southwest of the centre, graben enter a shield plains (psh) unit. The graben system within this unit exhibits a marked decrease in lineation density and intensity compared to outside this unit due to partial flooding of the graben. The system is likely older than the shield plains (psh) unit.

Isolated graben within the radiating system have limited interaction with a rift zone (rz) unit and an upper regional plains (rp_2) unit. The rift zone is clearly younger than the radiating system, but the age relation between the system and the upper regional plains (rp_2) unit is uncertain.

5.2. System 5

System 5 is centred within a rift zone (rz) unit – as mentioned in chapter 3.3, the system is centred on, and younger than, an arm of Hecate Chasma (Figure 5.3). The extensive radiating graben-fissure system also makes contact with several other geological units. Near the centre of the system are several smooth plains (ps) units. The smooth plains (ps) material near the centre and within the rift zone (rz) unit is largely unaffected by the radiating system. Age relations are difficult to determine, however,

given that the smooth plains (ps) appear to be mapped as the areas between lineations, they could be areas covered by lava plains or remnants of earlier smooth lava plains that have not been crossed by younger graben. The simplest, and most likely, interpretation is that the smooth plains (ps) are younger than the radiating system.

North of the centre, on the edge of the study area, the system encounters a lobate plains (pl) unit. The graben appear to encroach on the edges of the unit, but are obscured towards the centre. It is likely that the lobate plains (pl) unit here is younger, and possibly somewhat concurrent to the radiating system. To the northeast of the centre, graben from system 5 can be seen crossing both a shield plain (psh) unit and a lower regional plains (rp_1) unit. Each appear to be older than system 5.

Just east of the centre, there is a small shield cluster (sc) unit. It appears unaffected by the radiating system, and is likely younger. West of the center is a small (13 km in diameter) crater, the outflow material from which obscures graben in the radiating system. A larger (64 km in diameter) crater to the northwest also appears younger than system 5.

Lobate plains (pl) to the northwest are crossed by a few graben, but exhibit a much lower density of lineation overall. They are likely late-concurrent to younger in age than the radiating system. The same is true of lobate plains (pl) units west of the centre of system 5, and further west again – south of Minona Corona and systems 7 and 65. Alternatively, these lobate plains (pl) units could be entirely younger than the radiating system, and the visible graben are simply those that are large not to have been

filled in by the lava flows. A shield plains (psh) unit in this area appears clearly older than the radiating system.

The formation of smooth plains (ps) units to the west of the centre of system 5 appears to have occurred late during the formation of the radiating system, as there is once again a lower density of lineation but still some graben that are clearly defined and likely younger than the smooth plains. The lower regional plains (rp_1) units that are intermixed with the smooth plains are more heavily lineated and likely older than the system.

5.3. System 14

Radiating graben-fissure system 14 is centred away from major rift zone units, in geology dominated by plains units (Figure 5.4). The central part of the system is mapped as a groove belt (gb) unit, due to the density of the radiating graben and fissures. To the southwest is a rift zone (rz) unit, along a line of particularly dense lineations.

A smooth plains (ps) unit to the west is clearly older than the radiating system, as it is crossed by many graben in the system. Another smooth plains (ps) unit to the northwest obscures graben, except for a band running from north to south across the unit. Both smooth plains (ps) units are likely younger than the radiating system despite this band of visible graben. A smooth plains (ps) unit to the southeast and south of the centre of system 14 is crossed by very few graben and is likely younger.

A unit of shield plains (psh) south of the centre of system 14 is cut by graben except in its southernmost reaches. It appears that this unit may have been produced by two generations of volcanism, one younger and one older than radiating system 14.

A lower regional plains (rp_1) unit which covers ground to the east and west of the system centre obscures most graben in the radiating system. It appears likely that the portions of the unit from the centre out to a point about 150 km to the west are in fact related to the magmatism that emplaced the radiating system. Like other volcanic units related to the radiating systems, it appears to have begun forming during the late stages of the development of radiating system 14.

5.4. System 47

Radiating graben-fissure system 47, centred on the large volcano Ozza Mons, is the largest system in the study area (Figure 5.5). The region near the centre, and up to 600 km out from that point, is dominated by lobate plains (pl) material. There are also two large shield clusters (sc) units at the centre of the system. These shield clusters are largely unaffected by the radiating system, and are clearly younger. The lobate plains (pl) vary in their relationship with the graben; to the north to northwest and directly south of the centre of system 47, there are areas where graben cut the unit. However, the rest of the lobate plains (pl) around the centre and within the study area are largely uncrossed by radiating graben. It is likely that the lobate plains (pl) unit is concurrent with the later stages of the radiating systems as well as in part younger. There are two possible explanations for the regional variations: first, that the north and south trending

graben are the youngest in the radiating system, and second, that the north and south regions of the lobate plains (pl) represent the earliest flows within that unit, and the only ones concurrent with the radiating system.

There are three units of shield clusters (sc) within the lobate plains (pl) to the northwest of the centre. These are clearly younger than the radiating system. Surrounding much of the lobate plains (pl) material are rift zone (rz) units. As mapped, these appear to be a combination of dense graben of the radiating system with actual arms of Hecate Chasma, which converge on this region.

To the north, north-northwest, and west are patches of upper and lower regional plains (rp_1) and shield plains (psh) material. All three of these units appear to be older than the radiating system as they are all cut by graben in some areas. West northwest of the centre is a smooth plains (ps) unit, which is mostly uncut by the radiating system, except for one set of large graben that cross its northern portion. It may be concurrent with the early stages of system formation; however, the graben are certainly older than the lobate plains (pl) that are in contact with it.

5.5. General Stratigraphic Analysis

Age relations between mapped surface geology and radiating graben-fissure systems are detailed in Table 5.1. The two most common, and clear relationships between the radiating graben-fissure systems and stratigraphy are as follows: where present, the groove belts (gb) unit is defined by the systems themselves, and as such, is concurrent with system formation; the lobate plains material (pl) unit is usually found to

be related to the magmatic events creating the radiating systems, occurring after the formation of the systems, with some local concurrence.

Rift zone (rz) units vary in their stratigraphic relationship with radiating graben-fissure systems. There is an even distribution between younger than , concurrent with , and older than relationships. The various plains units (psh, rp_1, rp_2, ps)) also have varying relationships with the radiating systems – smooth plains tend to be younger while the others units (psh, rp_1, rp_2) are sometimes older. Where they are present, the shield clusters and craters vary in their relationships with the systems as they are relatively small and local features which may not be constrained to any common age of formation.

The challenge in this analysis lies in the root of the method; in comparing this project's mapping of tectonic features to Ivanov's geological mapping, two data sets are being discussed, both derived from the same source – the Magellan SAR images. Ivanov's map is primarily based on the morphological characteristics of the planet's surface. As such, all of the units are defined by the density or type of identifiable geological structures. This results in a mix of different unit types: those defined by the presence of volcanic or geologic structures (psh, rz, sc, pl) and those defined by the amount of deformation they show (t, pdl, gb, rp_1, rp_2, ps). While the shield volcanic units (psh, sc) generally retain their designation even when crossed by multiple sets of graben, the plains units (pl, ps) as mapped are not crossed by graben. Once they exhibit some lineaments, they are classified as one of the lineated plains units (rp_1, rp_2) – many

units of rp_2 can be seen with clear lobate flow forms. As such, the ages of these units are somewhat hard to define: typically, the increasing levels of deformation (from pl and ps up to rp_1) could be tied to increasing age, but a unit of pl formed in a tectonically inactive region (eg. not near a rift zone or large magmatic structure) could easily be older than a unit of rp_1 formed in active region.

The geologic units mapped in the vicinity of the better delineated radiating systems are somewhat defined by them: groove belts are generally mapped by the presence of denser graben near the radiating centres, regional plains units show fewer graben, and the lobate and smooth plains units are typically lava flows related to the systems that post-date the emplacement of the radiating graben. The notable exception to this rule is the rift zones, which are largely mapped independently from the radiating systems – except for some of the more significant radiating systems (e.g. numbers 5, 6, and 47) where it appears that the density and size of the radiating graben has led them to be mapped as rift zone units.

From a morphological perspective, the mapping method of Ivanov (2008) is fully defensible. The problem arises when the map is used in conjunction with the study of the magmatic radiating graben-fissure systems. With the identification of the ages of the radiating systems with respect to each other and to Hecate Chasma, it can be seen that these features formed over a relatively wide span of time. It follows that geological units related to these radiating systems (especially gb and pl) could also be formed throughout that same span of time. The possible variance of these ages means

that they do not provide tight constraints on regional stratigraphy and geochronology. Nevertheless, the study of radiating graben-fissure systems and their relation to the mapped geology has produced a few concrete results. It is clear that the radiating systems are younger than the tessera (t) and densely lineated plains (pdl) units. All other units encountered within the study area appear to have formed over the same span of time as the radiating systems.

Figure 5.1. Legend of geologic units used in Ivanov's surface geology map of Venus. Modified from Ivanov (2008).

Figure 5.2. Surface geology in the area of system 54, from Ivanov (2008). Radiating system 54 superimposed as dark blue lines.

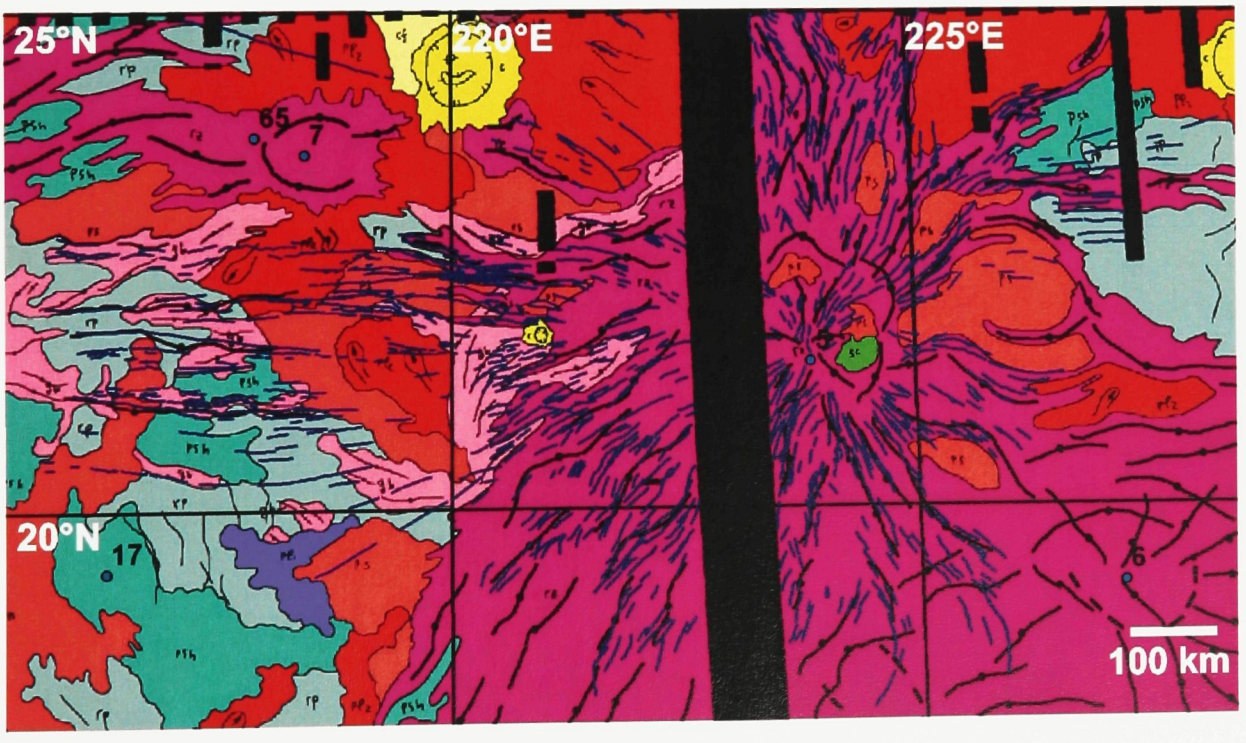

Figure 5.3. Surface geology in the area of system 5, from Ivanov (2008). Radiating system 54 superimposed as dark blue lines.

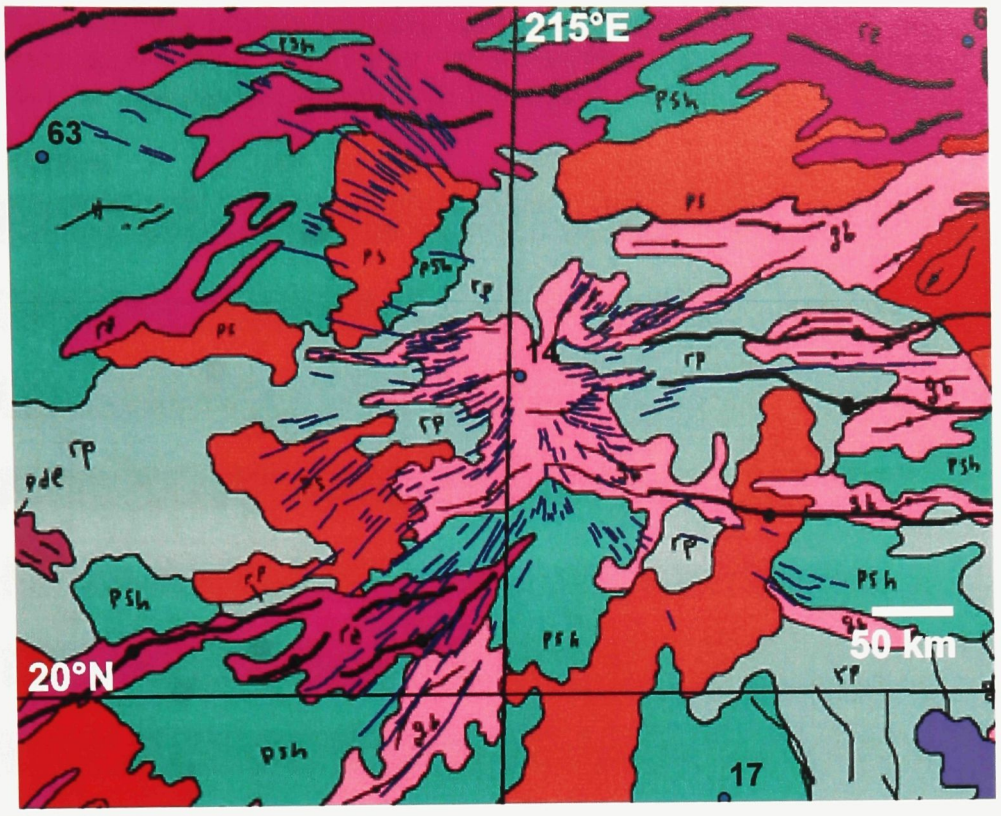

Figure 5.4. Surface geology in the area of system 14, from Ivanov (2008). System 14 superimposed as dark blue lines.

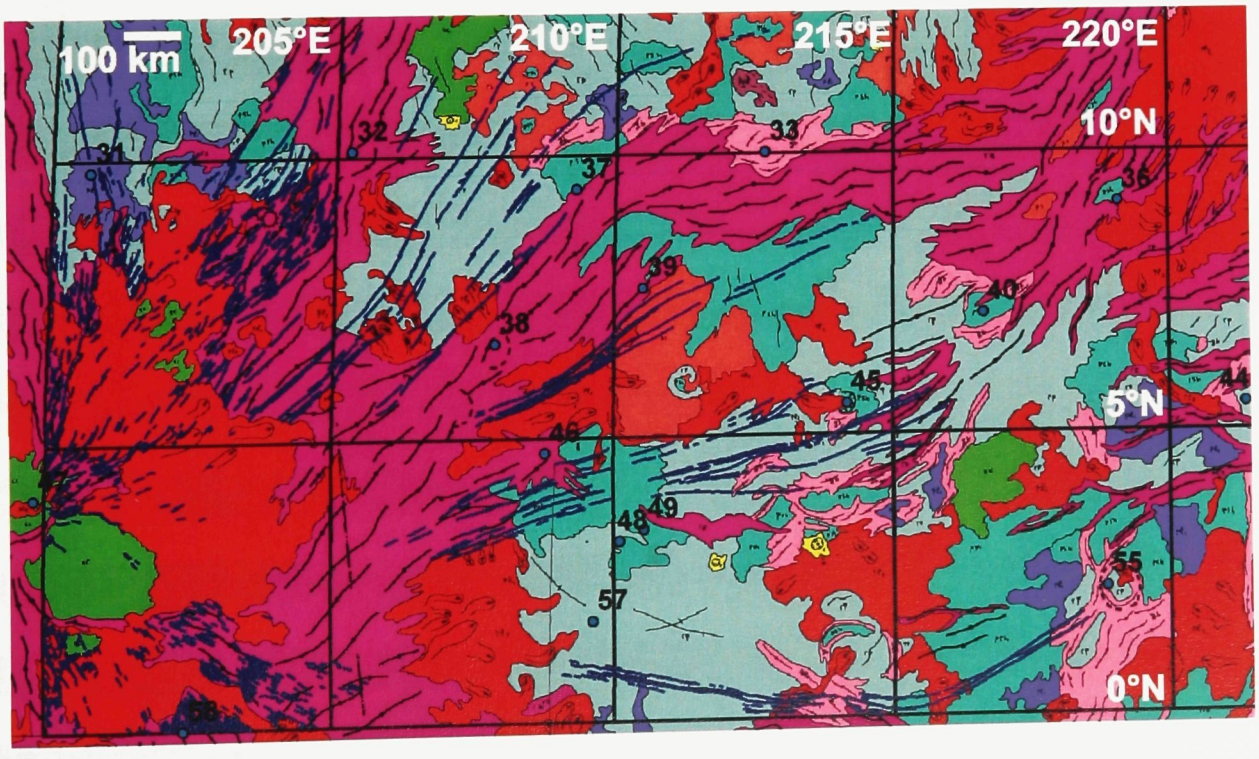

Figure 5.5. Surface geology in the area of system 47, from Ivanov (2008). System 47 superimposed as dark blue lines.

Table 5.1. Age relations between radiating graben fissure systems and mapped geology. Geological units abbreviated as in Figure 69. Within the table, "y" indicates that the system is younger than the unit, "o" indicates that it is older, "c" indicates coeval emplacement.

System	t	pdl	mt	pr	gb	psh	rp_1	rp_2	rz	ac	sc	ps	pl	c	cf
0									c						
1									o			o			y
2					c	y/c	y		y/c				y/o	o	
3					o	o/y	y	y/c	y/c				y/c		
4						o			o				o/c		
5							y		c		o	o/c	o/c	o	o
6					y		y		c		y	o/c	o/c/y		
7					c		y		y/c			o/c	o/c	o	o
8							y		y						
9							y		y				o/c		
10		y			c	y	y	y						y	y
11							y/c		y						
12						c	y		y						
13						c	y		y				o/c		
14					c	o/y	o		c			o/y			
15		y				c/y	y	y/c					y		
16						y/c									
17						y/c									
18					o/c	o	y	y	o		o	o/c	o/c	y	
19						c	c		o						
20									o						
21						o	y/c					o/c	o/c		
22				o		y	y/c		o			o	o/c		
23					y				y/c		y/c	y/c	c		
24						y	y	y	o/c				o/c		
25					y	y									
26					c	y	o/c		o/c				o	o	
27				y	c	y	y		y/c				o/c		
28					y/c	y			c			o	o/c		
29								o/c							
30								o/c							
31							c/y	c							
32						o/c	y	y	c		o		o/c		
33		y			c	y	y	y	o			o/c	o/c		
34					o						o	o			
35					o/c	y	o		y						
36		y			c	o			y/c				o/c		
37						y	y		o/c						

System	t	pdl	mt	pr	gb	psh	rp_1	rp_2	rz	ac	sc	ps	pl	c	cf
38									o			y	o/y		
39									o			y			
40					y/c	o	y		o						
41													c		
42					y	y	y						c		
44					o/c	y	y		c				o/c		
45					c	y	y		o/c				o		
46						y			o/c			y	y/c		
47						y	y	y	o/c		o		o/c		
48						y	y/c								
49						y	y/c								
51					c	y	y	y/c	o				o		
52					o/c	o/c	o/c	y	y/c				o/c		
53					o			y					c		
54					c	o	y		o				o/c		
55					o/c	y/o	y	y					y		
57							y						o	o	
58							y		o/c				o/c		
59						y	o	y/c							
60		y			c	y	o	o							
61					c	y	y		o						
62					y/c	y	y	y							
63						y									
64					c				o/c				y/c		
65					y/c	y	y		c			o	c		
66					o/c	y	y	y	o		y		y/c/o		
67							y/c	y					y/c		
68					c										

6.0. Width of Graben versus Distance from Radiating Centre

Several of the longer, better defined, and more continuous graben mapped in the study area have been surveyed, recording the width of the graben with respect to their distance from the associated radiating centres. The primary goal of this compilation is to ascertain whether graben width varies with position along the graben. For instance, if the width of graben were shown to decrease with distance from the centre, it could enable a more reliable identification of the location of the sources of the graben.

The graben selected for this study (shown in Figure 6.1) are predominantly related to system 47 – Ozza Mons – which is the largest and most extensive system in the study area. Several well-defined graben extend out to greater than 1500 km and even up to 2000 km from the system's centre. The only other graben mapped is associated with centre 6, and is abnormally long for that system – it is one of a set of graben that extend 1400 km to the southeast of the centre, more than twice as far as any other graben mapped in the system. However, the trend and morphology of these graben as they approach the system's centre fit with the rest of the graben in that region of the radiating graben-fissure system.

The graben were measured for width every 20 km along their length. These measurements were completed using the "measuring tape" tool in ArcMap. Due to the relatively coarse pixel size in the Magellan altimetry (75 m/px), there is a certain amount of error involved in measuring features that rarely exceed 20 pixels in width. Nevertheless, the measurements displayed in Figure 6.2 are accurate enough to reveal interesting patterns.

There are two patterns of note in these data: the rapid fluctuation of width along each graben, and the general trend in width along each set. First, the rapid fluctuation

is at least partially the result of measuring error due to the coarseness of data and difficulty of interpretation as mentioned above. However, some of these variations may also be the product of the local geology, whether the host geology had an effect on the morphology of the graben, or simply affected the visibility of the graben edges in the SAR data. A long-wavelength trend is also quite notable in a few of the graben: Ozza 1, Ozza 2, Ozza 3, and Ozza 4 all show a noticeable decrease in width as the distance from the centre increases. Ozza 6 shows the opposite trend, with a clear increase in width along its length. Graben 6 SE increases width for about half of its length before decreasing towards the far end. Ozza 5 shows no clear trend.

The graben identified as Ozza 1 and 6 SE have their widths compared against local geology (Ivanov, 2008) in Figures 6.73 and 6.74, respectively. Ozza 1 was chosen as representative of the graben that exhibit decreasing widths with distance, and 6 SE as representative of the graben which do not.

As seen in Figure 6.3, Ozza 1 is widest near the centre of the system, within the rift zone unit (rz). There is a sharp drop in width as the graben approaches the contact between this unit and the lower regional plains unit (rp_1). The drop does occur within the mapped rift zone unit, but it should be noted that there is not a clear contact between the two units in the SAR image, but rather a gradual transition. There is a local peak in width within the lobate plains unit (lp) at 780 km from the centre, but there is a local narrowing of the graben in the next section of lobate plains (lp), 100 km further from the centre. In between these two points, there is a continuous narrowing of the graben within a lower regional plains unit. It appears the only unambiguous relation between widths and mapped geology is found in the initial rift zone unit and the wide width found within it. However, the same problem arises in this analysis as in the interpretation of the radiating systems' ages with respect to the mapped geology (Section 5): the rift zone unit is defined by having large and abundant graben, predominantly aligned in one direction. It is therefore unsurprising that the widest

portion of the graben Ozza 1, found in a region of dense lineation, is also in a rift zone unit in Ivanov's map (2008).

A similar set of observations is found along graben 6 SE (Figure 6.4). While there are certain variations that could be associated with host geological units, there is no strong evidence for relations to be found between the width of graben and the surface geology in which they are found.

Ozza 6, which displays the widening trend along its length, is an outlier here. During the mapping portion of this study, it was attributed to system 47 – Ozza Mons. It fits well within this system, with its length and general directional trend. However, the eastern end of the graben does terminate in very close proximity to the centre of system 55. Its trend approaching the centre is sub parallel to graben within system 55. With a maximum mapped radius of 166 km for the system, though, the length of the graben Ozza 6 – which would increase the system radius to 980 km – is out of place within that system. If it is common for graben to decrease in width with distance from system centres, as this study may indicate, then it is possible that Ozza 6 is in fact part of system 55.

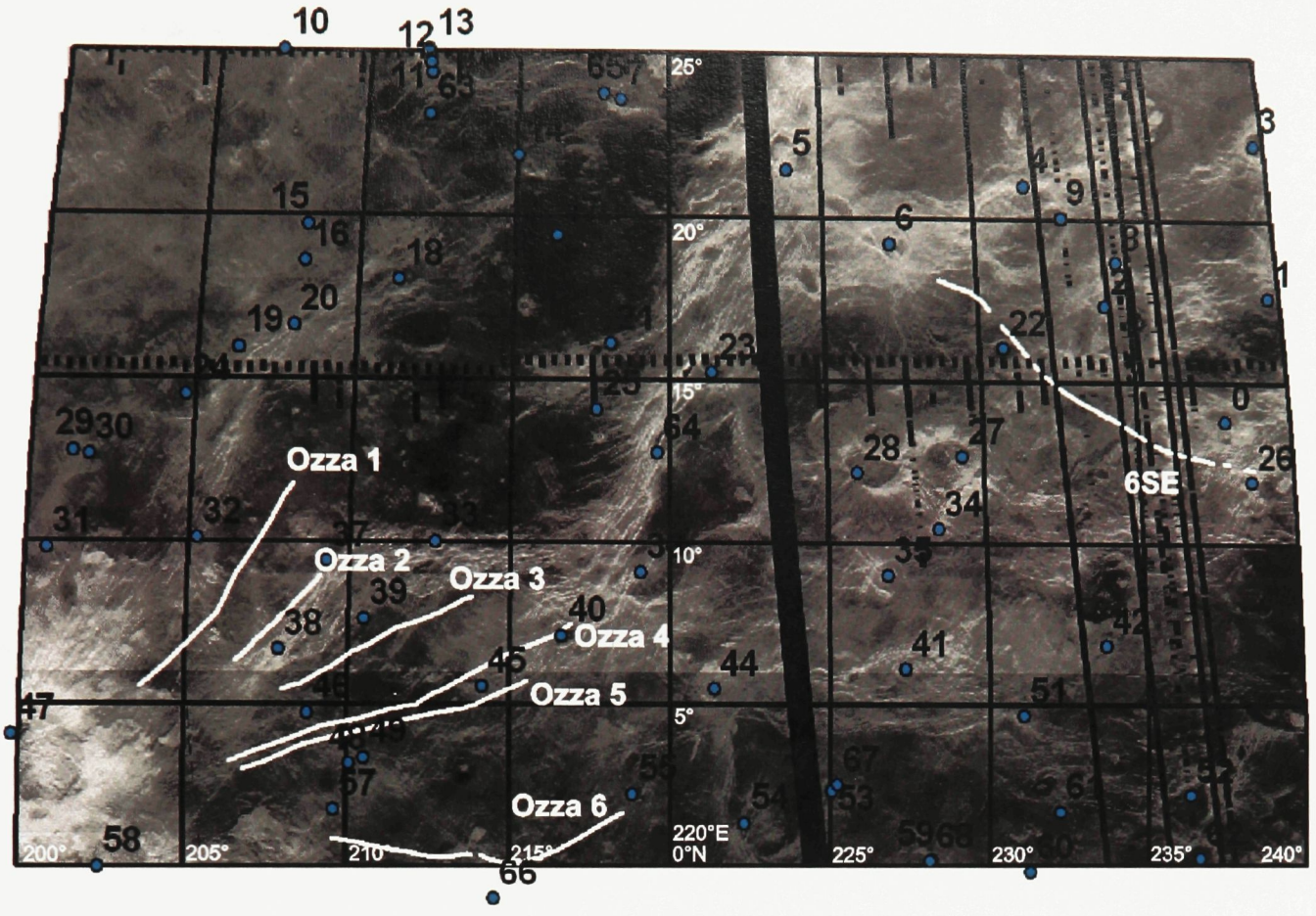

Figure 6.1. The graben included in the study of graben widths are indicated by white lines overlaid on the Magellan SAR data of the study area. Numbered dots indicate the centres of radiating systems.

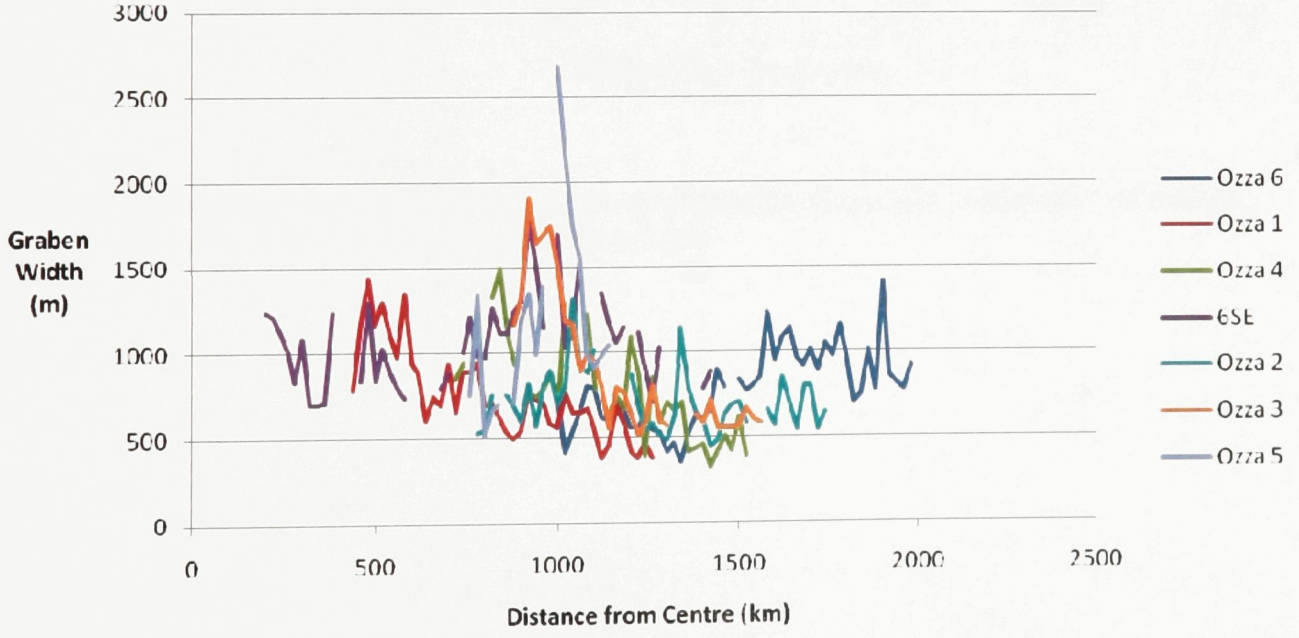

Figure 6.2. Plot of graben width versus distance from radiating system centre.

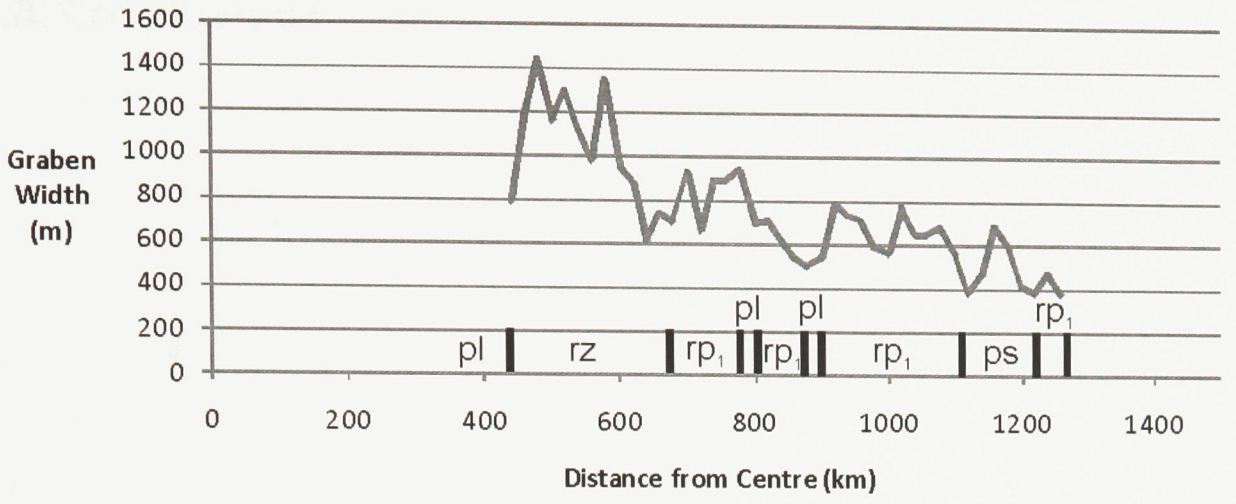

Figure 6.3. Widths of graben "Ozza 1" and geological units crossed by the graben. Symbology: "pl", lobate plains; "rz", rift zone; "rp_1", lower regional plains; "ps", smooth plains.

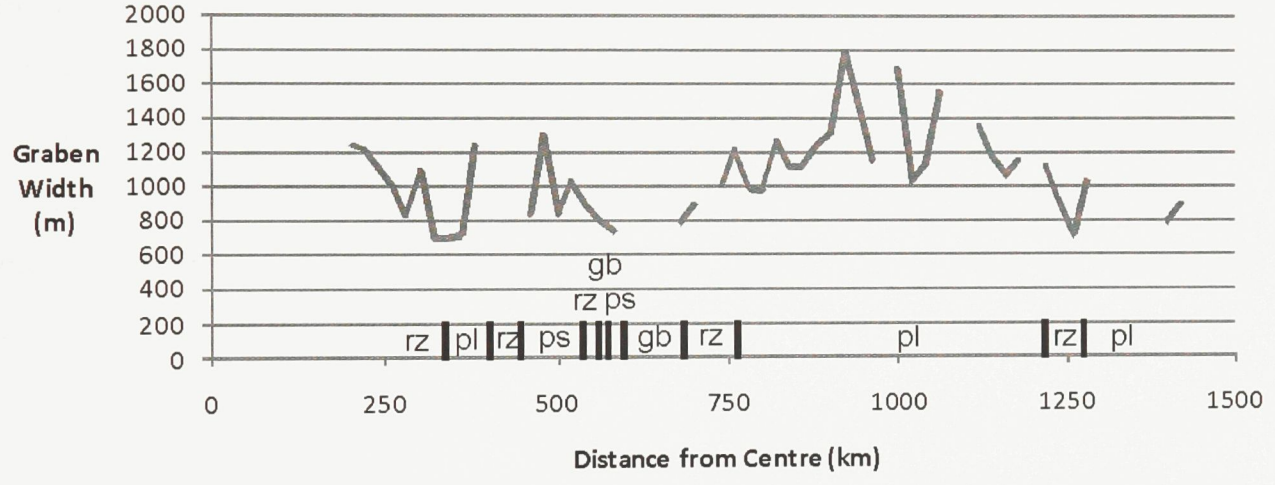

Figure 6.4. Widths of graben "6SE" and geological units crossed by the graben. Symbology: "pl", lobate plains; "rz", rift zone; "ps", smooth plains; "gb", groove belt.

7.0. Conclusions

A detailed map of radiating graben-fissure systems has been produced for an 11,000,000 km^2 area around northern Ulfrun Regio. There were 47,000 individual graben and fissures mapped from which 66 radiating graben-fissure systems, comprised of 13,000 graben and fissures, were identified. These systems range in radius from 10 km up to greater than 2000 km, including 19 systems with radii of greater than 500 km. In many cases these radiating systems are associated with coronae or major volcanic centres.

Cross-cutting relationships between these radiating graben-fissure systems have been identified and used to determine the relative ages of radiating systems that interact with each other. Cross-cutting relationships between rifting of Hecate Chasma and radiating graben-fissure systems were also identified. Using the two sets of cross-cutting relationships, and treating Hecate Chasma as having a constant age throughout the study area, 57 of the 66 radiating graben-fissure systems were placed on a relative timeline. There is found to be a general trend of younging from the southwest corner of the study area to the northeast.

Cross-cutting relationships and interactions between the radiating graben-fissure systems and surface geology as mapped by Ivanov (2008) have also been identified. The radiating graben-fissure systems are recognized to be younger than the tessera and densely lineated plains units. The systems are seen to each be individually older than lobate plains units which are related to them. It is also found that the various volcanic plains units (lobate plains, smooth plains, upper and lower regional plains, and shield plains) all formed over a similar period of time during which the radiating graben-fissure systems also formed.

The widths of seven major graben within two radiating graben-fissure systems were measured systematically with increasing distance from the centre of their respective systems. Of the seven graben, four exhibit a narrowing trend along their length away from their centres, and one shows a widening trend. It is proposed that the

widening trend may be helpful in identifying the magmatic centres from which long graben propagate.

References

Addington, E.A. 2001. A stratigraphic study of small volcano clusters on Venus. *Icarus* 149:16-36.

Aittola, M. and Kostama, V.-P. 2000. Venusian Novae and Arachnoids: Characteristics, Differences and the Effect of the Geological Environment, *Planet. Space Sci.,* 48:1479–1489.

Aittola, M. and Kostama, V.-P., Chronology of the Formation Process of Venusian Novae and the Associated Coronae, *J. Geophys. Res. E*, 2002, vol. 107, no. 11, p. 5112; doi: 10.1029/2001JE001528.

Basilevsky, A.T. and Head, J.W. 2002. Venus: timing and rates of geologic activity. *Geology* 30:1015-8.

Bilotti, F. and Suppe, J. 1999. The Global Distribution of Wrinkle Ridges on Venus. *Icarus,* 139:137-157.

Bullock, M.A., Grinspoon, D.H., and Head, J.W. 1993. Venus resurfacing rates: constraints provided by 3-D Monte Carlo simulations. *Geophys. Res. Lett.* 19:2147-50.

Crumpler, L.S., Aubele, J.C., Senske, D.A., Keddie, S.T., Magee, K.P., Head, J.W. 1997. Volcanoes and centres of volcanism on Venus. In: *Venus II: Geology, Geophysics, Atmosphere and Solar Wind Environment,* eds. S.W. Bougher, D.M. Hunter, and R.J. Philips (Tuscon: Univ. of Arizona Press), pp. 697-756.

Crumpler, L.S. and Aubele, J.C. 2000. Volcanism on Venus. In: *Encyclopedia of Volcanoes, ed. H. Siggurdson* (London: Academic Press), pp. 727-769.

Cyr, K. E., and H. J. Melosh. 1993. Tectonic patterns and regional stresses near venusian coronae. *Icarus,* 102:175-184, 1993.

Ernst, R.E. and Desnoyers, D.W. 2004. Lessons from Venus for understanding mantle plumes on Earth. *Phys. Earth Panet Inter.* 146:195-229.

Ernst R. E., Head, J.W., Parfitt, E., Grosfils, E., and Wilson, L . 1995. Giant Radiating Dyke Swarms on Earth and Venus. *Earth-Sci. Rev.,* 39:1–58.

Ernst R. E., Desnoyers, D.W., Head, J.W., and Grosfils, E.B. 2003. Graben-fissure systems in Guinevere Planitia and Beta Regio (264-312E, 24-60N), Venus, and implications for regional stratigraphy and mantle plumes. *Icarus,* 164:282–316.

Ernst, R.E., Harris, B.A., Studd, D., Samson, C., Grosfils, E.B., Head, J.W. 2008. The Global Distribution of Graben-Fissure Systems on Venus and Implications for Magmatism on Mars. Canadian Space Exploration Workshop 6, abstract 6121.

Ernst, R.E., Grosfils, E.B., Head, J.W., Samson, C., Ivanov, M.A., Studd, D., and Harris, B.A. 2009. Towards a Dyke Swarm Map of Venus. *Eos Trans. AGU*, 90(22), Jt. Assem. Suppl., GA13A-06.

Foster, A., and F. Nimmo. 1996. Comparisons between the rift systems of East Africa, Earth, and Beta Regio, Venus. *Earth and Planetary Science Letters,* 143:183-195.

Glaze, L.S., Stofan, E.R., Smrekar, S.E., Baloga, S.M. 2002. Insights into corona formation through statistical analyses. *J. Geophys. Res.* 107 (E12), 5135, doi:10.1029/2002JE001904.

Grosfils, E.B., Head, J.W. 1994. The global distribution of giant radiating dike swarms on Venus: implications for the global stress state. *Geophys. Res. Lett.* 21:701-704.

Hamilton, V.E., Stofan, E.R., 1996a. Global Characteristics of Arachnoids on Venus. *Lunar and Planetary Science Conference, Vol. XXVII,* pp. 483-484.

Hamilton, V.E. and Stofan, E.R. 1996b. The Geomorphology and Evolution of Hecate Chasma, Venus, *Icarus,* 121:171–194.

Head, J. W., L. S. Crumpler, J. C. Aubele, J. Guest, and S. R. Saunders. 1992. Venus volcanism: Classification of volcanic features and structures, associations, and global distribution from Magellan data, *J. Geophys. Res.,* 97:13,153– 13,197.

Head, J.W. and Coffin, M.F. 1997. Large igneous provinces: a planetary perspective. In: *Large Igneous Provinces: Continental, Oceanic, and Planetary Flood Volcanism*, eds. Mahoney, J.J. and Coffin, M.F. Geophysical Monograph 100. American Geophysics Union, pp. 411-438

Head, J.W. 1999. Interiors of the Terrestrial Planets. In: *The New Solar System, 4th ed.* Beatty, Petersen, and Chaikin, eds. Cambridge University Press.

Herrick, R.R. 1994. Resurfacing history of Venus. *Geology* 22:703-6.

Herrick, R.R., Izenberg, N., Phillips, R.J. 1995. Comment on "The global resurfacing of Venus" by R.G. Strom, G.G. Schaber, D.D. Dawson. *J. Geophys. Res.* 100:12255-9.

Ivanov, M.A., and Head, J.W., 2004. Stratigraphy of small shield volcanoes on Venus: criteria for determing stratigraphic relationships and assessment of relative age and temporal abundance. *J. Geophys. Res.* 109, E10001, doi10:1029/2004JE002252, 32 p.

Ivanov, M.A. 2008. Global Geological Map of Venus: Preliminary Results. *Lunar and Planet. Sci.* 39, #1017.

Janes, D.M. and Turtle, E.P. 1996. Gravity Signatures of Corona Precursors on Venus: Reality vs. Prediction, *Lunar and Planet. Sci. XXVII.* pp. 605–606.

Janle, P., and Meissner, R. 1986. Structure and Evolution of the Terrestrial Planets. *Surveys in Geophysics 8,* 107-186.

Lopez, I., Alvarez, M., and Oyarzun, R. 1997. Are coronae restricted to Venus?: Corona-like tectonovolcanic structures on Earth. *Earth, Moon and Planets,* 77:125-137.

McKenzie, D., Ford, P.G., Johnson, C., Parsons, B., Sandwell, D., et al. 1992. Features on Venus generated by plate boundary processes. *J. Geophys. Res.* 97:13533-44.

McKinnon, W.B., Zahnle, K.J., Ivanov, B.A., Melosh, H.J. 1997. Cratering on Venus: models and observations. In: Bougher, S.W., Hunten, D.M., Phillips, R.J. (Eds.), Venus II: Geology, Geophysics, Atmosphere, and Solar Wind Environment. University of Arizona Press, Tucson, AZ, pp. 103-140.

Namiki, N., and Solomon, S.C. 1994. Impact crater densities on volcanoes and coronae on Venus: implications for volcanic resurfacing. *Science* 265:929-33.

Nimmo, F., and McKenzie, D. 1998. Volcanism and tectonics on Venus. *Annu. Rev. Earth Planet. Sci.* 26:23-51.

Oliver, C. and Quegan, S. 2004. Understanding Synthetic Aperture Radar Images. SciTech Publishing.

Parfitt, E. A., and J. W. Head. 1993. Buffered and unbuffered dike emplacement on Earth and Venus: implications for magma reservoir size, depth, and rate of magma replenishment, *Earth Moon Planets,* 61:249-281.

Pettengill, G.H., Eliason, E., Ford, P.G., Loriot, G.B., Masursky, H., and McGill, G.E. 1980. Pioneer Venus radar results: altimetry and surface properties. *J. Geophys. Res.* 85:8261-70.

Phillips, R.J., Raubertas, R.F., Arvidson, R.E., Sarkar, I.C., Herrick, R.R., Izenberg, N., Grimm, R.E. 1992. Impact craters and Venus resurfacing history. *J. Geophys. Res.* 97:15923-48.

Phillips, R.J., and Hansen, V.L. 1994. Tectonic and Magmatic Evolution of Venus. *Annu. Rev. Earth Planet. Sci.* 22:597-654.

Price, M., Suppe, J., 1995. Constraints on the resurfacing history of Venus from the hypsometry and distribution of volcanism, tectonism and impact craters. *Earth Moon Planets* 71:99-145.

Prinn, R.G., and Fegley, B. 1987. The atmospheres of Venus, Earth, and Mars: a critical comparison. *Annu. Rev. Earth Planet. Sci.* 15:171-212.

Russell, C. T. 1980. Planetary Magnetism. *Rev. Geophys. Space Phys.* 18, 77-106.

Saunders, R.S., et al. 1990. The Magellan Venus Radar Mapping Mission. *J. Geophys. Res.* 95:8339-8355.

Schaber, G.G., Strom, R.G., Moore, H.J., Soderblom, L.A., Kirk. R.L., et al. 1992. Geology and distribution of impact craters on Venus: What are they telling us? *J. Geophys. Res.* 97:13257-301

Squyres, S. W., D. M. Janes, G. Baer, D. L. Bindschadler, G. Schumbert, V. L. Sharpton, and E. R. Stofan. 1992. The morphology and evolution of coronae and novae on Venus. *J. Geophys. Res.* 97:13,611–13,634.

Stofan, E. R., V. L. Sharpton, G. Schubert, G. Baer, D. L. Bindschadler, D. M. Janes, and S. W. Squyres. 1992. Global distribution and characteristics of coronae and related features on Venus: Implications for origin and relation to mantle processes. *J. Geophys. Res.* 97:13,347–13,378.

Stofan, E.R., Hamilton, V.E., Janes, D.M., and Smrekar, S.E. 1997. Coronae on Venus: morphology and origin. In: *Venus II: Geology, Geophysics, Atmosphere and Solar Wind Environment*, eds. S.W. Bougher, D.M. Hunter, and R.J. Philips (Tuscon: Univ. of Arizona Press), pp. 931-965.

Stofan, E.R., Smrekar, S.E., Tapper, S.W., Guest, J.E., Grinrod, P.M. 2001. Preliminary analysis of an expanded corona database for Venus. *Geophys. Res. Lett.* 28:4267-70.

Strom, R.G., Schaber, G.G., Dawson, D.D. 1994. The global resurfacing of Venus. *J. Geophys. Res.* 99:10899-926.

Strom R.G., Schaber, G.G., Dawson, D.D., Kirk, R.L. 1995. Reply to comment on "the global resurfacing of Venus" by R.G. Strom, G.G. Schaber, D.D. Dawson. *J. Geophys. Res.* 100:23361-65.

Studd, D., Ernst, R.E., Samson, C. 2008. Radiating graben fissure systems in Ulfrun Regio: A contribution to the Venus Global Dyke Swarm Map Project. Vernadsky-Brown Microsymposium on Comparative Planetology 50, abstract 91631.

Studd, D., R.E. Ernst, C. Samson, E.B. Grosfils, J.W. Head, M.A. Ivanov. 2010a. Radiating graben fissure systems in Ulfrun Regio: A contribution to the Venus Global Dyke Swarm Map Project. *Lunar Planet. Sci.,* 41, #1950.

Studd, D., R.E. Ernst, C. Samson, E.B. Grosfils, J.W. Head, M.A. Ivanov. 2010b. Mapping in the Ulfrun Regio area: A contribution towards a global Venus dyke swarm map. *CASI ASTRO Con.* 15, #03.

Studd, D., R.E. Ernst, C. Samson, E.B. Grosfils, J.W. Head, M.A. Ivanov. 2010c. Interaction between radiating graben-fissure systems and local geology, Ulfrun Regio, Venus: A contribution to the Venus Global Dyke Swarm Map Project. *COSPAR Sci. Ass.,* 38, B-10-0000-10.

Surkov, Yu. A., V. L. Barsukov, L. P. Moskalyeva, V. P. Kharyukova, and A. L. Kermurdzhian, New data on the composition, structure, and properties of Venus rock obtained by Venera 13 and Venera 14, Proc. Lunar Planet. Sci. Conf. 14th, Part 2, *J. Geophys. Res.*, 89, suppl., B393.B402, 1984.

Surkov, Yu. A., L. P. Moskalyova, V. P. Kharyukova, A.D. Dudin, G. G. Stairnov, and S. Ye. Zaitseva, Venus rock composition at the Vega 2 landing site, Proc. Lunar Planet. Sci. Conf. 17th, Part 1, *J. Geophys. Res.*, 91, suppl., E215-E218, 1986.

Woodhouse, I.H. 2006. Introduction to Microwave Remote Sensing. Boca Raton, FL. CRC Press/Taylor & Francis.

Appendix 1.

This table summarizes the important properties for each of the radiating graben-fissure systems mapped in the study area. The spread arc column refers to the amount of a full circle (in degrees) around a system's centre that is populated by graben from that system. The topography column relates whether there is a dome or depression at the centre of each system. A value of "-1" implies that there is a depression; "1" implies a central dome; "0" describes systems without a significant topographical change at the centre of the system.

System	Latitude (°)	Longitude (°)	Max Radius (km)	spread arc (°)	# of graben	central elevation (km)	vs. planetary mean (km)	topography	dome radius (km)	dome/swarm radius ratio	within corona?
0	238	14	33	30	6	6052.4	0.6	-1		0.00	Y
1	239.5	22.5	221	285	90	6054.3	2.5	0		0.00	Y
2	234.5	17.5	555	360	339	6055.2	3.4	1	165	0.30	Y
3	240	22.5	534	360	680	6055.6	3.8	1	68	0.13	Y
4	231.5	21	592	270	410	6056.0	4.2	1	266	0.45	Y
5	224	21.5	809	360	1011	6059.6	7.8	1	138	0.17	Y
6	227.5	19	1418	360	693	6059.0	7.2	1	82	0.06	Y
7	218.5	24	334	280	199	6057.2	5.4	1	69	0.21	Y
8	234.5	19	313	40/30	90	6056.8	5.0	0		0.00	N
9	233	20	816	100/45	221	6055.9	4.1	0	292	0.36	Y

10	207	25	768	180	367	6055.0	3.2			0.00	N
11	212	24	122	240	41	6054.7	2.9	1	36	0.30	N
12	212	24.5	349	210	130	6055.3	3.5	1	12	0.03	Y
13	212	25	290	20/10	35	6054.7	2.9			0.00	Y
14	215	22	300	360	275	6056.4	4.6	1	122	0.41	N
15	208	19.5	297	300	172	6054.5	2.7	-1		0.00	N
16	208	18	8	360	13	6054.8	3.0	0		0.00	N
17	216.5	19	114	360	26	6054.4	2.6	1	20	0.18	N
18	211.5	18	729	360	1075	6056.4	4.6	1	247	0.34	Y
19	206.5	16	164	90/10	19	6055.5	3.7	0		0.00	N
20	218	17	101	290	30	6059.4	7.6	1	110	1.09	N
21	218	16	292	100/40	58	6054.7	2.9	0		0.00	Y
22	231	16	242	330	121	6055.6	3.8	1	53	0.22	Y
23	221.5	15	391	360	353	6058.9	7.1	1	75	0.19	Y
24	204.5	14.5	508	250	321	6057.5	5.7	1	240	0.47	Y
25	217.5	14	64	70	14	6055.5	3.7	1	31	0.48	N
26	238.5	12	257	110	125	6054.4	2.6	0		0.00	N
27	229	13	564	200	205	6055.9	4.1	1	36	0.06	Y
28	226	12.5	486	360	287	6057.6	5.8	1	129	0.27	Y
29	201.5	2.5	74	90/10	5	6054.9	3.1	-1		0.00	Y
30	202	2.5	45	360	8	6054.9	3.1	-1		0.00	N
31	201	9.5	68	45/30	14	6057.1	5.3	1	37	0.54	N

32	205	10	475	360	288	6054.0	2.2	-1		0.00	N
33	212.5	10	581	360	313	6053.7	1.9	0		0.00	Y
34	228	10.5	126	190	19	6055.6	3.8	1	33	0.26	Y
35	237	9	367	360	128	6054.6	2.8	0		0.00	Y
36	219	9	560	360	207	6058.9	7.1	1	102	0.18	Y
37	209	9	292	100/80/30	194	6058.3	6.5	1	57	0.20	N
38	207	7	548	140/10	351	6053.4	1.6	0		0.00	N
39	210.5	7.5	81	260	29	6055.4	3.6	0		0.00	N
40	217	7.5	172	130/90	62	6055.2	3.4	1	68	0.40	Y
41	227.5	6.5	93	95	10	6052.6	0.8	-1		0.00	Y
42	234	7	207	120/60	59	6054.8	3.0	1	28	0.14	Y
44	221.5	5.5	224	270	51	6055.0	3.2	1	81	0.36	N
45	214	6	149	150/20	45	6053.9	2.1	0		0.00	Y
46	209	4.5	247	110/80	118	6054.0	2.2	-1		0.00	N
47	199.5	4	1985	180	1508	6061.8	10.0	1	301/969	0.17/0.52	N
48	210	3	48	260	11	6054.1	2.3	0		0.00	N
49	210.5	3	40	130	7	6053.5	1.7	0		0.00	N
51	231	4.5	365	60/50	42	6054.4	2.6	1	24	0.07	Y
52	236.5	2.5	350	250	134	6055.3	3.5	1	86	0.25	Y
53	225	2.5	163	75	8	6054.9	3.1	0		0.00	N
54	222.5	2	527	360	205	6056.6	4.8	1	353	0.67	Y
55	218.5	2	166	170	85	6053.9	2.1	-1		0.00	Y

57	209.5	2	254	50/40/30	46	6054.8	3.0	-1		0.00	Y
58	202.5	0	805	80	947	6061.3	9.5	1	230	0.29	N
59	228	0	67	90/30	38	6055.2	3.4	1	31	0.46	N
60	231.5	0	193	45	17					0.00	Y
61	232	2	168	60/40	19	6055.0	3.2	1	95	0.57	Y
62	237	0	366	180	51	6053.6	1.8	-1		0.00	Y
63	212	23	38	360	10	6054.8	3.0	0		0.00	N
64	219.5	13	219	110	48	6057.6	5.8	1	26	0.12	Y
65	218	24	190	330	135	6056.6	4.8	1	53	0.28	Y
66	214.5	-0.5	760	160	462					0.00	N
67	225	2.5	176	150	15	6054.9	3.1	1	25	0.14	N
68	228	0	263	70	8	6055.2	3.4	1	24	0.09	N

Appendix 2.

Included in this appendix are 2 items: 1) a large format copy of a map of the study area that aggregates most of the important findings of this thesis; and 2) a DVD carrying digital copies of this map and others, as well as the GIS files for the project. These can both be found in the attached envelope.

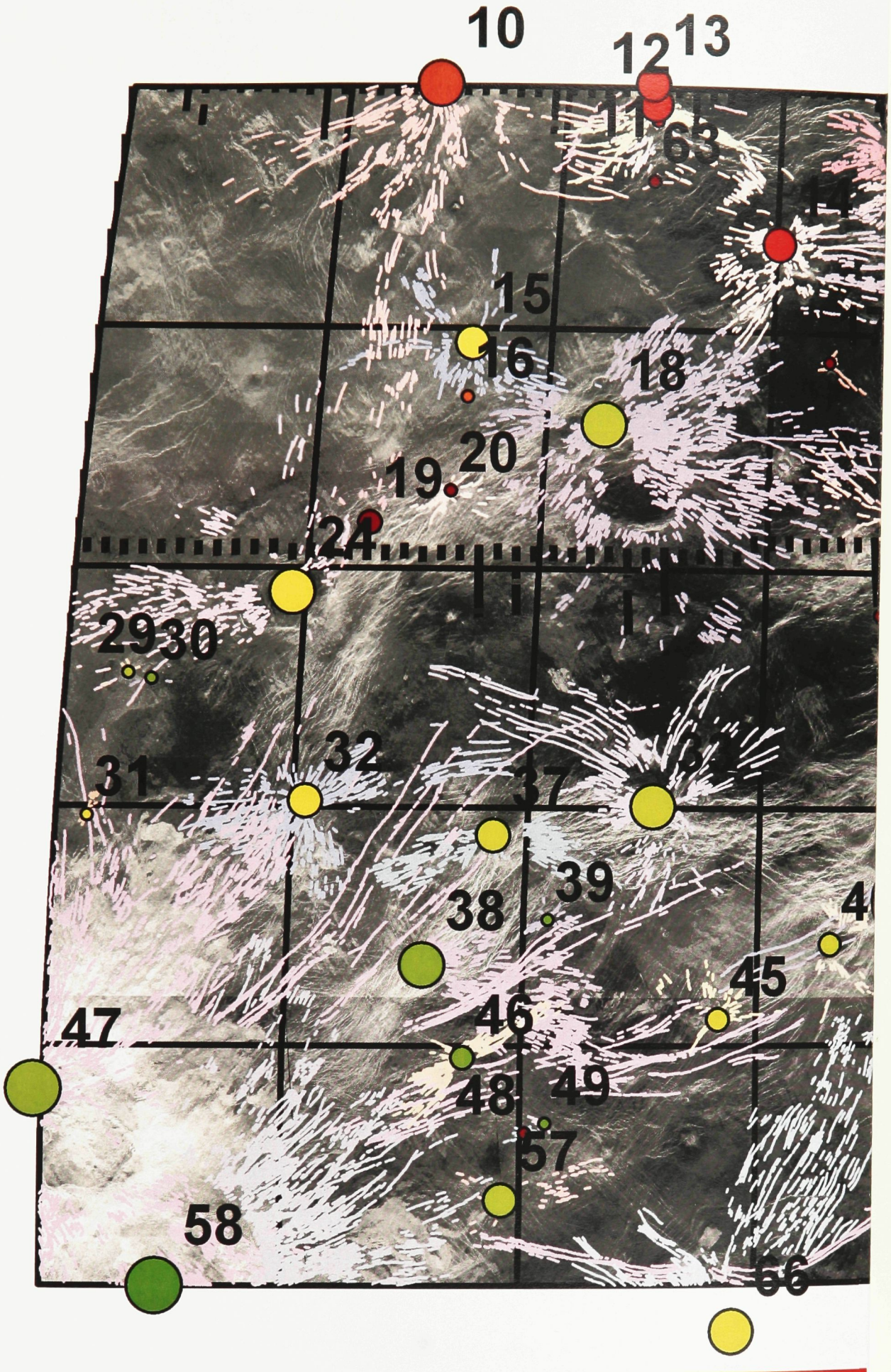
10
12
13
11
63
15
16
18
19
20
24
29
30
31
32
37
38
39
45
46
47
48
49
57
58
66
Older
System Age
Younge
Age Undetermined

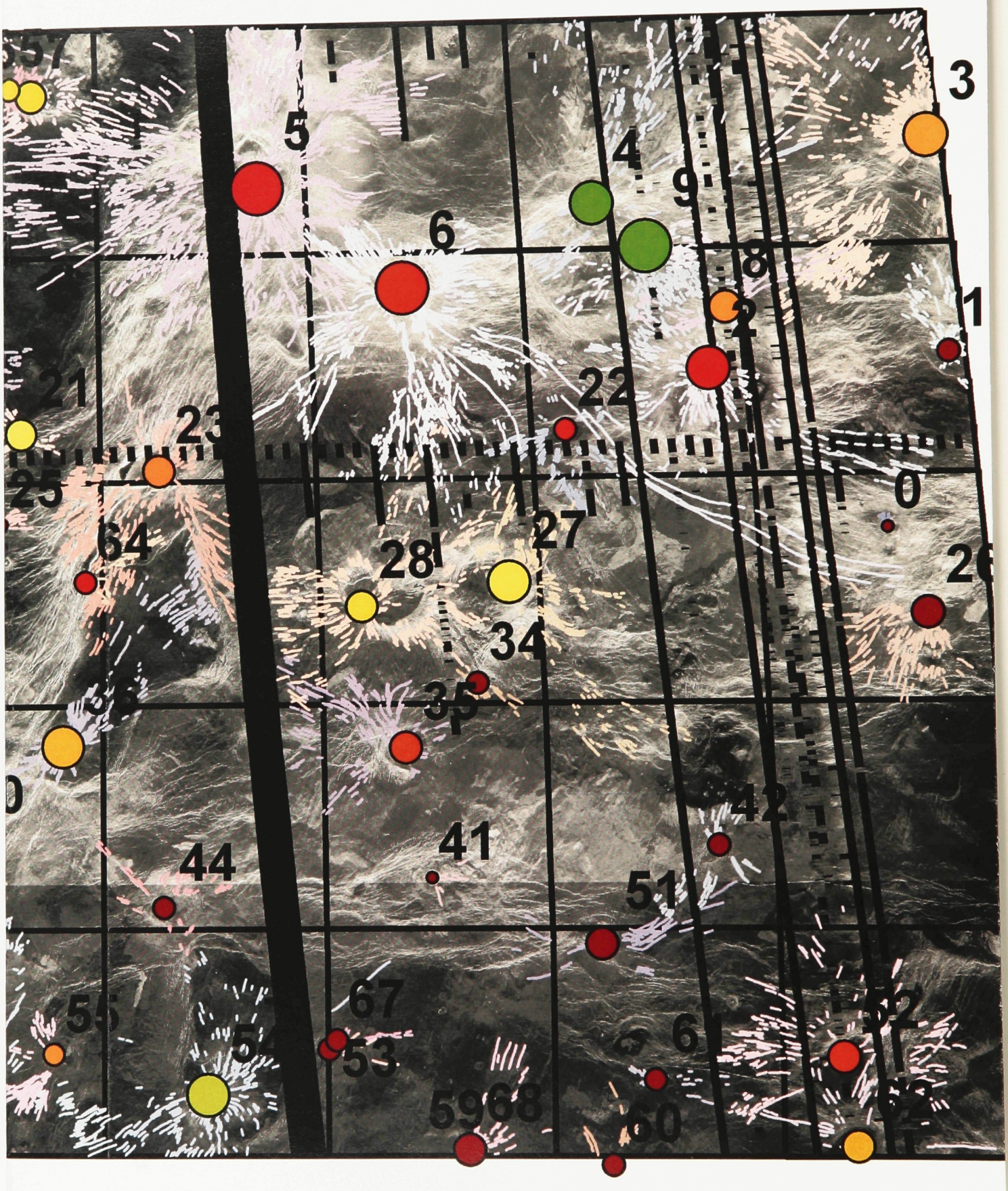
System Radius (km)
8-125
126-250
251-500
500-800
800-1985